Universität Bremen

INSTITUT FÜR BIOPHYSIK

Fachbereich 01

Faculty of Physics/Electrical Engineering

Influence of the microenvironment on the biomechanical properties of pancreatic ductal adenocarcinoma (PDAC) cells

Dissertation submitted towards the degree of

Doctor of Natural Sciences in Physics

(Dr. rer. Nat.)

Shruti G. Kulkarni, M.Sc.

Submission: Bremen, 01.11.2023

Defence: Bremen, 13.12.2023

Referees

Prof. Dr. Manfred Radmacher

Prof. Dr. Małgorzata Lekka

“All my life through, the new sights of nature made me rejoice like a child.”
Marie Skłodowska-Curie

This project has received funding from the European Union's Horizon 2020 research and Innovation program under the H2020-MSCA-ITN-2018 Grant Agreement n. 812772.

Acknowledgement

I sincerely thank Prof. Dr. Manfred Radmacher and Prof. Dr. Małgorzata Lekka, who supervised this doctoral work. I gained immensely from their knowledge and expertise. They supported me scientifically, and gave me the freedom to pursue any line of experiments. They gave me the freedom and confidence to learn at my own pace, and were always equally enthusiastic about both successes and failures. Prof. Lekka is kind and compassionate, and always happy to chat about work as well as life. As I travelled to Krakow under difficult circumstances, she always made sure I had the support I needed to complete my work in the limited time I had. Prof. Radmacher was always ready to discuss and tried to find the solution to any problem, big or small, without any judgement.

I developed an interest in biophysics because of Dr. Bidisha Sinha at IISER Kolkata, who was my master thesis supervisor. Her enthusiasm for research is infectious, and she will always be my motivation in the research I carry out. She spreads her passion to all her students and I was lucky to be one of them. I received great training under her and am incredibly grateful for that. I had the opportunity to practice research for the first time under the guidance of Dr. Jacinta D'Souza at UM-DAE CBS; Mumbai. I learned about good lab practices, planning projects, and many more invaluable lessons in the three months I spent in her group. Furthermore, I want to warmly thank Prof. Dr. Monika Fritz and Prof. Dr. Dorothea Brüggemann for their suggestions and feedback, as well as great discussions. They helped me grow as a scientist and as a person.

I would like to thank my colleagues at the Institute of Biophysics, University of Bremen: Prem Kumar Viji Babu, Nina Messerschmidt, Meike Gummich, Holger Doschke, Janka Heits, Thomas Mertens, Gaby Theimann, Mènie Wiemer, Saurabh Joshi, Jonas Michalewski, Jennifer Rothfischer, Deepanjali Dutta and Arundhati Joshi who have always been supportive and friendly. Carmela Rianna first introduced me to the lab at UB, and was also my first teacher as I started the PhD. Her kindness and dedication to her work were an inspiration to me, and I am very grateful to her. I am grateful to have supportive colleagues like Anna Piorecka-Ecken and Malte Ohmstede, especially in the most challenging part of my PhD. I want to thank Sandra Perez-Dominguez, who started the PhD with me in Bremen. We have shared our joys and successes, sorrows and failures, and the occasional research article. Because of her, I grew as a scientist, but most importantly as a human being.

Collaboration with colleagues from other departments also helped me to use instruments not present in our department. I am very grateful to Sina and Prof. Dr. Vellekoop for capturing electron microscope images. I also want to thank

Dr. Annette Peter and Prof. Dr. Rita Groß-Hardt for providing the Confocal facility and help with training.

As I carried out a large part of my work at the Institute of Nuclear Physics Polish Academy of Sciences, my lovely colleagues there always supported me. I want to thank Kajangi Gnanachandran, Renata Szyldak, Tomasz Zielinski, Marcin Luty, and Bartolomej Zapotoczny. Joanna Zemla and Joanna Pabijan taught me how to navigate the lab, use the various intruments, and have contributed the most to the development of my research at IFJPAN, and I thank them for it.

As part of the training and research in Phys2BioMed, I travelled to CMPI group in CNRS, Lille. Prof. Frank Lafont and Dr. Vincent Dupres were happy to welcome me to the group for my secondment. Dr. Elisabeth Werkmeister and Javier Lopez helped me to navigate the new lab and guided me to fulfil my experiments.

I also want to thank the Phys2BioMed network and all the colleagues and supervisors in the project. I received excellent feedback and co-operation from everyone at the regular meetings. It was also an incredible opportunity to participate in in Europe-wide scientific collaboration, and meet people from different backgrounds. I am especially grateful to Harinderbir Kaur and Khaldoun Gharzeddine, who are lovely and supportive people that I will be happy to call friends for life.

Many friends old and new supported me with their love and friendship in these years. Laura, Iliyana and Valeriia, I am so grateful for your friendship in Bremen. Joining Impro theatre classes was one of the best decisions I made in Bremen, which led me to meet incredible people who are fun, kind and empathetic. They made this city my home. Karishma, Rajiv and Himanshu were there for me Krakow, where I found a small corner of peace in the hectic time I usually had there. I want to thank Kimaya, Srishti, Sai Shipra, Supraja and Madhavi, who showed me that some friendships can grow even at a distance. I want to thank Shubhagata, with whom I shared all my joys and failures. I can't imagine my life without her and I am very grateful to her for supporting me during this journey from half way across the world.

My family is my strength and my guide. Their care, compassion and kindness sustains me. The love and care of my parents Ashwinee and Gopal Kulkarni raised me to be capable of attempting to undertake a PhD. My sister Saakshi is always there to cheer me on and support me. My extended family, late Archana Pillai, Anita Kulkarni, Ajay Kulkarni and Subbiah Pillai, and my grand father Vinayak Kulkarni, have all cared for me and supported me like I was their own child. My dear cousin Raaghav, who has been through a lot these last 3 years,

yet continues to work hard, truly inspires me every day to continue on my chosen path and meet the challenges of a new day. Anita and Shirish Yakkundi, my aunt and uncle, and excellent scientists themselves, have been my guides in the world of academics, and I am very grateful for this. Vinay believed in my ability when I found it hard to do so myself. He supported me through some of the most difficult personal times in the last four years, I find myself lucky to always have his love, support and kindness. As everything in my life, I share the outcome, the fruits of this work with him.

The past few years were marred by the COVID-19 pandemic for the entire world. As I dealt with the many unexpected repercussions of this situation, everyone supported me to continue and complete my doctoral work in many different ways. As I undertook the journey of completing a doctoral thesis, many people held my hand and walked by my side. I will always be grateful for their support and guidance.

Table of contents

List of Figures

List of Tables

Abstract

The pancreas is an abdominal organ with digestive and endocrine functions. Pancreatic ductal adenocarcinoma (PDAC) is a deadly disease with low survival rates and poor prognosis, which occurs in the digestive part of the pancreas, specifically due to the conversion of healthy epithelial cells to cancer cells. There are continuous efforts to understand the mechanisms of disease progression, as well as for expanding viable options for therapy.

PDAC is characterised by a dense and fibrotic extra-cellular matrix (ECM), which is a dense mass of protein fibers. There are also many cancer-associated cell types. Together, they form the unique milieu of the tumour microenvironment (TME). The various components of the TME promote the aggressive progression and metastasis of PDAC. While the molecular, genetic, and epigenetic mechanisms of the PDAC and its TME have been studied for a long time, the stiffness and mechanical properties of the TME are slowly emerging as important factors in the poor prognosis of PDAC.

This work used Atomic Force Microscopy (AFM) to elucidate the subtleties of PDAC mechanics. Two modes were used to study two distinct mechanical aspects: the stiffness or viscoelasticity of PDAC cells and the extent of cell-cell interaction. The AFM is a type of scanning probe microscope that detects piconewton-scale forces. A cantilever with a reflective gold coating on the back is indented upon a sample, and the deflection of the cantilever is detected by an optical-lever. A cantilever with an integrated tip was used to probe the viscoelastic properties of PDAC cell lines. A cantilever with an attached live cell was used to press against other cells, to probe the extent of cell-cell interaction via cell adhesion. A small study on the impact of measurement parameters like experimental CO_2 concentration and loading force of the cantilever was also carried out.

Four PDAC cell lines were studied in this work: two from the primary cancer site of the pancreas, one from a lymph node metastasis, and one from liver metastasis. The effect of physical cell confinement and ECM-based hydrogels on cell viscoelasticity was studied. The cell-cell interaction within the cancer cells, as well as the extent of their interaction with endothelial cells, was studied. The effect of a potential drug on cell-cell interaction was also studied.

Through this work, a mechanical paradigm of pancreatic cancer cells can be established. The interplay between cancer cells and the TME via mechanical clues can be understood better.

Chapter 1 - Introduction

The pancreas is a secretory organ located in the abdominal region of the human body (Fig. 1.1). It is responsible for both endocrine and exocrine functions. Pancreatic ductal adenocarcinoma (PDAC) accounts for about 85% of all occurrences of tumours in the pancreas [1]. Commonly referred to as PDAC cancer for this reason, this disease occurs in the exocrine region of the pancreas.

Vague presenting-features of the disease lead to late diagnosis. The most common symptom is jaundice, which sets in very late in the progression of the disease. The best available tools for prognosis are early-detection systems [2]. However, the relatively low prevalence of PDAC makes these systems infeasible. Recent therapies for PDAC have led to improvement in survival rates; however the lack of efficacy of therapies targeting agents that worked for other cancers shows that PDAC has unique challenges that need to be tackled [3]. What this boils down to is that PDAC has among the lowest 5-year survival rates in patients suffering from cancers. The most recent 5-year survival rate of PDAC worldwide stands at 4-6% [1][4]. Overall, the prognosis of PDAC is very poor, and indeed further steps after diagnosis are often expensive. Treatment options have limited efficacy, and one aspect of PDAC, which has proven to be a significant hurdle in treatment, in particular, is the strong and complex desmoplastic reaction in both primary and secondary tumour sites [5].

This chapter describes the important role played by microenvironmental factors in PDAC progression and metastasis, as well as mechanical perspectives on the disease. Biophysical tools that can be used to study PDAC and the role of the cancer microenvironment are also presented.

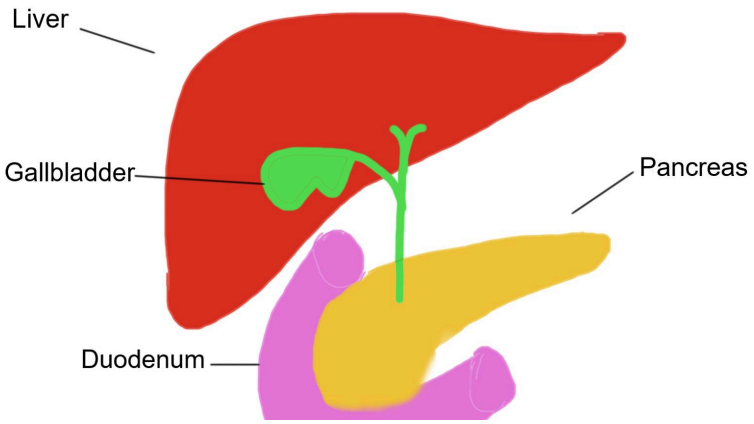

Fig. 1.1 The location of the pancreas in the body, surrounded by organs like the liver, duodenum (small intestine), and gallbladder.

1.1 Clinical and molecular characteristics of PDAC

The pancreas is a secretory organ and functions as a gland. Anatomically, it is divided into the head, neck, body, and tail. It contains tissue with both exocrine and endocrine roles. The endocrine region forms only 1% of the gland, and it is responsible for regulating blood sugar level. Its exocrine region comprises of 99% of the gland and is responsible for producing precursor digestive enzymes called zymogens. The acinar cells are responsible for producing zymogens. They are clustered around small ducts (epithelial cells) wherein the zymogens are collected in an increasing hierarchy of ducts till and secreted into the small intestine via the main pancreatic duct and the bile duct.

PDAC is characterized by a grim prognosis with low survival rates. The late diagnosis is perhaps the most significant cause of the low survival rate. The majority of patients with PDAC do not experience symptoms until the disease has already reached an advanced stage. About 10% of cases have a familial bias; however the genetic basis remains unknown. Other risk factors include tobacco consumption, alcohol consumption, and chronic pancreatitis among others [6]. Signs and symptoms may include yellow skin from jaundice, abdominal pain, loss of appetite, and explained weight loss, among others. Medical imaging techniques such as computed tomography and endoscopic ultrasound can be used to detect the spread of cancer and the possibility of removing it surgically (resectability). Once detected, the efficacy and outcome of treatment are heavily dependent on the stage of the disease. Only 20% of patients are eligible for initial surgical removal [7]. The only curative option is surgical resection of the tumour, followed by adjuvant therapy to prevent remission. Adjuvant therapy includes treatment with gemcitabine + capecitabine or mFOLFIRINOX. These drugs inhibit the DNA replication machinery and prevent cell replication, effectively ending tumour growth.

In patients with unresectable and/or metastasized tumours, the only prognostic option is neoadjuvant chemotherapy, which may be combined with chemoradiation. However, these are recommended case-per-case and not a standard care practice [8].

While the histopathological study is not necessary for forming the surgical plan, poorly differentiated tumours are the most typically observed form of cancer. The resulting feature is also considered desmoplasia and a consequent hypoxic environment [9]. The interplay of form and function is the cornerstone of biology. The disruption of tissue architecture is a marker of many diseases. In the case of PDAC, this is slowly considered to be more than a mere by-product of the disease. The exocrine region of the pancreas does not have a well-defined stem-cell compartment. Instead, acinar cells acquire progenitor-like abilities. This is followed by acinar-to-ductal metaplasia under normal circumstances, generating healthy exocrine tissue [10]. However, acquiring progenitor-like abilities by acinar cells renders them more susceptible to pro-oncogenic mutations like in the pro-oncogenic gene KRAS. Subsequently, acinar cells do not produce healthy tissue but instead produce precursor lesions of PDAC [11]. These are classified as high-grade pancreatic intraepithelial neoplasias or PanINs and are the most commonly occurring malignant tumours of the exocrine pancreas [12]. They are usually papillary lesions with loss of polarity, irregular stratification, tufting, severe cytological atypia, mitoses, and occasional intraluminal necrosis. Loss of cell polarity and irregular stratification are particularly dramatic alterations in cellular morphology. Whether the origin of cancer cells is ductal or acinar, is difficult to determine. This is because the plasticity of the acinar cells drives the homeostasis and regeneration of the exocrine tissue. The changes in morphology and gene expression are summarised in Fig. 1.2.

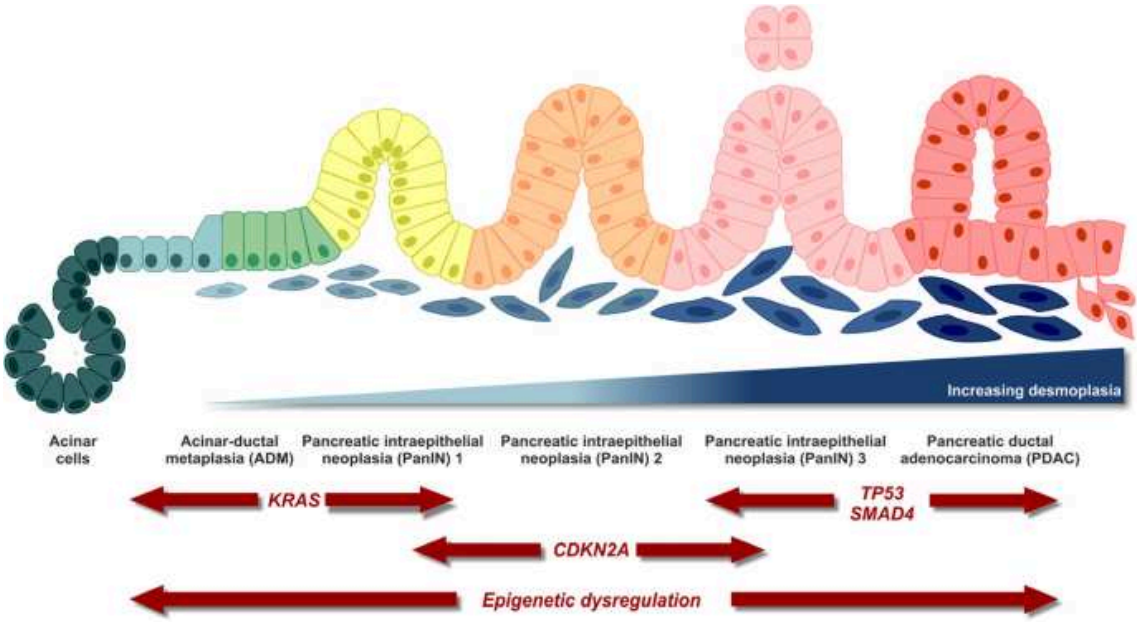

Fig. 1.2 The progression of PDAC (adapted from [13]*).*

The mutational and transcriptional landscape of PDAC has been explored using next-generation sequencing approaches. The gene encoding the proto-

oncogenic GTPase KRAS and several other tumour suppressor genes, including TP53, CDKN2A, and SMAD4, are frequently altered or mutated in PDAC [14]. For example, KRAS mutations were found in the majority of pancreatic tumours (> 90) [15]. Overexpression of RAC-beta serine/threonine-protein kinase (AKT2) [16] and elevated activity of its upstream regulator phosphoinositide 3-kinase (PI3K) [17] were also observed in PDAC, leading to increased tumour cell survival.

In addition to these key mutations, certain subsets of patients with PDAC exhibited less common alterations, such as germline mutations in DNA damage repair genes (e.g., BRCA1/2, PALB2, and ATM) and somatic mutations in DNA mismatch repair regulator genes, resulting in increased microsatellite instability [18]. Importantly, the transcriptomic landscape of PDAC is not solely governed by genetic alterations. Epigenetic regulatory mechanisms play a significant role, including DNA methylation, histone post-translational modifications, and non-coding RNA regulation. Thus, PDAC has a complex biomolecular progression, accompanied with changing tissue morphology.

1.2 Microenvironment factors that promote PDAC

PDAC tumour comprises of an extensive desmoplastic stroma. This is the abnormal growth of fibrous connective-like tissue in the tumour. The main components of the desmoplastic stroma are cancer-associated fibroblasts, immune cells, and the fibrous matrix (Fig. 1.3). One consequence of the abnormal tumour environment is hypovascularisation, where the vascular system is unable to penetrate the tissue and cannot supply adequate oxygen and nutrients. This leads to another key feature of the PDAC microenvironment, which is hypoxia.

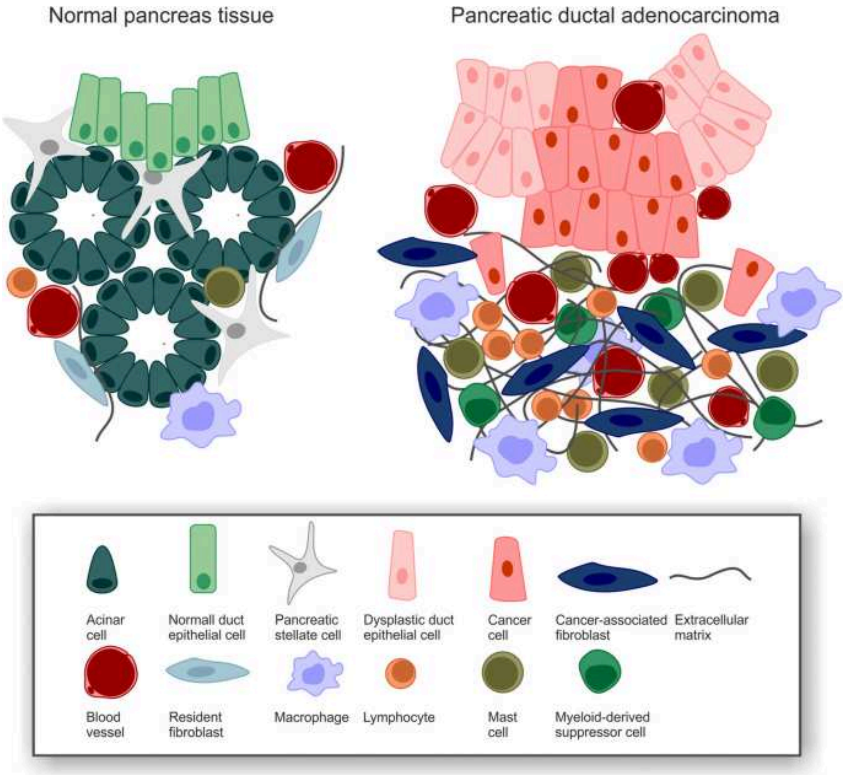

Fig. 1.3 The desmoplastic reaction and complex stroma of PDAC (adapted from [13]*).*

The desmoplastic reaction of PDAC tumours can be a direct result of pre-cursor stress conditions like chronic inflammation and injury. Pancreatic stellate cells are the precursors of fibroblasts found in the pancreas. In the healthy pancreas, they can be found in the quiescent stage, where they are neither dividing nor contributing to any normal functions of the pancreas [19]. However, under stress conditions, and under activation from cancer cells [20], stellate cells can activate and differentiate into cancer-associated fibroblasts (CAFs) that secrete ECM proteins and start the desmoplastic reaction. There are at least two distinct subpopulations of CAFs, namely myofibroblasts and inflammatory fibroblasts [21].

Thus, the PDAC microenvironment becomes highly fibrotic with tensile-resistant fibrillar collagen and compression-resistant hyaluronic acid (HA) [22]. Hyaluronic acid provides a favourable microenvironment for PDAC progression, with high expression of HA and its receptors in cancer cells [23]. Pancreatic stellate cells play a major role in this desmoplastic reaction, leading to one of the stiffest tumour stroma among all cancers. Activated pancreatic stellate cells can stiffen the ECM and activate the release of the pro-inflammatory molecule transforming growth factor – ß (TGF-ß) in the ECM [24]. PANC-1, which is a cell line from the primary tumour site, has been shown to have enhanced matrix-metalloproteinase activity on stiffer collagen substrates [25]. Activated pancreatic stellate cells have been shown to have increased Collagen – I deposition and ECM remodelling, which is dependent on matrix-metalloproteinase activity and TGF-ß [26]. Stellate cells, which become activated to form cancer-associated fibroblasts, form the tumour ECM which promotes cancer progression and hinders treatment [27]. While cells that can provide in vitro ECM, or direct ECM from PDAC tumours is difficult to obtain, ECM components can be used to study the effect of the ECM on PDAC.

Hyaluronic acid (HA) or hyaluronan is a glycosaminoglycan, a type of polysaccharide found in the connective parts of tissues. It is shown to be abundantly secreted [28] and detected in [29] PDAC. It stimulates cancer cell motility [30], at the same time impairing vascular function. Overall, it contributes to drug resistance in PDAC, and it is considered a good target for therapeutic development [31], [32]. The role of HA is an emerging concept. The role of collagen in PDAC progression, however, is well-established. Collagen is a group of fibrillar proteins that form part of the ECM throughout the body. In its different forms, it can promote various functions. However, in PDAC it is known to promote chemoresistance [33]. Collagen type-I [34]–[36], collagen type-IV [37], [38] and collagen type-V [39] all contribute to cancer progression, malignancy, invasion and metastasis. 3D collagen-nitrocellulose matrices could model the tumour microenvironment of PDAC [40]. Matrix stiffness has been shown to produce chemoresistance in PDAC [41], while also being linked to the mechanical memory of cancer cells [42]. This suggests that the mechanical properties of the tumour microenvironment could potentially influence PDAC initiation and progression. This also calls for a significant mechanical response of the cancer cells themselves.

1.3 Epithelial-to-mesenchymal transition (EMT) and metastasis in PDAC

Epithelial-to-mesenchymal transition can be simply defined as a morphologic cellular program where the cell phenotype transitions from an epithelial to a mesenchymal state. It occurs at the tumour invasive front and in circulating tumour cells (Fig. 1.4). However, the significant role of epithelial-to-mesenchymal (EMT) is very clear. The EMT-inducing transcription factor Zeb-1 is important for inducing invasion and metastasis [43]. EMT is a morphologic cellular program that changes cells from the epithelial to the mesenchymal phenotype. Intermediate hybrid epithelial and mesenchymal cell states or semi-EMT states are observed in vivo, particularly in circulating tumour cells [44]. A peculiar characteristic of the semi-EMT state is the expression of cell-cell interaction molecules found in both epithelial and mesenchymal cells. E-cadherin is responsible for forming adherens junctions in epithelial cells [45]. N-cadherin is the marker of the mesenchymal state. In 3D spheroid models of PDAC cells, while there was more expression of mesenchymal markers, E-cadherin expression continued as well, indicating a semi-EMT and the role of E-cadherin in collective migration [46][47]. Epithelial stabilisation in circulating tumour cells also leads to the enhanced collective migration of cancer cells, as well as enhanced metastasis to the liver [48]. Recapitulating the matrix stiffness of PDAC tumours in mice and 3D substrates shows markers of EMT like increased vimentin expression and reduced E-cadherin expression [41]. While EMT was classically considered a promoter of metastasis, the role of the two cadherin forms, E-cadherin and N-cadherin is obscured. The overall cell-cell attachment of PDAC cells is also not characterised, neither other cancer cells nor with the endothelium that the cells pass through during metastasis .

Early progression to metastasis is a common and typical feature of pancreatic. Patients show invasion of the liver, peritoneum, lungs, colon, and sections of the vasculature, like lymph nodes [6]. However, key genetic drivers of metastasis are not well understood. Stem cells show mechanical dependence for differentiation [49]. Pancreas lacks a stem cell compartment, and since the proliferating cells, which are stellate cells, are considered the ones to form the tumour by becoming cancerous, we could theorise that they depend on matrix stiffness and composition for progression.

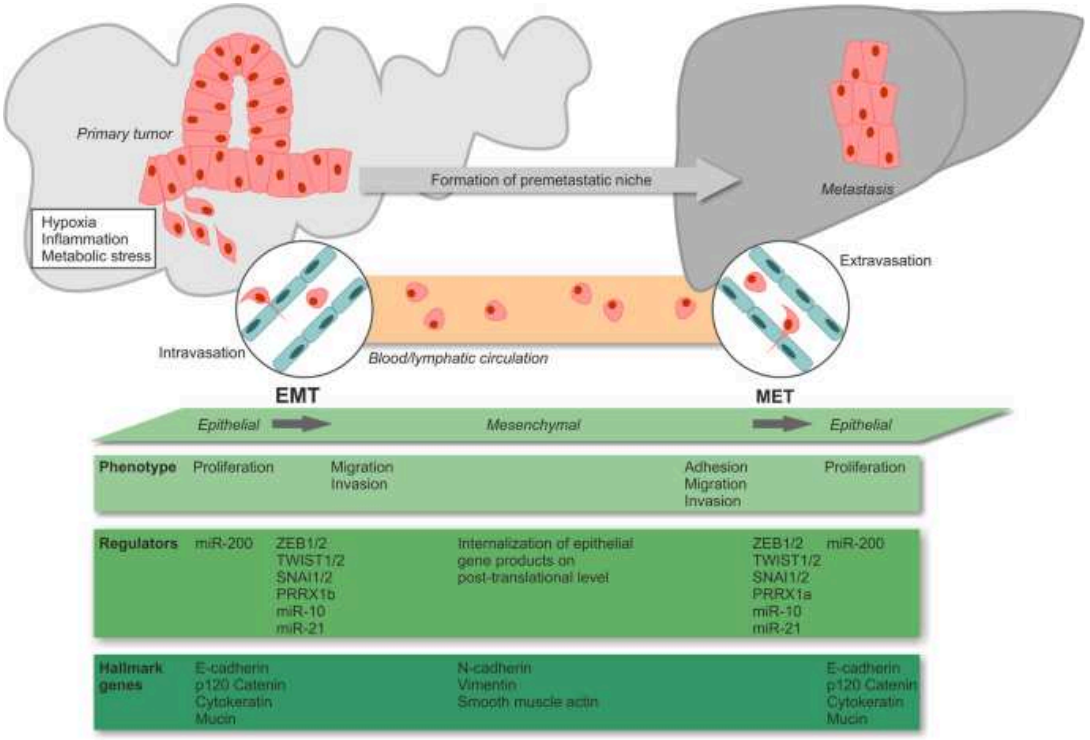

Fig. 1.4 The epithelial-to-mesenchymal transition and metastasis formation in PDAC (adapted from [13]*).*

1.4 Atomic Force Microscopy

Atomic force microscopy (AFM) [50] is a scanning probe technique inspired by the scanning tunnelling microscope [51]. The scanning tunnelling microscope is based on the principle of a tunnelling current between a metal tip and a conductive sample, while AFM is based on the principle of a force between a tip and the sample. AFM can be utilized in various modes for surface imaging and examining mechanical properties. Upon its invention, the AFM was used to image non-biological samples. It was theorised as an instrument that can image materials at angstrom resolution [52]. The AFM could however be used in a liquid or fluid environment, and this was fully exploited, especially prior to the invention of immunohistochemistry. While immunohistochemistry and fluorescence-based super resolution techniques now dominate high- and even-atomic resolution imaging of cells, AFM was used earlier to image interesting biological phenomena like the activation of live human platelets [53]. AFM was used in imaging mode to obtain high-resolution images of biological samples like proteins [54] and cells [55] in liquid. Using segment-wise analysis of the indentation and finite element models, the underlying features of cells could be imaged using stiffness tomography [56]. With the emergence of the study of mechanical properties of biological samples and cells, AFM was soon used to elucidate interesting mechanical properties like the mechanical-dynamics of motile fibroblasts [57] and comparison of the stiffness of normal and cancerous cells from the bladder [58]. Probing and measuring a sample with the AFM cantilever directly was used to image and measure the mechanical properties of samples. However, AFM cantilevers could also be modified to perform indirect force-based experiments that can characterise the surface properties of samples. Cantilevers were chemically functionalised, and then used to probe samples. Thus, the interaction properties between the sample and the functionalised cantilever were characterised. Early studies with this approach showed the interaction between melanoma cells and extracellular matrix protein fibronectin or endothelial cells [59]. Starting with the possibility of high-resolution imaging, the AFM was used for several applications in material sciences as well as in biological systems.

The AFM has two principal abilities: force measurements and imaging of surface topography. Here, we will delve deeper into the applications of force measurements mode. The AFM functions on the principle of an Optical Lever System (OLS). The OLS consists of a lever and an optical sensor that detects the movement of the lever. A cantilever, coated with a reflective material, is pressed with a piezoceramic element in the z-direction against the sample. The sample deflects the cantilever, and the optical sensor detects the bending of the cantilever. The optical sensor consists of a laser that is reflected off the back of the cantilever, and the reflected beam is detected by a photodiode. The AFM is used in the contact-mode for force measurement. The cantilever applies a fixed amount of force on the sample, and the sample's response to the force is measured. The material properties of the sample determine its response to the applied force. These properties can be measured using AFM. The applications of the AFM-based force measurements can be divided into two classes of experiments, i.e., those devoted to estimating the mechanical/rheological properties of cells or tissue and those focused on the determination of adhesion applied to describe unbinding of single molecular complexes or to elaborate cell-ECM or cell-cell adhesion.

The stiffness of biological materials is frequently expressed by Young's (elastic) modulus. Multiple studies measured the stiffness of cells from different tumour types like breast, bladder, cervix, and pancreatic cancer. Cancer cells were shown to be softer than healthy cells, albeit up to a different extent. Cancer cells also lost stiffness sensing [60], a result observed in other tumour types like thyroid cancer [61]. While the above results were observed for cancer cells, the cells were from the primary tumour site. Breast cancer is probably the most studied cancer in terms of mechanics and rheology. The results showed that more invasive breast cancer cells show less cell-cell adhesion and reduced E-cadherin expression [62]. They are also softer and have less filamentous actin in the cytoskeleton, as shown in multiple studies [63]. Invasive breast cancer cells MCF-7 also respond to microenvironmental factors like hypoxia and the stiffness of the environment. MCF-7 cells displayed markers of EMT under hypoxia and when the stiffness of the environment was increased [64]. The results obtained for other cancer types, like, e.g., renal cancer, which shows that normal, cancerous, and metastatic cells behave differently as a response to the stiffness of the substrate being changed. While healthy cells stiffen with increased substrate stiffness, as in the case of the other cancer types studied, cancerous cells from the primary tumour site had the same cell stiffness regardless of substrate stiffness. This indicated that compared to normal cells, cancerous cells were unable to sense the mechanical properties of the substrate. However, metastatic cells softened when they were grown on stiffer substrates, perhaps because cells exerted large forces on soft substrates during invasion

[65]. Bladder cancer cells preferentially grow on softer substrates presenting more adhesive groups [66]. Local mapping of bladder cancer cells revealed that more aggressive cancer cells are stiffer at the cell periphery than at the centre of the cell [67]. Healthy bladders were shown to be stiffer than cancer cells using AFM nanoindentation. However, a more complex microrheology technique was required to distinguish between cells and cancer spheroids at different stages of cancer progression [68]. Malignant bladder cancer cells also have a higher number of N-cadherin complexes than benign cells, which are also more stable as compared to benign cells [69]. In a single colorectal cancer cell line, two morphological populations of cells were identified, having similar adhesive properties. However, they differed in cell stiffness, which is suggested as a marker for more invasive or aggressive cells in the tumour [70]. Metastatic colorectal cancer cells are stiffer and less migratory than primary site cells; however the evaluated metastatic cells have a better prognosis than the primary site cells [71]. Cancer cells could use two theories of mechanics to migrate and metastasise. One is to exert force via actomyosin and the other is to soften and allow to be squeezed. The microenvironment tunes these abilities. If the cells exert force, then we can find out in what microenvironment are they likely to do it. On the other hand if they soften, then they need good cell-cell interaction.

Pancreatic cells and tissues have also been the object of mechanical measurements. In Rubiano *et al.*, the moduli for inflamed tissue (pancreatitis) and cancer PDAC tissue were reported to be 2.15 ± 0.41 kP and 5.46 ± 3.18 kPa, respectively. The viscoelastic properties were measured, and the Steady-State modulus (SSM) or elastic modulus and viscosity could be calculated. Pancreatitis tissue had higher SSM than normal tissue (1.06 ± 0.25 kPa; $p < 0.005$). The average viscosity of pancreatitis samples (63.2 ± 26.7 kPa.s) was, however; significantly lower than that of both normal tissue (252 ± 134 kPa.s) and tumours (349 ± 222 kPa.s; $p < 0.005$). Thus, healthy, inflamed, and cancerous pancreatic tissues show unique mechanical markers [72]. The study performed on two PDAC cell lines from the primary site showed that the more invasive cell line (BxPC-3) is softer but lacks an elongated morphology or well-oriented F-actin stress fibers as compared to the less invasive cell line (MIAPaCa-2). Ex-vivo studies were performed on murine orthotropic tumour models derived from both cell lines. In this study, cancer cells are injected into healthy mice to observe the progression of the cancer. Using AFM, it was observed that the desmoplastic region of the tumour was stiffening the cell microenvironment or the extracellular matrix (, while the cancer cells themselves were softening [73]. Another attempt at modelling PDAC behaviour in in-vitro models showed that pancreatic stellate cells are vital for capturing the mechanical microenvironment of PDAC in PANC-1 cell cultures. Standard drug treatment is less effective over stiffer tumours [74]. PANC-1 cells were

shown to have stiffness ranging from 100-500 Pa with an indentation force of 0.5 nN [75]. Another study compared healthy or normal pancreatic epithelial cells (HPDE6-C7) with cells from the primary site with increasing invasiveness (MIAPACA-2 and BxPC-3) and a metastatic cell line from invasion into the abdomen (AsPC-1). The Young's modulus of HPDE6-C7 (11.07 ± 7.1 kPa) is larger than that of MIA-PaCa-2 (4.13 ± 2 kPa), BxPC-3 (6.91 ± 4 kPa) and AsPC-1 (2.98 ± 1.5 kPa). The metastasised cells were the softest [76]. A different study measuring Young's modulus of normal pancreatic epithelial cells (HPDE) with cells from the primary site (MIAPACA-2 and PANC-1) and a metastatic cell line from invasion into the lymph node (Hs 766T) found very different results. The Young's modulus of the cell lines was 3.7 ± 1.2 kPa (HPDE), 1.7 ± 1.0 kPa (MIA PaCa-2), 2.4 ± 1.1 kPa (PANC-1) and 3.0 ± 2.0 kPa (Hs 766T). In this case, the cells from the primary site were softer [77]. While the absolute values of cells from similar regions (healthy and primary sites) varied in both cases, the trend was similar. Healthy cells are stiffer than cancerous cells. However, when comparing those to cells from metastatic sites, the actual site of metastasis affects the comparison. There seems to be no general rule about the relative stiffness of cells from metastatic sites. Mechanical properties of PDAC cell lines have been studied previously studied; however most studies were limited to the study of cell lines from the primary tumour site and at most one metastatic site.

1.4.1 Cell stiffness and viscoelastic properties of cells

While the stiffness of PDAC cells has been measured, the cells were always modelled as elastic samples, while in fact cells are more complex and are viscoelastic in nature [78]. In the case of purely elastic materials, the strain response occurs instantaneously after applying stress. Conversely, the strain lags behind the stress in purely viscous materials by a phase difference of 90°. Viscoelastic materials display behaviour that falls between the two ideal cases, with a certain degree of lag between stress and strain. Viscoelastic materials have some hallmarks:

1. The stress-strain curve shows hysteresis, because there is some relaxation because of the slow response of the viscous component
2. A constant strain is observed at increasing stress, termed as stress relaxation
3. Constant stress causes the strain to increase, which is described as a creep response
4. The stiffness of the material depends on the strain rate or the stress rate

The elastic component can be modelled as spring representing a linear elastic solid that follows Hooke's law and has the ability to recover fully from a stress (within the elastic limit). The viscous component can be modelled as a dashpot that obeys Newton's law and deforms at a constant rate on the application of a stress, never recovering once the stress is removed. Combining a spring and dashpot in forms the Maxwell model for a viscoelastic liquid, and combining them in parallel forms the Kelvin-Voigt model for a viscoelastic solid. The elastic response of strain dominates at shorter time scale while the viscous response of strain dominates at longer time scales for the Maxwell model. The opposite is true in the Kelvin-Voigt model. A combination of both models in series, termed as the Burgers model can describe real viscoelastic systems.

Viscoelastic properties can be measured using many types of tests. Creep compliance tests measure the creep response of biological samples by applying a constant force while allowing the sample to relax [79]. A jump in z-height in contact with the sample [80] can also be added. This technique allows evaluating the creep response of a well-defined step instead of looking at the global creep after approach. Oscillatory frequency sweep measurements can be carried out, where the AFM cantilever is oscillated over a range of frequencies to capture the range of timescales of the viscoelastic response. Cell microrheology can be defined by its complex shear modulus (G* (w)) [81]–[85]. The real and the imaginary parts of G*(w) describe the elastic energy stored and the viscous energy dissipated within the cell at different frequencies. The ratio between the imaginary and the real parts is called loss tangent, and indicates the solid- or liquid-like mechanical behaviour of the cell.

Polymer networks of made up of monomers of protein molecules, form the cytoskeleton of the cell. This is the main framework that maintains the shape and structural integrity of a cell. Since polymers are rearranged in viscoelastic material experiencing deformation, it is necessary to characterise the polymer network that the sample has. As cancer cells have been known to differentially regulate the expression and arrangement of cytoskeletal networks beyond actomyosin, proteins like keratin [86]–[88] and vimentin [89], [90] might play a role in awarding differential mechanics to cancer cells in different stages of disease. When oscillatory stress is applied on the cell, the strain response follows a power-law as a function of frequency of oscillation. The soft-glassy model of rheology can be used to model the power-law behaviour. The cytoskeleton of the cell, specifically the actomyosin network, can be conceptualized as a collection of components held in place by attractive or repulsive bonds formed between adjacent components. The components here are made up of chains of actin cross-linked by myosin molecules. The bonds are the cross-links. These have relatively weak binding energies, allowing the

elements to occasionally escape their traps and change their positions. The occurrence of power-law rheology can be attributed to a broad range of energy of the bonds, resulting in a scale-free distribution of lifetime of the bond [91].

The multi-frequency oscillation technique called sweep methodology is used here to extract the elastic and viscous properties of materials from AFM force curves. This is a subset of frequency-dependent characterisation of the rheological properties of cell. Applying a sinusoidal oscillation on a viscoelastic sample generates a delayed response from the sample. The phase shift θ in the strain curve is calculated. The larger then phase shift, the more viscous a sample is. The word "*sweep*" in this terminology simply comes from the fact that the cantilever in contact is swept across many frequencies over multiple decades. As the loss tangent falls around the value for soft-glassy materials [84], [91], the structural damping model, a power law-based model, is used to describe the viscoelastic properties of cells. The structural damping model models the sample as a variation of a soft glassy material. This model uses a single power-law exponent, which scales the storage and loss moduli, and could be used to characterise the fluidity of the sample. Materials with less fluidity might have a network that is less prone to deformation. Thus, cell fluidity could indicate the difference between cancer cells at different stages of progression. There is an additional component to account for the energy loss due to hydrodynamic drag experienced by the cantilever during oscillation. This work uses corrects the hydrodynamic drag placed on the cantilever by applying the structural damping model. The mechanical properties of cancer cells are compared by quantifying the Young's modulus indicating the stiffness of samples and power-law exponent indicating the viscoelasticity or fluidity of samples.

1.4.2 Cell-cell interaction

Cells in the human body interact with each other directly for many different purposes. Cells in the immune system interact to activate pathways for protecting from intruders. That is an example of temporary cell-cell interaction. Most cell-cell interactions in the body are more long-term. The entire body is held together because layers of epithelium form all the surfaces of organs, sarcomeres form muscle layers and fibroblasts form the plethora of connective tissue in the body. Morphologically, pancreatic ductal adenocarcinoma is the disruption of the epithelial cell-cell relations [92]. Neoplastic disorganisation occurs. The normal epithelium is rests on a continuous layer of basement membrane or ECM, with cells having polar organisation of organelles. In contrast, the neoplastic or cancerous tissue has a disorganised ECM and

randomly oriented epithelial cells. The key feature here is the loss of appropriate contact between epithelial cells.

Atomic Force Microscopy (AFM) is a technique that can measure small forces, including the interactions between single molecules like proteins at the order piconewtons . Similarly, the interaction between cells can be quantified using an AFM-based technique called Single Cell Force Spectroscopy (SCFS) [59]. In SCFS, a cell is attached to a cantilever, and then this cell-cantilever is used to perform an AFM force curve on a sample of cells mounted on the AFM stage as the sample. The force curve can be used to extract information about the strength of attachment between the cell-cantilever and the sample. An SCFS experiment involves three steps: (1) functionalising a cantilever such that a living cell can be attached to it (2) preparing cell samples for the experiment (3) performing force curves on a cell sample using a cell-cantilever.

Cantilevers used for SCFS experiments are made from silicon nitride. The cantilever surface can be activated using ozone or UV irradiation, which cleans it and makes it possible to coat with a hydrophilic silane material like 3-(aminopropyl)triethoxysilane abbreviated as APTES. A layer of glutaraldehyde is then coated onto the APTES. Glutaraldehyde does not directly attach to activated silicon nitride, but forms a cross-linked network on APTES. This mesh can form covalent bonds with the anime groups of proteins. Thus, at the final step of cantilever functionalization, a protein is deposited on the cantilever [69]. The cantilever is now chemically functionalised and can easily attach to a cell, in a process termed as “catching a cell”. The sample for SCFS is usually a layer of the cells whose interaction properties are to be probed. Additionally, a cell suspension is added fresh to the layer of cells right before AFM measurements, to have cells that could be caught on the functionalised cantilever to achieve a cell-cantilever.

To carry out the cell-cell interaction experiment, two cells are pressed against each other. When they detach, they release the energy required to connect them in the attachment phase. Using an AFM, the cell-cantilever is pressed against the sample of a layer of cells. The z-piezo is used to move the cell-cantilever towards the cell layer at a fixed velocity during the approach. The cell-cantilever and cell layer make contact for a brief period of time called dwell, usually on the order of seconds, and then the cantilever is retracted at the same fixed velocity as the approach. The cantilever deflection is recorded as a force curve, where the retract portion of the curve is the most interesting part. In the approach, the cells come in contact and stay in contact during the dwell period. This enables the formation of cell-cell adhesions. As the cell-cantilever retracts, it is deflected and pulled back towards the cell layer because of the adhesion between the two cells. Eventually, the retracting z-piezo causes the formed

adhesions to break, and the force of the breaks is recorded in the retract curve. Clusters of adhesion complexes form bonds, which when broken during the retract process, are observed as ruptures of forces. The magnitude of the rupture force characterises the type of complex that was ruptured. The number of ruptures indicates the strength of the adhesion. The total energy required to break the adhesion between the cell-cantilever and layer can also be calculated. This is termed as the work of adhesion, and characterises the ability of the cells to remain attached to each other [93].

1.5 Mechanical properties of cancer and their measurement

Cellular response to external forces is mediated by load-bearing sub-cellular structures such as cell-adhesion complexes, cell membrane, and cytoskeleton. The effect of microenvironment stiffness on cell development is well established. Since cells are inherently mechanosensitive [94], the use of contact-based mechanical probing needs to be carried out carefully. Cell mechanical response can strongly depend on cell culturing parameters like temperature, and on sample preparation parameters like cell confluency, starvation and growth passage number [95][96]. Live cells show more variability as the duration of measurement of a sample increases. However, fixed cells don't have the same mechanical properties as live cells [97]. Some work shows that the PDAC cell cycle stage can affect cell stiffness. PANC-1 cells measured with a pyramidal cantilever tip stiffened as they progressed through their cell cycle [98]. Thus, it is better to tune measurement parameters than to measure fixed samples, which would be unaffected by cell culturing conditions. Different parts of the cell can be felt at different depths, thus, the depth of indentation and range of data analysis are crucial [99]. Epithelial cells can show two types of phenotypes in culture, i.e., spindle-like and oval-like. Increasing cantilever loading rate shows increased stiffness in the spindle-like phenotype associated with the mesenchymal state and not with the oval-like phenotype associated with the epithelial state [100]. PDAC cells partially change from epithelial to mesenchymal phenotype and biochemistry [101]. When comparing the mechanical properties of cell lines from different types of tumours, that is, from a primary and secondary site, it is important to note that the cells may not all have the same phenotype. It is, therefore important to choose the indentation parameters carefully.

AFM offers a wide range of forces to be exerted compared to other methods. The cell elasticity of fibroblasts has repeatedly been shown to be higher when estimated by a sharp tip as opposed to a blunt tip [102], [103]. This raises questions about how much force is needed. For example, short-term peak-force exhibits dependency on loading rate [104]. To measure the mechanical properties of a soft sample, the force applied and the achieved indentation have to be analysed with an appropriate contact mechanics model. The Apparent Young's modulus of cells was calculated with the Hertz contact model [105]. This is the case of a spherical indenter indenting semi-infinite elastic half-space. The Hertz model is built upon several assumptions. These include the assumptions that the sample is an isotropic, homogeneous, and linear elastic material. Additionally, it assumes that the sample is flat and infinitely thick.

While these assumptions do not strictly hold true for cells, the Hertz model can nevertheless accurately describe the mechanical properties of cells, and is widely utilized in this context. However, it is crucial to consider three important factors: the internal structures of the cell, its finite thickness, and its contributions from viscosity or viscoelasticity. These factors play a significant role in the mechanical behaviour of cells and should be taken into account when applying the Hertz model in cell mechanics studies.

The pH of tumour microenvironment is variable and usually hypoxic. This means that there is a deficiency of oxygen in the microenvironment. Hypoxia originates from the strong desmoplastic reaction, and, in turn, propagates the desmoplastic progression by activating stellate cells to differentiate into cancer-associated fibroblasts. PDAC microenvironment is hypoxic and acidic. Cells experience chronic low pH in the range of 6.4-7-.0 because of the metabolic activity. Metabolic reprogramming occurs in early PanIN lesions. Metabolic reprogramming of cancer cells is important, because it sustains uncontrolled proliferation by rapid ATP and macromolecule synthesis, as well as maintaining a redox state necessary for preventing apoptosis [106]. Healthy cells generate ATP via the oxidative phosphorylation pathway; however cancer cells shift to the less-efficient glycolytic pathway. Poor distribution vascularisation of the tumour results in a low glucose supply in the TME. While many types of tumours show adaptation to the glycolytic pathway, PDAC, in fact, faces glucose starvation and shows considerable metabolic plasticity. Cancer tissue mechanics and metabolism go hand-in-hand [107], and the cross-talk between mechanotransduction and tissue mechanics is gaining more recognition [108]. Glycolysis in healthy lung epithelial cells was shown to be reduced by actin cytoskeleton disassembly. However, glycolysis in transformed small-cell lung carcinoma cells is unresponsive to substrate stiffness [109]. Cell metabolism is dependent on substrate sensing.

While PDAC tumours have chronic low pH, cell lines are cultured under 5% CO_2, 37°C, humidified and air-filtered environment in an incubator. 5% CO_2 atmosphere maintains a physiological pH of 7.4 in a culture medium supplemented with bicarbonate buffer [110]. Normal pancreatic ducts from rat pancreas have bicarbonate exchangers [111], which indicates that correct pH is required for the physiological function of the pancreas. Furthermore, bicarbonate buffer systems with CO_2-supplemented air are the most physiologically relevant method of maintaining pH [110]. However, studies on cells using AFM usually do not use pH control but rely on buffers [112] instead of using a medium with an appropriate CO_2 environment. Unfortunately, CO_2 is not available in most commercial AFMs. Fibroblasts cultured in a bicarbonate-independent medium were softer than those cultured in the typical growth medium [102].

Apparent Young's modulus might be different with and without 5% CO_2. Moreover, cancer cells from different tumour sites might not have the same change in mechanical properties because of the changed pH. While there could be complex factors affecting the molecular mechanisms of cells, we need to measure the mechanics directly to be able to argue about comparing and using mechanics as a biomarker. If all measurements are carried out under sub-optimal CO_2 conditions, then this may be acceptable anyways. However, not all cells can survive under sub-optical pH conditions. For example, melanoma cells measured using AFM without CO_2 control can die in 2-3 hours [113]. While PDAC cell lines may survive on that time scale, their mechanical properties might still be affected.

AFM provides a versatile approach for studying cellular mechanics, but understanding the appropriate force ranges, maintaining constant conditions, and considering environmental factors are crucial for accurate measurements. The response of cellular materials to mechanical stimuli depends on various factors, including temperature, cell confluency, starvation, and cell passages. Additionally, the viscoelastic nature of cells and the influence of pH and CO_2 levels further complicate the mechanical characterization of cellular materials. A thorough understanding of these factors will enhance the interpretation of AFM measurements and advance our understanding of cellular mechanics.

Chapter 2 - Aim

To study the mechanical properties of Pancreatic Ductal Adenocarcinoma (PDAC), cell lines from different tumour sites were used. A cell line is a culture of cells from a set of cells from a tissue. The cells are of the same type. In this case, all cells in a cell line are cancerous cells. Cells from a cell line proliferate indefinitely under appropriate culture conditions. PANC-1 and PL-45 cell lines, derived from the primary tumour site of the pancreas from different patients, were used. Cell lines derived from metastatic sites were also used. Hs 766T cell line was derived from a metastasis to the lymph node, and the CFPAC-1 cell line was derived from a metastasis to the liver. Because of the lack of accessibility to normal pancreatic cell lines, one of the cell lines from the primary site, namely PANC-1, was used as a control. This cell line is widely used in various pancreas-related studies, thus, it seems to be well-characterized and established among various research laboratories [45], [75], [114]–[116].

The first part covered in Ch. 4 of the work was to settle the measurement conditions of the mechanical properties. The mechanical properties of cells were measured using the Atomic Force Microscope (AFM). While it is not always possible to maintain the right CO_2 and pH conditions, we needed to investigate the mechanics of cells under certain conditions of CO_2 and loading force.

The second part of the work covered in Ch. 5 investigated the viscoelastic properties of all four cell lines under varying confinement and substrate conditions. The effect of mechanical properties and substrate composition on the stiffness of cells from the primary site and metastatic sites were compared. The aim of this part was to understand the mechanoresponsiveness of cancer cells before and after they have metastasised.

The third part of the work covered in Ch. 6 investigated the cell-cell interaction of cancer cells with self-cells and with endothelial cells. The effect of N-cadherin masking drug ADH-1 on the cell-cell interaction was also investigated. Cancer cells were shown to change adhesive proteins during semi-EMT, which could correlate with their ability to exit the primary tumour and colonise a secondary, metastatic site. The aim of this part was to understand the changes in adhesive properties that cancer cells undergo before and after metastasis, and if this can be targeted to prevent further spread.

Chapter 3 - Materials and methods

Several physical, biochemical, and biological techniques were used here to carry out this work. The topic of interest in this work is pancreatic cancer. Thus, cell lines derived from two primary and two metastatic sites were used. The cells were studied on various substrates to mimic the natural cancer cell microenvironment. Two mechanical aspects of cells were elaborated, i.e., viscoelasticity and intercellular adhesion. The effects of measurement conditions on cell stiffness were also studied. Finally, the cytoskeletal network of cells was characterised.

The mechanical properties of cells were measured using the Atomic Force Microscope (AFM). The viscoelastic properties of cancer cells were measured using a novel microrheology technique. By applying the structural damping model, the power-law exponent was calculated. The cell-cell interaction between cells was measured as well. The data was analysed using software developed by other group members.

This chapter describes the protocols for preparing substrates, culturing cells, and sample preparation for various experiments, and the measurement techniques used, i.e., atomic force microscopy and optical/fluorescence microscopy.

3.1 Cell culture and sample preparation

3.1.1 Cell lines used and their sub-culturing protocol

The following human pancreatic cancer cell and human endothelial cell lines were used:

1. PANC-1 (CRL-1469, ATCC) is a primary site tumour cell line derived from the pancreatic duct.
2. PL-45 (CRL – 2558, ATCC) is a primary site tumour cell line derived from the pancreatic duct.
3. Hs 766T (HTB-134, ATCC) is a secondary or metastatic site tumour cell line derived from the lymph node.
4. CFPAC-1 (CRL-1919, ATCC) is a secondary or metastatic site tumour cell line derived from the liver.
5. EA.hy926 (CRL-2922, ATCC) is an endothelial cell line.

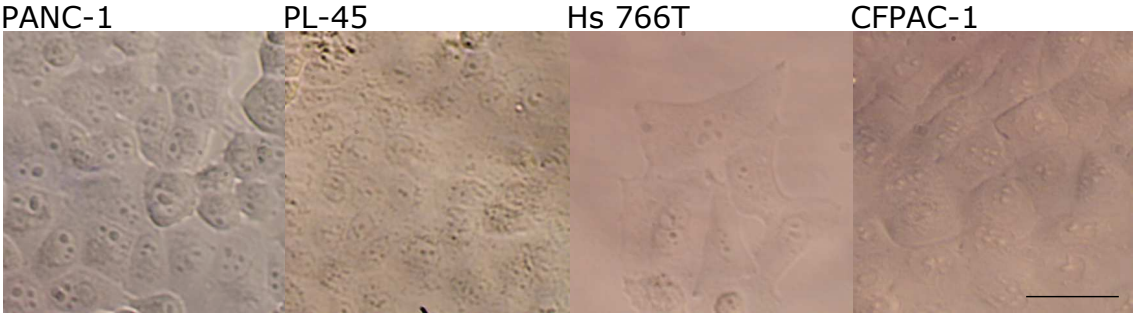

Figure 3.1 Optical images of pancreatic cancer cell line cultured on the stiff Petri dish surfaces in a CO_2 incubator at 37°C. The scale bar is 50 μm

When cultured in high density on plastic petri dishes (Fig. 3.1), the pancreatic cells display round/cubic morphology, regardless of the cell type. However, PANC-1, PL-45, and CFPAC-1 were able to form a monolayer, while Hs 766T tended to grow in clusters where the cells were not often observed to adhere to their neighbours. Although cells originated from PDAC, each cell line was cultured in a specific medium best suited for its growth.

3.1.1.1 Materials used for sub-culturing PANC-1, PL-45, Hs 766T and EA.hy926 cell lines.

Dulbecco's Modified Eagle Medium (DMEM, Gibco), 0.025% Trypsin-EDTA solution (Sigma), 0.05% Trypsin EDTA solution (Sigma), Penicillin-Streptomycin (P/S, Sigma), Fetal Bovine Serum (FBS, Sigma) and Phosphate

Buffer Saline (PBS, Merck). The complete medium comprises of DMEM supplemented with 10% FBS and 1% P/S.

3.1.1.2 Materials used for sub-culturing CFPAC-1 cell line:

Iscove's Modified Dulbecco's Medium (IMDM, ATCC), 0.025% Trypsin-EDTA solution (Sigma), Penicillin-Streptomycin (P/S, Sigma), Fetal Bovine Serum (FBS, (Sigma) and Phosphate Buffer Saline (PBS, Merck). The complete medium comprises of IMDM supplemented with 10% FBS and 1% P/S.

3.1.1.3 General protocol for sub-culturing all cell-lines

Cells were cultured in the following way. The culture medium was removed from the flask of cells and discarded. The cell layer was briefly rinsed with 4 mL of PBS solution to remove all traces of serum that contained the trypsin inhibitor. Then, 2.0 ml of pre-warmed Trypsin-EDTA solution was added to the culture flask, and the flask was placed in the CO2 incubator for 5 minutes. CFPAC-1 cell line was cultured with 0.025% Trypsin-EDTA solution for all experiments. PANC-1, PL-45, Hs 766T, and EA.hy026 cell lines were cultured with 0.025% Trypsin-EDTA solution for cell-cell interaction AFM experiments and with 0.05% Trypsin-EDTA solution for rheology and elasticity measurements.

When ≥ 90% of the cells had detached, 4 mL of complete medium was added. The solution was transferred to a 15 mL centrifuge tube and centrifuged at 1800 rpm for 4 minutes. The supernatant was discarded. Then, 2 ml of complete medium was added, and cells were aspirated by gently pipetting. Aliquots were prepared accordingly, and culture flasks or samples were placed into the 5% CO_2 incubator.

3.1.2 Preparation of cell samples for measuring cell mechanics/rheology

Cells were seeded and grown on the petri dish as per the table for preparing different samples. Then, 4 mL of suitable complete culture medium was added. The cells were incubated for the specified duration for each experiment. Table 3.1 presents the number of cells seeded for an experiment and the incubation time. PANC-1 and Hs 766T cells required about 1 day less than PL-45 and CFPAC-1 to fully spread on any substrate that they were seeded on. The

duration of incubation varied accordingly. Since single cells and cells on patterns only require cells to spread on the substrate before measurement, they were incubated for the duration required for cell spreading. A higher concentration of cells was seeded to form layers. The cells were also seeded for 1 extra day, to ensure that they spread fully. Cells on hydrogels were seeded for longer than those on single cells, because the cells needed longer time to spread on the hydrogels.

Table 3.1. Number and incubation period of cells seeded for microrheology and stiffness measurements carried out by AFM.

	PANC-1	PL-45	Hs 766T	CFPAC-1
Single cells, micropattern	50,000 cells for 1 day	50,000 cells for 2 days	50,000 cells for 1 day	50,000 cells for 2 days
Layer of cells	120,000 cells for 2 days	120,000 cells for 3 days	120,000 cells for 2 days	120,000 cells for 3 days
Cells on hydrogels	50,000 cells for 2 days	50,000 cells for 3 days	50,000 cells for 2 days	50,000 cells for 3 days

3.1.3 Preparation of cell samples for measuring cell-cell interactions

3.1.3.1 Preparation of cell samples for measuring cell-cell interactions

Cells were split and counted following the sub-culturing protocol. Solutions of 4,000 cells (to be grown for up to 10 days), 8,000 cells (to be grown for up to 7 days), or 12,000 cells (to be grown for up to 5 days) per mL of complete media were prepared. Subsequently, 1 mL of the respective cell solution was added to each well of a 24-well plate. The medium was changed every 2 days until the cells were ready for use.

3.1.3.2 Seeding cells to grow layers

The cells were split and counted following the sub-culturing protocol. Solutions containing 100,000 cells (PANC1), 120,000 cells (PL45), 120,000 cells (Hs766t), 100,000 cells (EA.hy926), and 120,000 cells (CFPAC1) per 1.5 mL of complete

media were prepared. Subsequently, 1.5 mL of the respective cell solution was added to each 35 mm Petri dish to prepare the samples. The cells were grown for 3 days before the AFM experiment.

3.1.3.3 Preparation of cell suspension to catch cells with a cantilever

The medium was discarded, and one well was rinsed with 500 µL of PBS. Then, 100 µL (for PANC1, PL45, Hs766T) or 200 µL (for CFPAC1) of 0.25% trypsin-EDTA solution was added, and the well was placed in the incubator for 1 minute. The trypsinized cells were brought up to a volume of 1 mL with complete media, and the entire 1 mL was transferred to a 15 mL centrifuge tube. The tube was centrifuged at 1800 rpm for 4 minutes. After discarding the supernatant, the cells were re-suspended in 100 – 500 µL of medium, depending on the size of the pellet.

3.1.3.4 Preparation of the cell cluster sample for the cell-cell interaction experiment

The medium in the sample petri dish was discarded, and then the petri dish was washed with 1 mL PBS. 1 mL of fresh medium was added to proceed with AFM cantilever calibration.

3.1.3.5 Preparation of ADH-1 solution

To inhibit cadherin-cadherin interaction between cells, Exherin (Adherex Technologies, UK, referred to as ADH-1 in the thesis) was applied. The powder should be weighed under sterile conditions. A 10X solution (4 mg/mL) was diluted with a raw medium. 100 µL of the 10X solution was then diluted with 900 µL of complete medium to prepare a working solution of 0.4 mg/mL and introduced to cells for drug treatment for 3 hours in a 37°C incubator with 5% CO_2. The stability of ADH-1 solution in raw DMEM is compromised when stored for extended periods at -20°C, and hence should be stored for up to 1 week.

3.2 Substrates used to confine cell spreading and mimic cancer microenvironment

3.2.1 Micropatterning rings of fibronectin on a glass coverslip

Cells for in vitro experiments are typically cultured on hard glass or plastic substrates, allowing them to spread to their full extent. The first level of confinement that can be imposed on these cells is by restricting spreading to a circular area on glass substrates. In this work, glass coverslips were coated with the ECM protein fibronectin in a ring shape through a series of steps (illustrated in Figure 3.2). Cells grown on these coverslips were confined to the ring pattern in a circular geometry. To generate patterns, we used a chromate synthetic quartz photomask. The photomask lacks quartz coating in the ring pattern (Delta Mask B.V., Netherlands). It has rings with the following dimensions: outer diameter of 25, 35 and 45 µm and ring width of 7 µm. Only cells growing on the 25-µm-diameter ring were measured using AFM. Coverslips are coated with PLL-PEG, and then the PEG is depleted specifically from the ring using the photomask and UV oxidation. When a PEG molecule is removed, the carbon group at that spot is oxidised to a carboxyl group, which can attach to fibronectin [117].

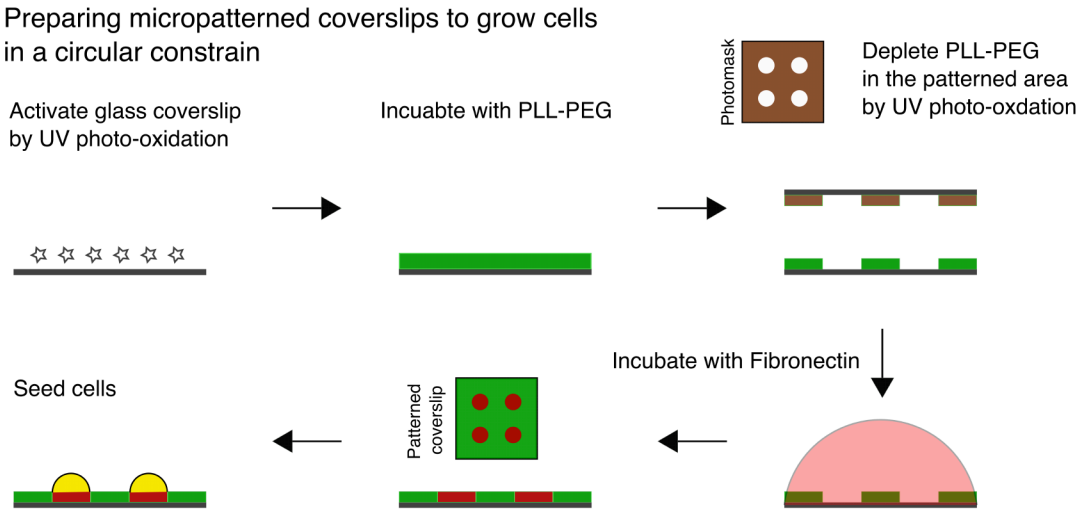

Figure 3.2 The workflow of micropatterning glass coverslips to have a ring pattern coating of fibronectin. Cells can then adhere on the fibronectin and be confined to spread on the ring geometry.

15-mm-diameter round glass coverslips were cleaned by sonication, first with acetone for 2 min and then with water for 2 min. The coverslips were washed with absolute ethanol for 1 min and air-dried completely. Next, the coverslips were placed in a UV ozone chamber (UVO Cleaner 30–220, Jelight Company Inc., USA) for 5 min to activate the surface. The activated surface of the coverslip was incubated with the PLL (20)-g [3.5]-PEG (2) solution (SuSoS AG, Switzerland) in milli-Q water at a concentration of 0.1 mg/mL for 1 h at room temperature (RT) in a wet chamber. Next, the coverslips were rinsed, once with D-PBS once and four times with milli-Q water. The coverslips were attached to the mask with 5 μL milli-Q water and exposed to UV for 5 minutes. These coverslips can be stored at 4°C in a humid chamber for up to 1 month. Before seeding cells, the coverslips were hydrated for 30 min with PBS and incubated with 25 μg/mL fibronectin (Sigma) in 100 mM $NaHCO_3$ (pH = 8.6) for 1 h at RT.

3.2.2 Silanizing coverslips for use in hydrogel sandwich

Hydrogels were prepared in a sandwich between hydrophilic and hydrophobic coverslips. Once the hydrogel was formed, the hydrophobic coverslip was removed to reveal a flat gel firmly attached to a coverslip [61], [118]. The hydrogel can be used to seed cells used for mechanical measurement using AFM. This method was chosen since AFM measurement requires cells to be grown on a flat and level surface.

3.2.2.1 Preparation of hydrophobic coverslips

The coverslips were washed with absolute ethanol and air-dried in the hood for 30 min. 200 μL of Sigmacote (Sigma: SL2 SIGMA) per coverslip was added in a glass petri dish. The coverslips were immersed in Sigmacote for 10 s. Then they were air-dried in the hood for 2 h. Remnants of salinization were rinsed off in a large petri dish filled with milli-Q water. Lastly, the coverslips were air-dried in a hood for 2 h. These can be stored in a sealed plastic petri dish for up to 1 week.

3.2.2.2 Preparation of hydrophilic coverslips

The coverslips were washed with absolute ethanol and air-dried in the hood for 30 min. 200 μL of 0.1 M NaOH per coverslip was added to a large glass petri dish, and the coverslips were placed in it for 3 min. 200 μL of amino-silane *N*-

[3-(Trimethoxysilyl)propyl]ethylenediamine) 97% (Sigma) per coverslip was added to a large petri dish, and the coverslips were transferred here for 3 min. The amino-silane was discarded, and the coverslips were washed 3x for 10 min with milli-Q water. Next, they were incubated with 200 µL 0.5% glutaraldehyde (in milli-Q water) per coverslip in a large petri dish for 30 minutes. The glutaraldehyde was discarded, and the coverslips were washed 3x for 10 min with milli-Q water. Lastly, the coverslips were air-dried in a hood for 2 h. These can be stored in a sealed plastic petri dish for up to 1 week.

3.2.3 Preparing Collagen and Collagen-Hyaluronic acid hybrid hydrogels

To prepare hydrogels from Collagen I and Hyaluronic acid, we adapted the protocol provided by AdvancedBioMatrix for their Collagen I (PhotoCol®-IRG) and Hyaluronic acid (PhotoHA®-IRG) hydrogel preparation kits. Figure 3.3. illustrates the workflow of collagen I hydrogel preparation.

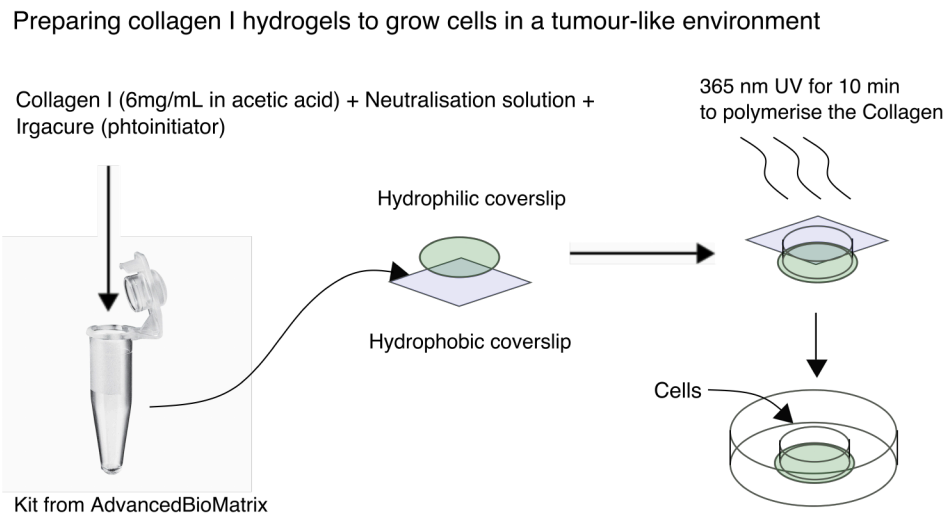

Figure 3.3 Illustration of collagen I hydrogel substrate preparation used to pancreatic cancer cells culture in a condition mimicking collagenous microenvironment of cancer tissue.

The collagen (or collagen-hyaluronic) hydrogel substrates were prepared using the protocols described below.

3.2.3.1 Preparation of collagen I solution

A beaker filled with crushed ice was placed on the sterile bench to keep the acetic acid (AdvancedBioMatrix) and lyophilised collagen I (PhotoCol®, AdvancedBioMatrix) at 4°C. The lyophilised collagen I was weighed into a sterile and chilled glass bottle. Based on the weight of the Collagen I, the appropriate amount of acetic acid was calculated to obtain the right concentration of the Collagen I solution. The concentration of Collagen I for pure collagen gel was 7 mg/mL and for hybrid gels it was 6 mg/mL. The collagen I solution was immediately transferred to a shaker at 4°C to mix overnight at medium speed. The solution can be stored at 4°C for up to 2 months.

3.2.3.2 Preparation of hyaluronic solution

A beaker filled with crushed ice was placed in the sterile bench to keep raw medium and lyophilised hyaluronic acid (PhotoHA®, AdvancedBioMatrix) at 4°C. The lyophilised hyaluronic acid was weighed into a sterile and chilled glass bottle. Based on the weight of the hyaluronic acid, the requisite amount of raw medium required was calculated and added to prepare a 2% w/v volume solution. Transfer the hyaluronic acid solution immediately to a shaker at 4°C and mix for 1 h at medium speed. The solution can be stored at 4°C for up to 1 month.

3.2.3.3 Preparation of Irgacure solution

The Irgacure powder was weighed out to a glass bottle, and the requisite amount of MeOH was added to prepare 10% w/v solution. The solution can be stored at 4°C for up to 2 weeks.

3.2.3.4 Preparation of collagen I gel

All coverslips were placed in the sterile chamber. Up to 4 hydrophobic coverslips were placed on the lid of a 90 mm petri dish. The items placed on ice were Eppendorf tube, 7 mg/mL collagen I solution, Irgacure solution (IRG), and Neutralisation solution (NS). The requisite amount of each solution was added to the Eppendorf tube based on the amounts given in Table 3.2.

Table 3.2 Composition of Collagen I hydrogel solution for preparing 2 hydrogels.

Concentration of Collagen I stock solution (mg/mL)	Volume of Col I (μL)	Volume of Col I (μL)	Volume of NS (μL)
6	180	9	15.3
7	180	9	14.8

Shortly, 90 μL of collagen I per gel was mixed, but 70 μL was distributed to each hydrophobic coverslip. The hydrophilic coverslip was gently placed on top of the gel droplet. The gels were placed in the incubator at 37°C for 30 minutes to ensure that collagen formed a gel. If not, gels were placed back in the incubator for 10 additional minutes. A strip of parafilm was placed on the UV stand, and the gels were placed hydrophilic-coverslip-side down on the parafilm. The stand with gels was placed under the UV for 10 minutes. After UV polymerisation, the gels were placed in the petri dish again. 200 – 500 μL of PBS was added to each gel to facilitate the release of the hydrophobic coverslip. The hydrophobic coverslip was pulled out with tweezers. The coverslip with the gel was glued to the petri dish with bio-friendly glue for 10 minutes before adding a complete medium.

3.2.3.5 Preparation of hyaluronic acid – collagen I hybrid gel

All coverslips were placed in the sterile chamber. Up to 4 hydrophobic coverslips were placed on the lid of a 90 mm petri dish. The Eppendorf tube, hyaluronic acid solution, 6 mg/mL collagen I solution and IRG solution were placed on ice. The requisite amount of each solution was added to the Eppendorf tube, based on the amounts given in Table 3.3, to form the hybrid gel solution.

Table 3.3 Composition of Hyaluronic acid - Collagen I hybrid hydrogel solution for forming 2 gels

Concentration of hyaluronic acid stock solution (% w/v)	Volume of HA (µL)	Concentration of Collagen I stock solution (mg/mL)	Volume of NS (µL)	Volume of Col I (µL)	Volume of IRG (µL
2%	144	6	1.3	16	8

Briefly, 80 µL of the hybrid gel solution per gel was mixed, but 70 µL was distributed to each hydrophobic coverslip. The hydrophilic coverslip was gently placed on top of the gel droplet. The gels were placed in the incubator at 37°C for 30 minutes to ensure the collagen formed a gel. If not, gels were placed back in the incubator for 10 additional minutes. A strip of parafilm was placed on the UV stand, and the gels were placed hydrophilic-coverslip-side down on the parafilm. The stand with gels was placed under the UV for 10 minutes. After UV polymerisation, the gels were placed in the petri dish again. 200 – 500 µL of PBS was added to each gel to facilitate the release of the hydrophobic coverslip. The hydrophobic coverslip was pulled out with tweezers. The coverslip with the gel was glued to the petri dish with bio-friendly glue for 10 minutes before adding a complete medium.

3.3 Atomic force microscopy (AFM)

3.3.1 Principles of AFM

A typical AFM setup comprises several key components, including a microfabricated cantilever, often integrated with a tip, a *xy*-piezo scanner to position the sample, and the AFM head. The AFM head consists of a laser, a position-sensitive photodiode to measure the cantilever's deflection, and a z piezo-scanner to position the cantilever. The cantilever, functioning as a spring, makes contact with the sample, and its deflection (d) is measured using the optical lever scheme. A laser beam is directed onto the gold reflective coating on the back of the cantilever, and the reflected beam is detected by a split photodiode. The difference in photocurrents between the photodiode segments indicates the deflection of the cantilever. The z piezoceramic transducer performs precise movement and control of the cantilever, and this measured quantity is called the z-height (z). The sample is moved precisely using the xy piezoceramic transducer to position on a pre-set *xy* grid (usually square).

During mechanical measurements of cells, the tip gradually approaches and indents the sample until it reaches a predefined maximum loading force (usually defined in terms of (cantilever deflection). Subsequently, the tip is retracted from the sample, returning to its original position above the surface. Throughout the approach and retraction processes, the deflection of the cantilever is recorded and displayed as a force curve plotting the cantilever deflection as a function of the z height of the cantilever.

The two measured variables are the deflection of the cantilever (d) and its accurate z-position or z-height (z). The z-position is controlled accurately by the z-piezoelectric ceramic that drives the vertical movement of the cantilever. A Linear Variable Differential Transformer sensor measures the z-position. This variable does not need to be calibrated for every experiment. However, the deflection signal from the photodiode varies from cantilever to cantilever, the positioning of the laser, and the medium of measurement, hence it must be calibrated for every experiment. This is essentially a calibration of the cantilever in use.

When the cantilever comes in contact with the sample, the sample physically deflects the cantilever. The distance by which the cantilever is deflected is referred to as the cantilever deflection or simply the deflection (d). The system does not measure the cantilever deflection directly; it rather measures the bending of the cantilever caused by its deflection. At the beginning of an experiment, the laser position is adjusted such that it is reflected to the centre of the split photodiode, and the difference of the photocurrent between the two

segments is reasonably close to 0. When the cantilever is physically deflected by the sample, the reflected laser position changes, and we see a difference in voltage between the segments of the photodiode. This voltage difference between the photodiode segments is related to the cantilever deflection by the optical lever sensitivity (*OLS*). The OLS has to be calibrated in every experiment.

By applying Hooke's law, the force exerted by the cantilever on the sample can be calculated. The cantilever displacement in the form of deflection can be measured as described above. We also need to know the spring constant of the cantilever. The spring constant of the cantilever can be found by three methods. The first is where the manufacturer uses a vibrometer to calibrate the cantilever and measure its spring constant. A cantilever whose spring constant is measured by the manufacturer using a vibrometer, is often expensive. PFQNM-LC-A-CAL cantilevers were purchased pre-calibrated for microrheology experiments. A second technique is by calculating the spring constant of a lever using the following formula for the relation between the dimensions of the cantilever, its elastic modulus, and its spring constant. The following relation describes the spring constant for a rectangular cantilever [119]:

$$k = \frac{Ewt^3}{4L^3} \tag{1}$$

where k is the spring constant, E is the elastic (Young's) modulus, t is the thickness, w is the width, and L is the length of the cantilever. To use this formula, the dimensions of each cantilever used in the experiments must be measured accurately since the spring constant is heavily dependent on the thickness and length of the cantilever. Nevertheless, equation (1) may be reasonably used to estimate the spring constant of cantilevers known to be from the same chip during the manufacturing process and used in the same set of experiments. Similarly, equations can be used to calculate the spring constant of triangular cantilevers [120].

A third technique is the thermal fluctuations method. Water molecules in the measurement medium continuously collide with the cantilever surface, giving rise to small but random fluctuations of the cantilever bending. By applying Boltzmann's equipartition theorem, the energy of these fluctuations in the vertical direction can be written as follows:

$$< E > = \frac{1}{2} k_B T \tag{2}$$

where <*E*> is the mean energy per degree of freedom, k_b is the Boltzmann's constant, and T is the temperature of the system in Kelvin. Cantilever thermal fluctuations can be recorded using the cantilever deflection and then converted to a power spectrum shown in Fig. 3.4 for NP-OW-D tipless cantilevers. Thus, the mean square displacement $< d^2 >$ can be measured.

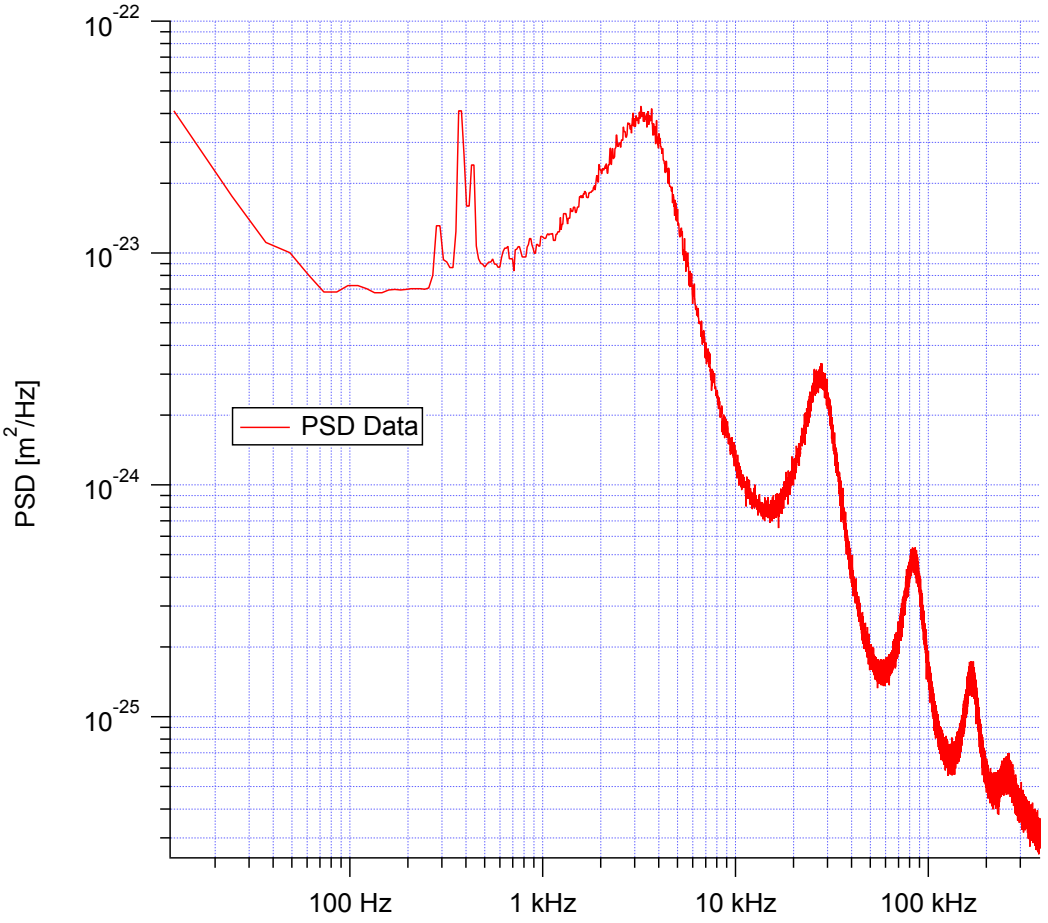

Figure 3.4 Raw power spectrum density of cantilever NP-OW-D showing multiple peaks corresponding to the various resonance modes that the cantilever can engage in. The energy of oscillation of each mode is the same, following Boltzmann's equipartition theorem. However, the measurement of the first peak (corresponds to oscillation in the direction of AFM indentation) is the most accurate.

An AFM cantilever has several vibration modes, each corresponding to different spring constants and effective masses (due to the distribution of mass along the cantilever). A typical power spectrum has multiple peaks corresponding to the different resonance modes that the cantilever can engage in. Boltzmann's equipartition theorem can be rephrased such that the mean square displacement of each mode will have the appropriate thermal energy.

$$\frac{1}{2} k_B T = \frac{1}{2} k_c < d^2 > \quad (3)$$

The thermal energy of fluctuations is equal to the energy of the cantilever motion in the vertical direction, which occurs in the. Thus, we obtain an equation for calculating the spring constant.

$$k_c = \frac{k_B T}{<d^2>} \tag{4}$$

Inversely, if we know the spring constant of a cantilever, we can readjust (recalibrate) the deflection signal such that the thermal (Fig. 3.5) reproduces the same known force constant. Thus, we can calibrate the OLS. Cantilever manufacturers can provide pre-calibrated cantilevers with a known spring constant. The spring constant, in this case, is pre-calibrated by the manufacturers using a vibrometer.

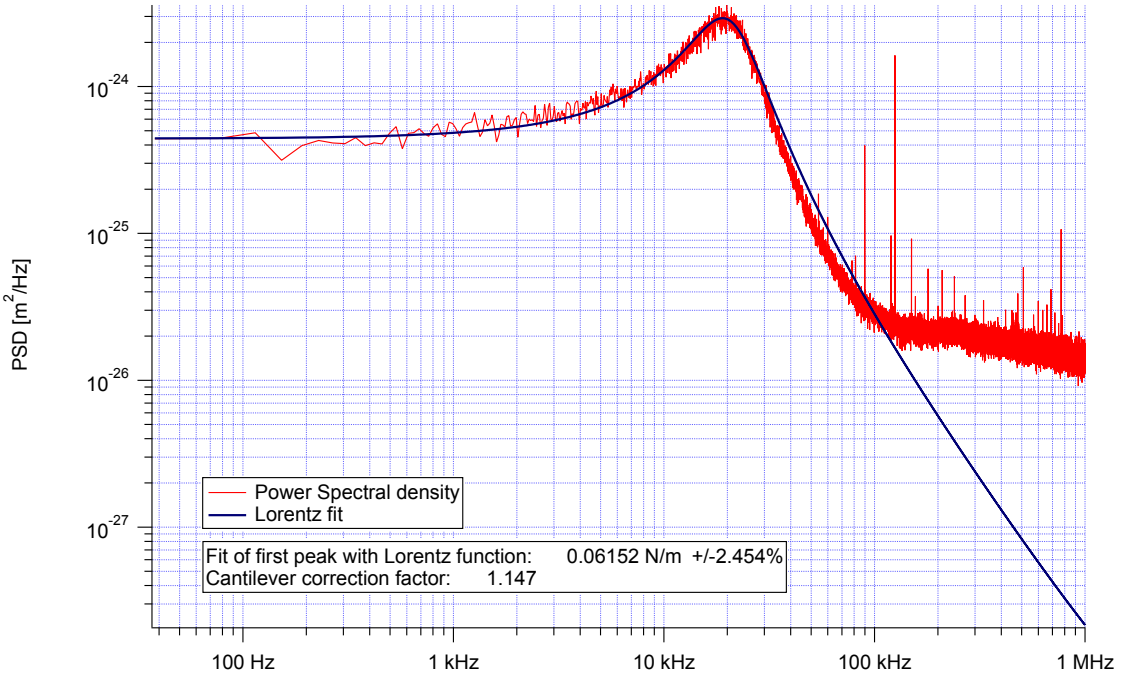

Figure 3.5 Power spectrum density of PFQNM-LC-A-CAL cantilever with Lorentz function fit to obtain the PSD at peak frequency of the first peak.

The OLS can also be calibrated by applying force against a sample whose stiffness is known to be much larger than that of the cantilever. In this case, glass or plastic substrate is the ideal choice. The cantilever deflection is exactly the same as the z-piezo movement when a cantilever presses against a stiff substrate. Thus, the voltage difference in the photodiode segments corresponds to the measured z-piezo movement, and the ratio of the two is the OLS. Once

the OLS is measured and calculated, the photodiode output can be directly observed as the cantilever deflection or simply deflection.

3.3.2 Principles of AFM for measuring cell stiffness and microrheology

After calibrating the OLS and cantilever spring constant, AFM mechanical measurements in contact mode are possible. Benefitting from the OLS calibration, the cantilever deflection is now measured in units of the actual distance by which the cantilever is deflected (Figure 3.6).

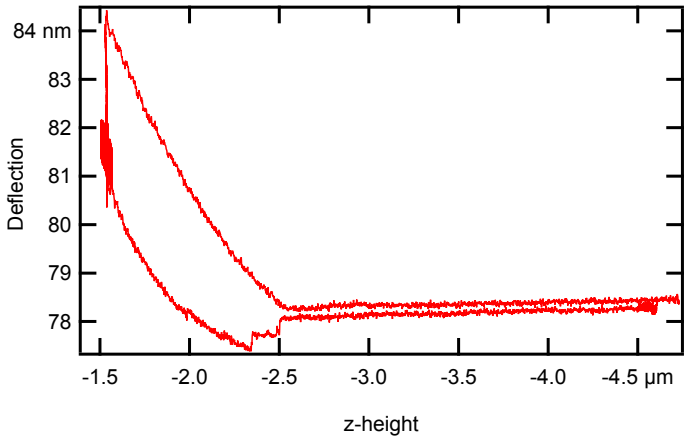

Figure 3.6 Force curve captured using PFQNM-LC-A-CAL cantilever on a single PANC-1 cell.

A sweep methodology force curve (Fig. 3.7) is used to measure the rheological properties of cells. The cantilever approaches the cell till the set-point is reached. Here, the cantilever dwells for a duration of 8.7 s. For the first 0.5 s, the cantilever holds a constant z-height, and the cell undergoes a creep to stabilise at a certain deflection. Then, the cantilever is oscillated at 51 frequencies, which are logarithmically increasing from 1Hz to 1000Hz. One wave per frequency is employed. The phase difference between the z-height and deflection for each frequency is the phase difference θ between the stress and strain response.

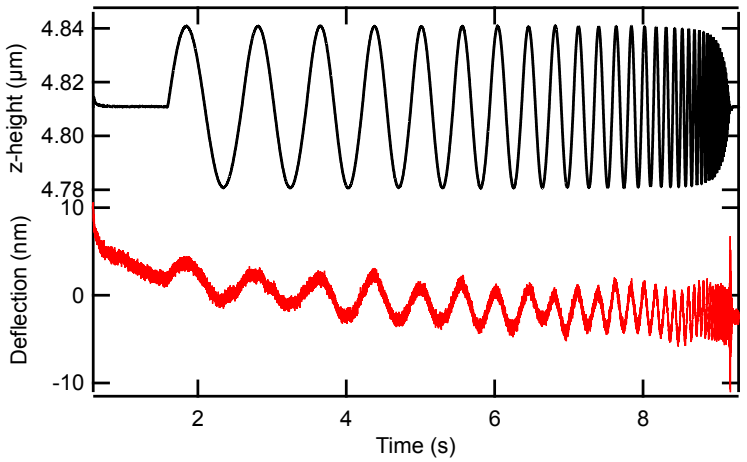

Fig. 3.7 The z-piezo movement (black) and cantilever deflection (red) in the contact part of a multi-frequency sweep methodology force curve.

As the cantilever probes the sample, the start and end z-position of the cantilever changes because of the topography of the sample. This introduces a deflection offset (d_0) and z-height offset (z_0) for each force curve. The deflection offset is the baseline deflection recorded at in the non-contact part of the force curve. To obtain the true deflection of the cantilever, this is subtracted from the raw deflection signal during contact. The final force exerted by the cantilever is calculated as follows:

$$F = k(d - d_0) \tag{5}$$

The z-height values have to reflect the relative position of the cantilever tip with respect to the sample. The z-height offset, commonly referred to as the contact point, is the z-height in the force curve where the cantilever tip makes contact with the sample. At the contact point, the value of the z-height should be set to 0 µm [121]. Thus, the contact point offset is subtracted from the raw z-height, before using it to calculate the cantilever indentation (δ) into the sample. The distance up to which the cantilever is able to penetrate the sample is referred to as the indentation. A sample, which is significantly stiffer than the cantilever, will not be deformed and indented. However, a soft sample can be deformed and indented into by a cantilever of similar stiffness at low forces. This is the deformation that can be modelled to find the mechanical properties of the sample. The indentation can be calculated as follows:

$$\delta = (z - z_0) - (d - d_0) \tag{6}$$

The non-contact part of a force curve is not directly relevant to the derivation of mechanical properties. However, it often has some features that are relevant for data processing. The deflection should be close to 0 V. However, often two

features are observed. First, there is always a slight offset in deflection, and this is never 0 V at the beginning of the measurement. This is because the location where the laser spot hits the photodetector tends to drift during the course of a measurement. Second, a small slope might appear in the entire. This might be because the large-scale z-scanners face a slight distortion during the cantilever approach. Fitting the non-contact region to a straight line and using the predicted deflection values to correct the curve can correct these issues.

To determine the mechanical properties, the deflection (in nm) and z-height signal collected from the AFM (Figure 3.8(left)) are converted to the force applied (F) by the cantilever tip and indentation (δ) into the sample (Figure 3.8(right)) using eq. (5) and (6), because these quantities can be used in the Hertz model, which describes the contact between a semi-infinite half-space and a spherical object [105].

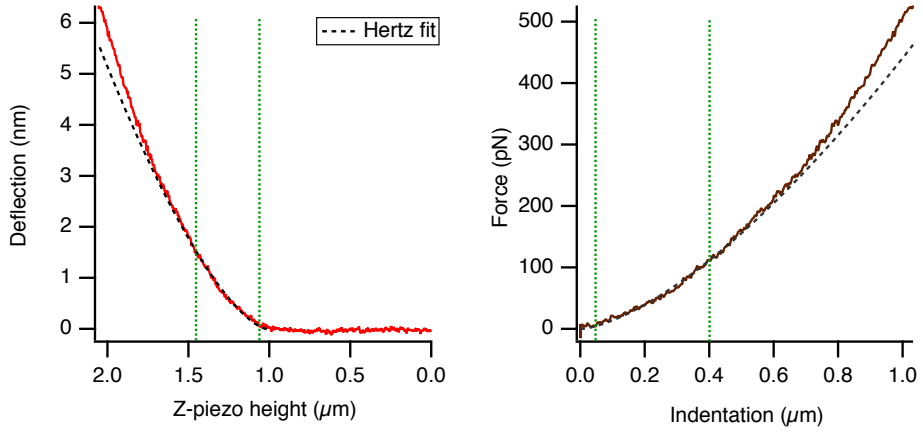

Figure 3.8 Hertz fit along the chosen deflection (left) and indentation (right)

The cantilever used to measure the mechanical properties of cells was a 3-sided pyramidal tip with a spike at the end. The spike can be modelled as a paraboloid with an end radius of 70 nm [103]. Cell mechanics is described by Young's (elastic) modulus, which is calculated from the Hertz model as follows:

$$F = \frac{4}{3}\frac{E}{(1-\nu^2)}\sqrt{R}\,\delta^{3/2} \tag{7}$$

where F is the loading force, E is Young's modulus, R is the radius of tip, ν the Poisson's ratio of the sample, and δ the indentation. The Poisson's ratio of cells is generally assumed to be 0.5 because a large fraction of the cells is incompressible water. The Young's modulus, however, does not fully describe the mechanical properties of cells, which are viscoelastic materials. Thus, the property calculated using the Hertz model is henceforth referred to as the Apparent Young's modulus, and a complex modulus E^* that describes the

elastic and viscous response of cells more accurately can be used to describe the rheological properties of cells:

$$E^* = E' + iE'' \tag{8}$$

where i is the imaginary unit, E' is the elastic modulus or storage modulus, and E'' is the viscous or loss modulus. The loss and the storage moduli are a function of frequency, and in the simplest case, power law behaviour is observed. The tangent of the phase difference θ between the stress and strain response, also known as the loss tangent, and can be defined as:

$$\tan\theta = \frac{E''}{E'} \tag{9}$$

However, in the case of these measurements, the cantilever experiences prominent hydrodynamic drag beyond 10 Hz. The hydrodynamic drag occurring because of the cantilever's geometry and movement is corrected (Appendix A). Power-law behaviour of complex elastic modulus over frequency was expected and observed. By using the structural damping model for calculating rheological properties, the power-law of the loss modulus is assumed to be the same as that of the storage modulus, which was shown to be able to describe cell micro-rheological properties [81].

$$E^*_{(\omega)} = E_0(1 + i\eta)\left(\frac{\omega}{\omega_0}\right)^{\alpha} + \mathrm{I}\,\mu\,\frac{\omega}{\omega_0} \tag{10}$$

where E_0 is the absolute value of the modulus, i is the imaginary unit, η is the loss tangent, ω_0 is the frequency scale (in our case, we use 1 Hz) α is the power law exponent of the sample, and μ is the strength of the hydrodynamic damping, which will depend on the shape of the cantilever and the viscosity of the medium. The real part of eq. (10) represents the storage modulus, and the imaginary part corresponds to the apparent loss modulus, which has two contributions: one from the sample, which scales with the same power law exponent as the storage modulus, and the hydrodynamics, which is directly proportional to the frequency. Thus, we can first obtain the power law exponent α by fitting the storage modulus as a function of frequency and then, in a second step, obtain the loss tangent η AFM set-up and the hydrodynamic damping coefficient μ.

3.3.3 Measuring cell stiffness and microrheology

3.3.3.1 AFM set-up

Microrheology experiments were conducted with an MFP3D AFM (Asylum Research, Santa Barbara, USA). The AFM head was mounted on an inverted optical microscope Axiovert 135 (Zeiss Oberkochen). The sample was mounted on the stage of the microscope, which was also used to position the sample correctly. The AFM head, sample, and stage were enclosed in a homebuilt polymethacrylate box. This was injected with 5% CO_2 when the experiment called for it.

3.3.3.2 Cantilever

The Apparent Young's modulus of cells was measured using PFQNM-LC-A-CAL cantilevers with an integrated tip (Bruker, Santa Barbara, USA). The cantilever is rectangular, 54 μm long (Figure 3.9).

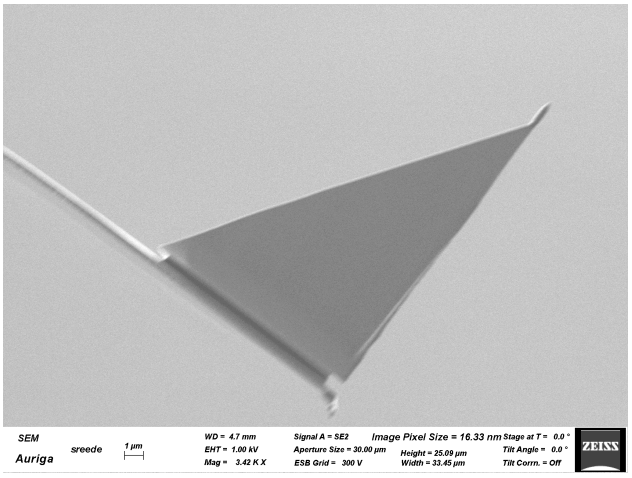

Figure 3.9 Image of PFQNM-LC-A-CAL cantilever captured using a Scanning Electron Microscope

It has a pre-calibrated stiffness in the range of 75 – 85 pN/nm and a nominal resonance frequency of 45 kHz in air. The tip is a 3-sided pyramid with an end radius of 70 nm and a height of 17 μm. The spring constant of this cantilever is relatively low, and hence makes it suitable for measuring soft samples such as cells and hydrogels. Since the cantilever's spring constant is pre-calibrated, the known value of the spring constant is used to calibrate the deflection sensitivity of the system, as described below.

3.3.3.3 *Cantilever calibration*

The cantilever is mounted on the holder and then onto the AFM head. The cantilever is calibrated to obtain the Optical Lever Sensitivity.

The sample is then placed in the sample holder. The trigger point of the force curve is calculated in nm as deflection (*d)* from the spring constant (*k*) and desired trigger force *(f):*

$$d = \frac{f}{k} \tag{11}$$

3.3.3.4 *Mapping the elastic or rheological properties of cells*

The various mapping parameters are set for each experiment. Experiments have macros that can automatically set-up the mapping parameters. They are described below for each experiment. Approach the central region (above the nucleus) of a suitable cell. For experiments on single cells, a suitable cell is one, which does not have any neighbouring cells or connections to other cells via filopodia or protrusions. For experiments on layers of cells, the cell must be completely surrounded by and connected to other cells, and those cells must be in turn also fully surrounded. An optical image of each cell is captured. The approach set-point is always 0.5 V and the z-distance is in the range of 0.5 μm – 5 μm. The force curve capture frequency is adjusted to maintain the ramp speed in the range of 6 – 8 μm/s. The gird size for all experiments is 5 μm x 5 μm.

Parameters for capturing force maps of cells with different trigger force:

- No. of curves in the grid – 8 x 8
- Trigger forces used (in nN) – 0.5, 1.0, 2.5 and 5.0.

Parameters for capturing force maps of cells that measure only the Young's modulus:

- No. of curves in the grid – 6 x 6 or 12 x 12
- Trigger force (nN) – 0.5

Parameters for capturing force maps of cells to measure rheological properties using sweep frequency methodology:

- No. of curves in the grid – 4 x 4
- Trigger force (nN) – 0.5
- Parameters of the multi-frequency oscillation are shown in Table 3.4

Table 3.4 shows the parameters used to generate multi-frequency oscillations in the dwell region of force curves using the sweep frequency methodology.

Dwell 1	Z -Step amplitude	Oscillation range	No. of frequencies
8.7 s	30 nm	1-1000 Hz	51

3.3.4 Principles of measuring cell-cell interaction

The atomic force microscope is a powerful tool for measuring forces. With piconewton force-resolution, this is a good tool to measure interaction forces between cells (Figure 3.10). A cantilever without an integrated tip is chemically functionalised, so biological material can be attached. A cell is attached to the cantilever to make a cell-cantilever. The cell acts as the tip of the cantilever and makes it possible to measure the adhesion between the cell on the cantilever and a sample of cells mounted on the stage. The approach and dwell part of the force curve can be used to extract information about cell stiffness and viscoelasticity. The retract curve usually has information about the adhesion between the cantilever tip and the sample. Cell-cell interaction can be measured if we replace the cantilever tip with a cell.

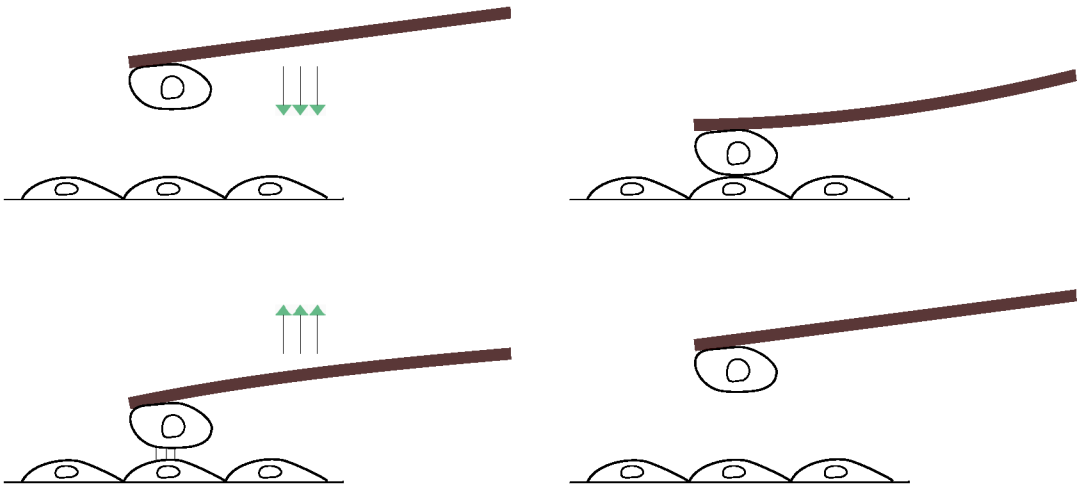

Figure 3.10 Schematic of cell-cell interaction experiment

During a cell-cell interaction experiment, the cell-cantilever comes in contact with the sample after approaching it, as is described later in section 3.3.5. After indenting into the sample up to a fixed trigger force, it dwells for a pre-determined duration of time, usually in the order of seconds. During the dwell,

the two cells form both specific and non-specific adhesions. Specific adhesions might be between particular cell-cell interaction proteins like cadherins, among others. Non-specific interactions include electrostatic or non-covalent interactions and other weak molecular interactions. Then, the cell cantilever is retracted. During the retraction, all adhesions are broken. Since the formation of adhesions requires some work, this is released when the adhesions are broken. As specific adhesions are broken in clumps, the bond rupture force suddenly causes the cantilever to bend. This can be observed as jumps or rupture events in the retracting part of the force curve. The first-order derivative of a retract curve will be 0 if the curve is flat. However, the retract curve of a cell-cell interaction experiment has several rupture events in the deflection. Thus, calculating the first-order derivative can filter rupture events and give the value of the force required to cause the rupture. This is usually the force of the rupture event between cell-cell adhesion molecules. Following Hooke's law, the product of the spring constant and the deflection gives the rupture force. The total work done to detach the two cells can be calculated by finding the area under the retract curve. The area is calculated from the point of the lowest deflection in the retract curve.

Further data analysis was performed with custom-built software in Igor Pro 9 (Wavemetrics, Portland, USA). Each force curve captured with AFM has 2 segments, approach (Fig.3.11, grey line) and retract (Fig.3.11, blue line). The cell probe is approached to the substrate and makes contact, and after applying 0.5 nN force, it retracts. The cell probe is retracted from the substrate by the z-piezo movement. However, because of the connections between the cell probe and substrate, the cell probe resists retraction and produces a deflection (d) of the laser on the photodiode. Since the force (f) exerted by the cell-substrate contact causes the deflection (d), it can be calculated as follows:

$$f = d \times k_c \tag{12}$$

where k_c is the spring constant of the cantilever. The cell-cantilever is deflected till the force is large enough to start breaking the connection between the cell probe and the substrate. While this is observed as the minimum deflection value of the force curve, it is, in fact, the total adhesion force. The area under the force curve, starting from this point till the cell probe retracts completely, can be integrated to obtain the total work of adhesion between the cell probe and the substrate. Detachment events can be observed on the force curve during the retract step. Receptors on the cell probe that were binding with substrate molecules, detach in step-wise events called ruptures. Substrate-receptor complex bends the cell probe by exerting a rupture force, until the complex breaks. This is observed in the force curve by a sharp change in deflection,

which is above a set threshold. The number of rupture events signifies the adhesion scale between the cell probe and the substrate. The force of binding and nature of binding between the cell probe and substrate can cause the membrane to be folded outward and pulled out as tethers at a steady force, till the tether breaks off from the substrate in a rupture event. This is observed in the force curve by a plateau of constant deflection between two rupture events. As the cell probe detaches completely from the substrate, the deflection in the retract curve reaches a constant value close to the deflection during the approach. The z-piezo distance covered from the point of minimum deflection to the point where there are no more detachment events is the total length of adhesion.

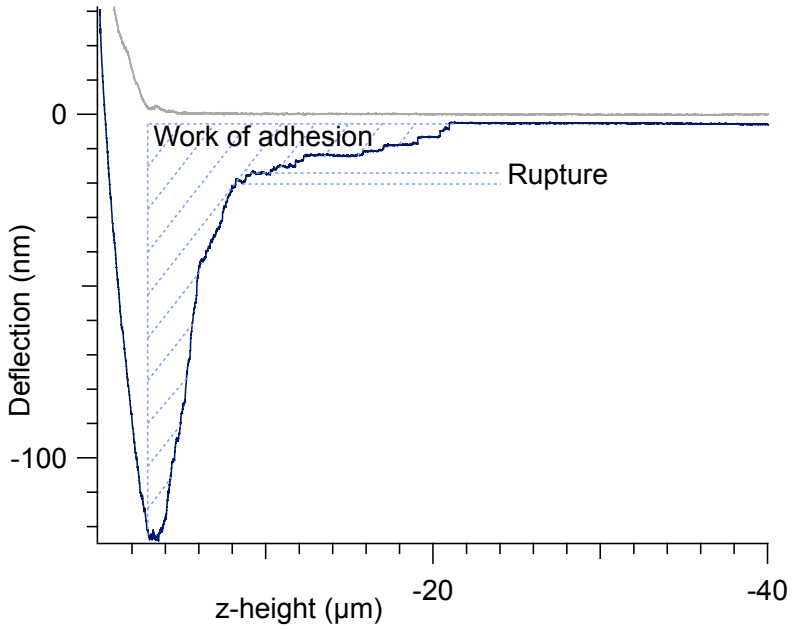

Figure 3.12 Force curve of cell-cell interaction between PANC-1 cell-cantilever and PANC-1 layer, with approach in grey and retract in blue.

3.3.5 Measuring cell-cell interaction

3.3.5.1 AFM set-up

Cell-cell interaction experiments were conducted with a CellHesion AFM (Bruker – JPK instruments). The AFM head was mounted on an inverted optical microscope IX71 (Olympus). The sample was mounted on the stage of the microscope, which was also used to position the sample correctly.

3.3.5.2 *Functionalization of cantilevers*

To measure cell-cell interactions using an atomic force microscope, we need to chemically functionalise the cantilever, so that cells can adhere to it. The cantilever was functionalised in a series of steps. It was first activated with UV treatment, then incubated with glutaraldehyde and APTES to form a hydrophobic polymeric mesh that can covalently bind to biomolecules. In the final step, the cantilever was incubated with a suitable protein (Table 3.5), which has receptors on the cell surface and can make them adhere strongly to the cantilever. The attachment has to be strong enough to last the measurement time of 35 - 45 min.

Table 3.5. shows the appropriate protein that could capture a cell onto the cantilever.

Cell line	Protein used for cantilever functionalization
PANC-1	Concanavalin-A (MP Biomedical) - a plant lectin that binds to mannose residues on glycoproteins
Hs 766T	Maackia Amurensis Lectin I or MAL I (Vector) – a plant lectin that binds to galactose (β-1,4) glcNAc residues on cell membrane glycoproteins
CFPAC-1	Fibronectin (Sigma) – Human ECM protein that binds to integrins
Ea.hy926	Concanavalin-A (MP Biomedical) - a plant lectin that binds to mannose residues on cell membrane glycoproteins

The functionalization protocol is based on a protocol provided by Dr. Joanna Zemla, IFJPAN, Krakow. First, the following solutions were prepared:

- 1% glutaraldehyde in PBS – store at 4° C
- 2 mg/mL Concanavalin A solution in PBS – prepare 200 μL aliquots and store at -20° C. Do not re-freeze after first use.
- 2 mg/mL MAL-1 solution in PBS – prepare 200 μL aliquots and store at -20° C. Do not re-freeze after first use.
- 0.5 mg/mL human Fibronectin solution in PBS – stable at 4° C for at least 2 weeks

Before functionalization, cantilevers were cleaned using plasma cleaner (oxygen open valve plasma with 0.5 mBar pressure for 40 s or with 0.5 mBar pressure for 60 s) or UV ozone cleaner (the exposure to UV for 5 minutes). I will check what we have). Afterward, cantilevers were functionalized using the following protocol:

- Add 1 mL (30 mm) or 5 mL (60 mm) of (3-Aminopropyl)triethoxysilane (APTES, Sigma) to a glass petri dish.
- Stretch and place parafilm on the Petri dish.

- Place cantilevers on the parafilm.
- Place the Petri dish in the desiccator under vacuum for 2 h.
- Place cantilevers directly in a glass Petri dish filled with 1% Glutaraldehyde in PBS, for 1 h.
- Rinse cantilevers by dipping in PBS for a few seconds.
- Stick a piece of parafilm on a 35 m plastic dish lid.
- Arrange 6 cantilevers on the lid, such that they are in a circle and the tips are facing inwards/each other.
- Place 200 μL of the protein solution to coat the tips completely.
- Incubate Concanavalin A and MAL-1 for 2 h at RT, and fibronectin for 1.5 h at 37°C 5% CO_2.
- Functionalised cantilevers can be stored at 4° C for up to 12 days.

3.3.5.3 Cantilever calibration

The cantilever was calibrated in the cell sample to which the cell suspension was not yet added. Since the cantilever is chemically functionalised and has a protein coating, it should be used within 5 min of removal from the fridge. Adjust the laser on the cantilever tip to obtain the maximum possible sum and deflection of close to 0 V. Contact-free calibration based on the Sader method was carried out. Attempts at contact-based calibration showed poor outcomes when catching a cell on the cantilever. Thus, the spring constant and deflection sensitivity of the cantilever were calibrated using the Sader method.

3.3.5.4 Catching a cell to make a cell-cantilever

Next, the cell suspension was added to a relatively cell-free region of the sample layer. A cell with the following features should be identified: rounded, bright, displays significant Brownian motion, and, preferably over plastic and not over a cluster of cells. Approach the cell to try and have it under the tip of the cantilever. Set approach target height to 90 um and approach set point to 1 nN. Approach the cantilever over the cell and remain in contact for 10 min.

Here, the following steps were applied (Fig. 3.12):

1) Lower head to bring it within 50 μm of the surface

2) Withdraw by 20-30 um in steps of 10 um, and move the stage a bit to ensure that the cell is adhered to the cantilever. Then, leave in this manner for 10-20 min for further attachment. The cell should attach at the same position on the cantilever for each experiment. Since the spring

constant of the cell-cantilever is calculated by the formula, which is heavily dependent on the length of the cantilever.

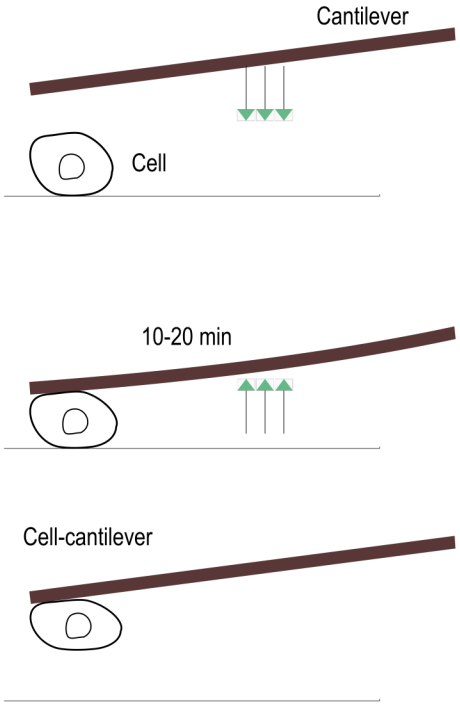

Figure 3.12 Schematic of cell capture using tipless AFM probe.

3.3.5.5 *Mapping the cell-cell interaction*

Enter force mapping mode, and set the scan size to 20 um and the grid size to 3 x 3. Identify a region of the cell layer with the following features. Looks about 35 μm in size, all cells in that area are completely surrounded by other cells, and there are no floating objects in the visible field. At 50 μm from the surface, place the cantilever-cell tip (CCT) over the selected area. Approach and start force map. A single force curve was recorded on each pixel of the map. An exemplary force curve recorded for the interaction between a PANC-1 cell and PANC-1 monolayers is shown in Figure 3.11. A large adhesion force characterized the PANC-1 – PANC-1 interaction, followed by rupture events.

3.3.6 Statistical tests

The difference between the mechanical parameters obtained for each comparison of the experimental groups was determined with the Wilcoxon signed-rank test and Cohen's d test using IGOR 9. For each force volume, the median of the force volume was calculated. The effect size (Cohen's *d*) between the log of medians of the parameter was calculated, and the significance of difference (Wilcoxon signed-rank) between the medians of the medians of the parameters was calculated. For *p*-values obtained from the Wilcoxon signed-rank test, ** and *** indicate statistically significant differences for $p < 0.001$ and $p < 0.0001$, respectively. For d values from Cohen's test, ## indicates a high effect size ($d>0.8$) and # indicates a medium effect size ($0.8>d>0.5$).

Chapter 4 - Effect of AFM measurement conditions on cell mechanics: CO_2 and loading force

All cells require optimum pH, CO_2, O_2, concentration, and pressure to perform their regular activity. Since this might affect cell mechanics, in this chapter, I describe how CO_2 conditions and loading force affect cancer cell mechanics. As compared to cells measured under conditions with 5% CO_2, cells from the primary site (PANC-1 and PL45 cells) measured under conditions without 5% CO_2 are stiffer, while cells from the secondary site (Hs766T and CFPAC1 cells) measured under conditions without 5% CO_2 are softer. Long-term cell survival also depends on appropriate CO_2 conditions. Contrary to expectations, cells from all cell lines studied softened as the loading force increased.

Users generally apply a fixed loading force for each force curve to conduct contact-based measurements of mechanical properties. When comparing samples with different properties, in this case, comparing cancer cells originating from various sources, the applied loading force is kept fixed across samples. However, as the samples do not all have the same stiffness, they are not indented to the same extent at a fixed force. Thus, while force curves were performed with a set loading force in this work, the data was analysed within a fixed indentation range. The Hertz contact model was used to analyse the approach part of AFM force curves to calculate Young's modulus of the cells. Data in a fixed indentation range were analysed. An important exception to this was the set of experiments measuring the effect of leading rate on cell mechanics. Force curves were analysed within a fixed indentation range.

4.1 Cell survival depends on appropriate CO_2 conditions

As a first step, PDAC cells were observed with a light microscope over a period of 20 h. Figure 4.1 shows that all cell lines for which culture conditions were supplemented with 5% CO_2 moved in the petri dish over the observed period.

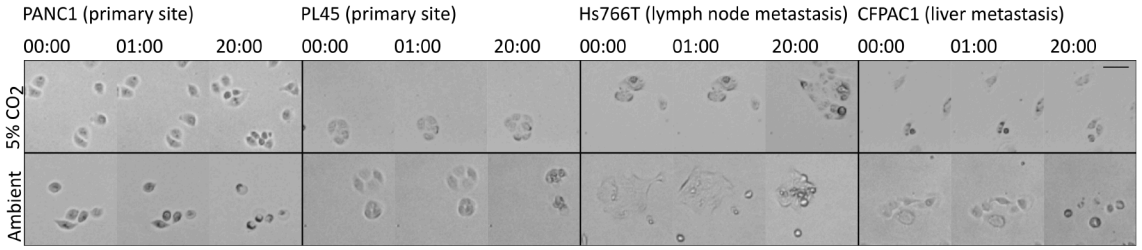

Fig. 4.1. Optical images of the studied pancreatic cancer cell lines (PANC-1, PL45, Hs766T, CFPAC1) collected between 0 to 20 hours during the culture with and without a 5% CO2 supplement show that cells do not survive in the long-term with 5% CO2 supplement.

PANC1, PL45, and Hs766t also multiplied over time. CFPAC1 cells did not multiply but maintained their shape and were highly motile. All cell lines without a 5% CO_2 supplement were motile and maintained shape during the initial observation period. However, as the cells approached hour 14:00, they began to round up, and by hour 20:00, all cells had rounded up and apparently died. No cell divisions were observed.

4.2 CO_2 has a varying effect on the mechanical properties of different cell types

Typically, AFM measurements on cells are carried out in the first few hours after taking the sample out of the incubator. Microscopy observations showed a reasonable time where cell morphology was similar for conditions with and without 5% CO_2 was 1.5 h. At the 1.5 h mark, cells observed using light microscopy as well as cells in AFM, were well-spread and showed normal morphology under studied culture conditions. Thus, after removing them from the incubator, cells were measured with AFM for up to 1.5 h. In the next steps, the mechanical properties were quantified. The comparison was obtained for the indentation range of 50 – 500 nm. The results are presented in Table 1 and Figure 4.2.

Mechanical properties of three out of four PDAC cell lines were sensitive to the presence or absence of 5% CO_2 in the AFM measurement conditions. Cells originating from cell lines established from the primary tumour site (PANC-1, PL45 cells) show similar relation, i.e., the apparent Young's modulus (E) of cells kept in conditions without 5% CO_2 is larger than the corresponding modulus value for cells kept in conditions with 5% CO_2 (Fig. 4.2A). Statistical tests Cohen's d and Wilcoxon- rank test confirm this. The metastatic cell lines (Hs766T and CFPAC1 cells) show the opposite effect; their E decreases when they are in conditions without CO_2. These results reveal cell softening or stiffening of cells in response to CO_2, indicating the importance of keeping the proper culture conditions during the AFM measurements.

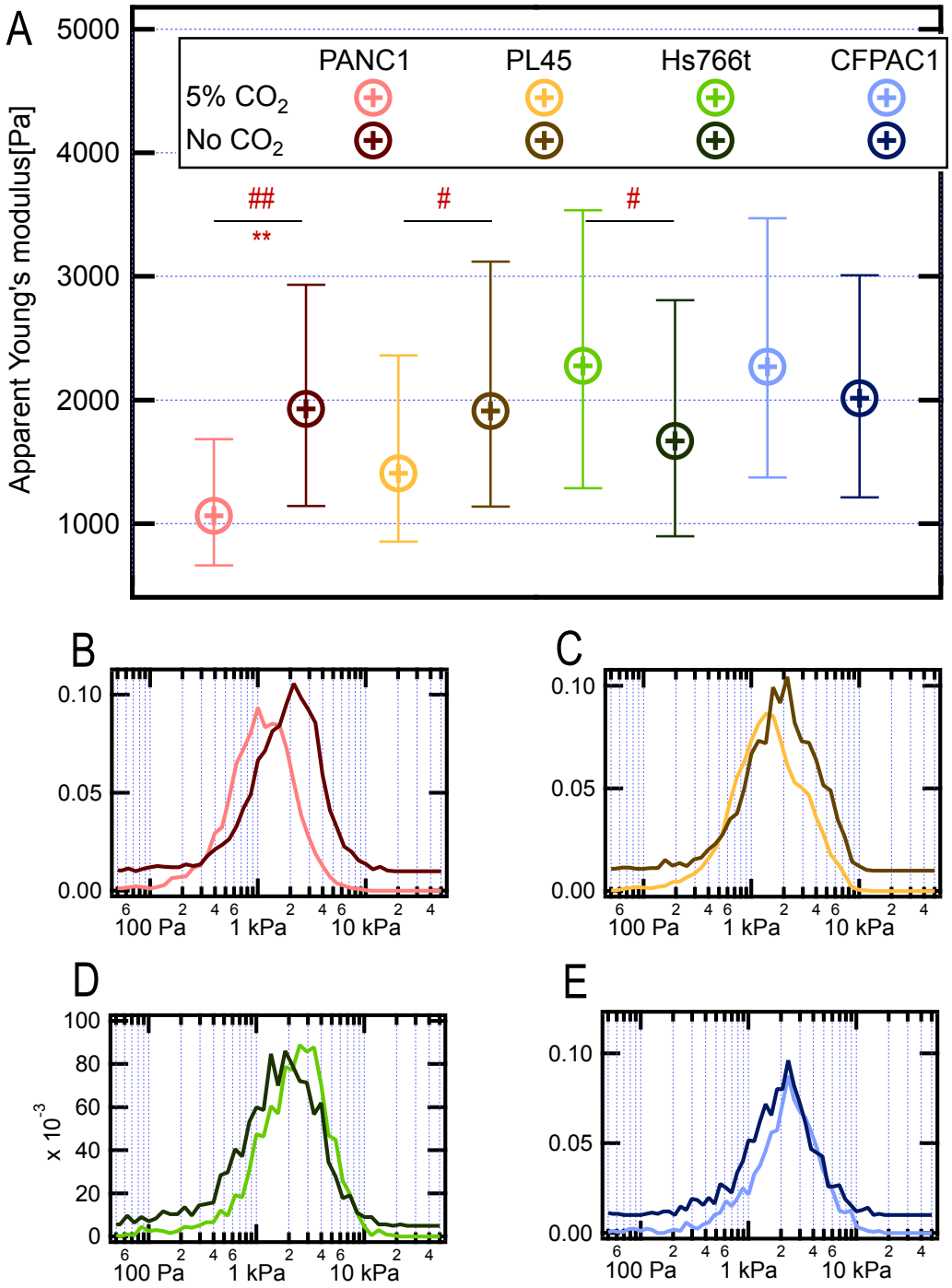

Fig. 4.2 The apparent Young's modulus (E) determined for four studied pancreatic cell lines originating from various stages of pancreatic cancer progression. PANC-1 and PL45 were collected from a primary tumour site, while Hs 766T and CFPAC1 were established from the secondary tumour site (a metastasis). A) shows a comparison of median ± interquartile region. (B-E) show the histogram distribution of the apparent Young's modulus for (B) PANC-1, (C) PL-45, (D) Hs 766T and (E) CFPAC-1.

Table 4.1. The median of the apparent Young's modulus obtained for pancreatic cancer cell lines from AFM measurements conducted with and without 5% CO_2.

Cell line	PANC-1	PL-45	Hs 766T	CFPAC-1
5% CO_2	1171 Pa	1409 Pa	2469 Pa	2243 Pa
No CO_2	2000 Pa	2005 Pa	1829 Pa	2024 Pa

The fluidity of the cells was quantified in parallel by determining the power law exponent (α). The power law exponent delivers a measure of the contributions from viscous and elastic components of the cell. The results, shown in Table 2 and Fig. 4.3, showed no change in the fluidity of cells kept during the AFM measurements with and without 5% CO_2. Only one exception is seen for PANC-1 cells. The power law exponent of PANC-1 without CO_2 is lesser, indicating it is more elastic in the absence of CO_2. Instead, the power law exponent was only dependent on the cell line. The power law exponent was the smallest for PANC-1 and CFPAC1 cells and the largest for Hs766T cells. This indicated that PANC-1 and CFPAC1 cells have larger elastic component, while in Hs766T cells, the viscous component dominated.

Table 4.2. The median of the power law exponent obtained for pancreatic cancer cell lines from AFM measurements conducted with and without 5% CO_2.

Cell lines	PANC-1	PL-45	Hs 766T	CFPAC-1
5% CO_2	0.126	0.128	0.143	0.117
No CO_2	0.113	0.126	0.140	0.101

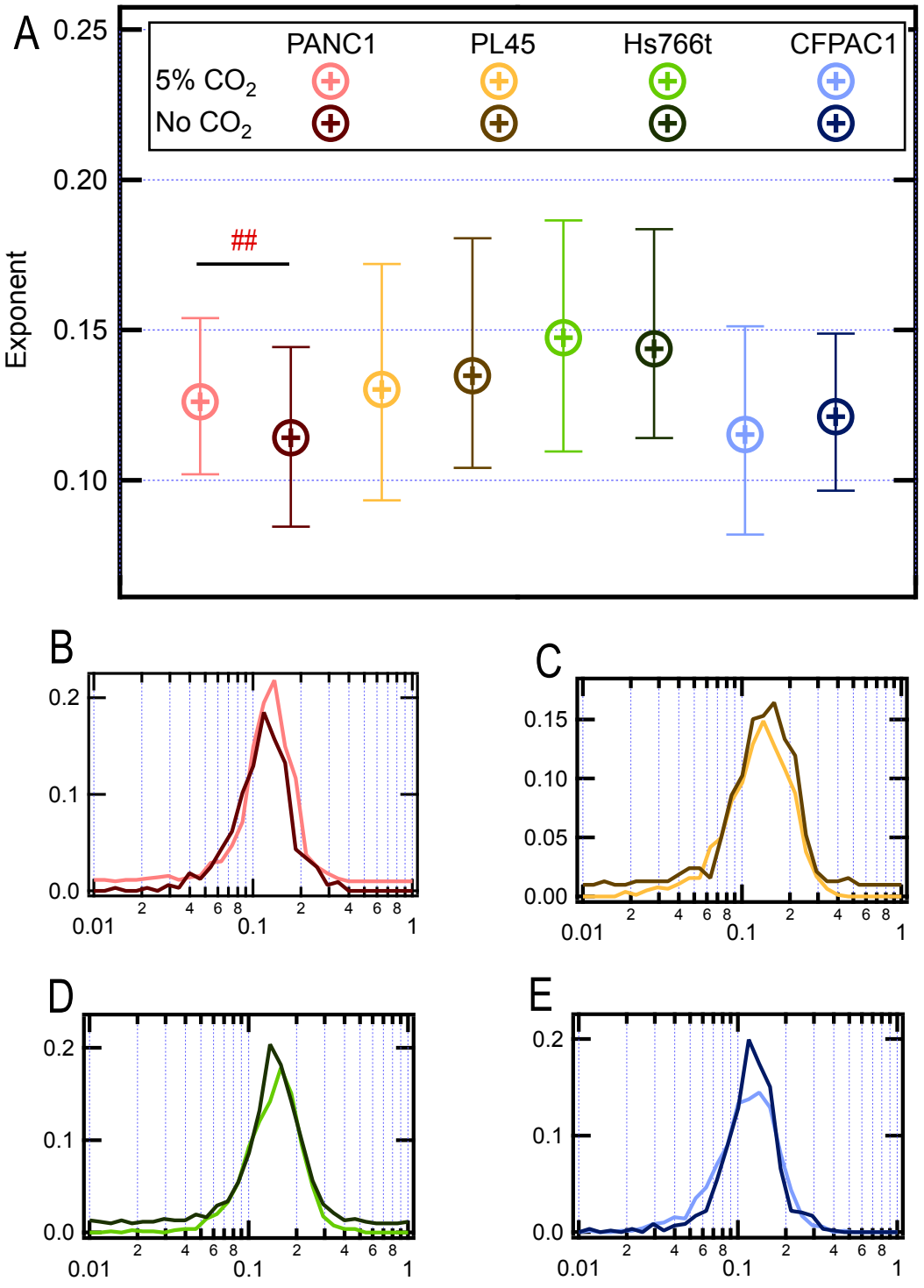

Fig. 4.3 The power law exponent (α) determined for four studied pancreatic cell lines originating from various stages of pancreatic cancer progression. A) shows a comparison of median ± interquartile region. (B-E) show the histogram distribution of the apparent Young's modulus for (B) PANC-1, (C) PL-45, (D) Hs 766T and (E) CFPAC-1.

The apparent Young's modulus shows a trend that the exponent does not follow. *E* represents the overall stiffness of a cell, which could be said to be related to the bulk of the cytoskeleton inside the cell. Since it largely depends on the amount of actin filaments rather than their organisation, the results indicate that metastatic site cell lines have a reduced cytoskeleton than that observed for cell lines collected from primary tumor sites when deprived of CO_2.

Several works aim to highlight the relative difference between healthy, benign and cancer cells [60], [61], [122], [123]. Cells and tissues are being studied extensively to use mechanical properties as markers of cancer [124], [125]. While several other physiological as well as measurement conditions have been shown to effect cell mechanics, this is the first instance of testing the effect of CO_2 conditions on cancer cell mechanics. Since the CO_2 concentration of the environment might not affect the cell mechanics of all cell lines in the same way, using cell mechanics to differentiate between normal and cancer cells becomes dependent on the measurement condition as well. Since AFM-based cell mechanics is a contact-based method, creating a CO_2 chamber for measurement is challenging. The chamber must enclose both the sample stage and the AFM head for the duration of the experiment. This work suggests that since cell lines being compared are differentially affected by CO_2 concentration, implementing systems to control CO_2 concentration in the surroundings of the sample during AFM measurements is important.

4.3 Loading force has a mild effect on cell mechanical properties

Force curves obtained on cells by using the AFM are usually analysed by selecting the data points in a range of force exerted on the cell. However, since most studies are carried out to determine if there is a difference in the stiffness of cells, analysing data in the same force range might introduce a bias. Stiffer cells will be indented to a lesser degree than softer cells. Thus, not all samples will be analysed for the same cell region. However, cell stiffness can depend on depth, indentation, and loading rate [100]. However, most studies that use large forces do not implement indentation analysis, but implement force range analysis. Another reason to use indentation analysis is to see if any cytoskeletal rearrangements occur due to large forces and cause changes in cell mechanics. The heterogeneity of the cytoskeleton of fibroblasts and erythrocytes can also be detected by probing deeper into cells during AFM measurements [126]. This highlights the need to probe cells in the same region when comparing cell lines from different disease stages. Thus, all force curves in this thesis that measure the cell stiffness are analysed by choosing an indentation range. This is because indentation is the parameter where the part of the cell, that is studied, can be kept constant.

AFM-based mechanical measurements are often carried out with large loading forces, which might result in indentations deeper than 10% of the cell's thickness and exert more than 10% strain on the cell. These conditions violate the assumptions under which the Hertz model can be applied to force curves. In this study, cells were measured using AFM with three loading forces: 0.5 nN, 1.0 nN and 2.5 nN. Around 10 cells were measured per cell line and per loading force. The experiments were divided into two categories of force maps based on whether the same cell was probed with all three loading forces or whether a different cell was probed for each loading force. This is elaborated below in the rest of the chapter.

In the first category of force maps, three force maps were captured on each cell. The first map used a loading force of 0.5 nN, the second map used a loading force of 1.0 nN and the third map used a loading force of 2.5 nN. Loading force does not influence the measured Apparent Young's modulus of any cell line differentially. Qualitatively, when the same cell is probed with three different forces, E remains the same for all cell lines (Fig. 4.4 and Table 4.3).

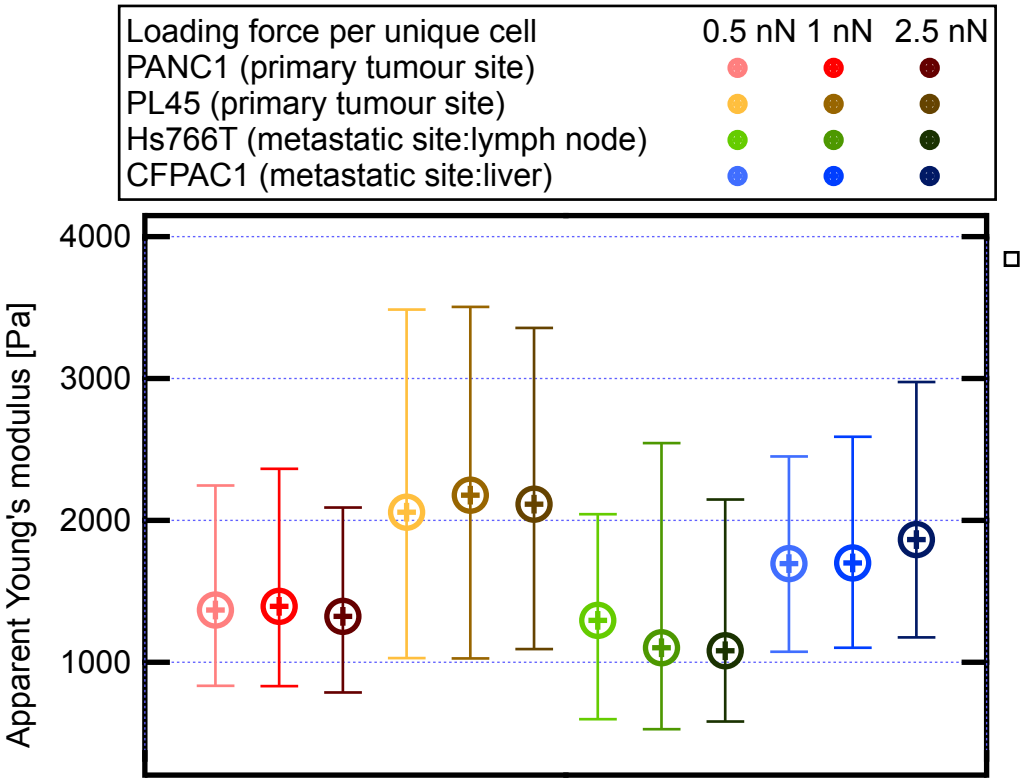

Fig. 4.4 A comparison of the median ± interquartile region of the apparent Young's modulus (E) determined for four studied pancreatic cell lines originating from various stages of pancreatic cancer progression. Each cell was measured three times with loading forces 0.5 nN, 1.0 nN and 2.5 nN (lighter to darker).

Table 4.3. The median of the apparent Young's modulus (in Pa) obtained for pancreatic cancer cell lines from AFM measurements conducted on the same cell with three different loading forces: 0.5 nN, 1.0 nN and 2.5 nN.

cell lines	PANC-1	PL-45	Hs 766T	CFPAC-1
0.5 nN loading force	1302	2269	1219	1682
1.0 nN loading force	1582	2238	1076	1495
2.5 nN loading force	1342	2121	1044	1623

In the second category of force maps, one force map was captured on one cell. For each cell, one of the following three loading forces was used: 0.5 nN, 1.0 nN and 2.5 nN. Increasing the loading force shows a general trend of increase in the measured Apparent Young's modulus of PL-45, Hs 766T and CFPAC-1 cell lines (Fig. 4.4 and Table 4.3). The trend is marked most sharply in PL-45 cell line. However, statistical tests showed no significant difference, although this might be due to the small sample size.

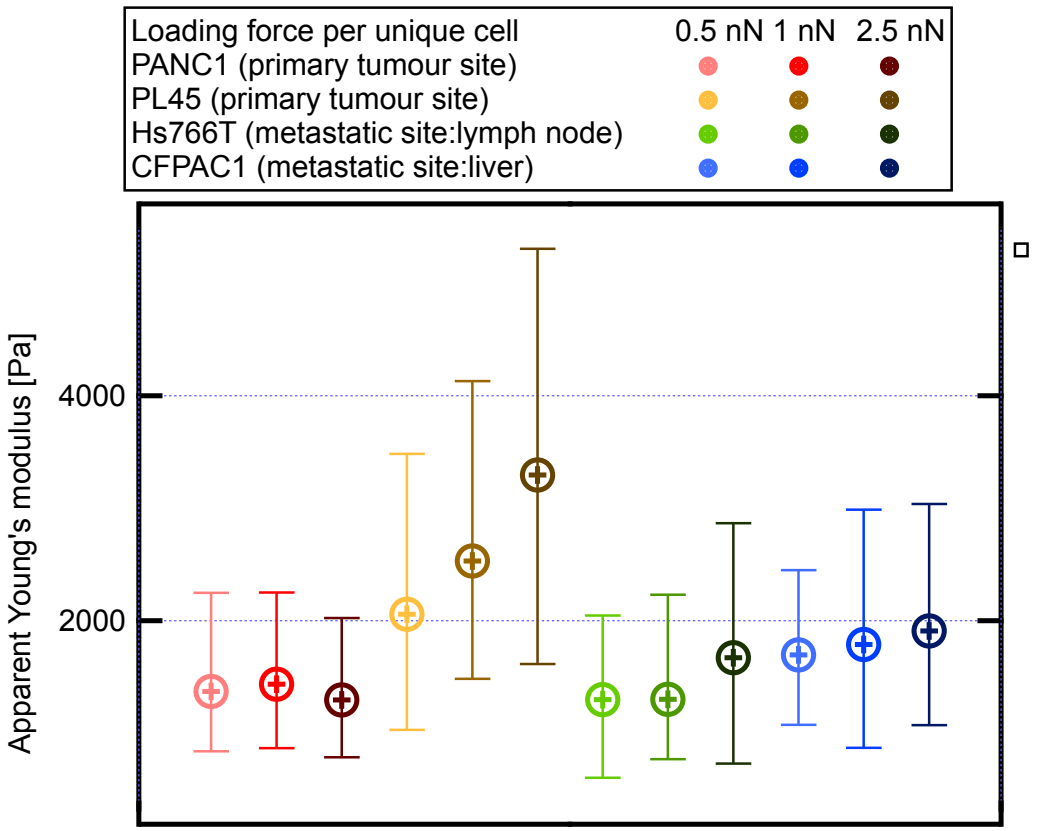

Fig. 4.5 A comparison of the median ± interquartile region of the apparent Young's modulus (E) determined for four studied pancreatic cell lines originating from various stages of pancreatic cancer progression. Three different cells were measured with loading forces 0.5 nN, 1.0 nN and 2.5 nN (lighter to darker).

Table 4.4. The median of the apparent Young's modulus (in Pa) obtained for pancreatic cancer cell lines from AFM measurements conducted on three different cells with three loading forces: 0.5 nN, 1.0 nN and 2.5 nN.

Cell lines	PANC-1	PL-45	Hs 766T	CFPAC-1
0.5 nN loading force	1302	2269	1219	1682
1.0 nN loading force	1346	2779	1362	1821
2.5 nN loading force	1333	3195	1924	1994

Usually larger force can cause stiffening of the cell [94], as is observed in this case. There is a trend of stiffening with increasing loading force, in the second category of force maps; however there is no significant change (Fig. 4.5 and table 4.4). When comparing the stiffness of cell lines to establish distinct mechanical characteristics of the stages of pancreatic cancer, it is certainly useful to choose the data acquisition and analysis parameters carefully. This set of experiments demonstrated that when measuring a population of cells, improper experimental parameters could produce misleading mechanical characterisation.

Chapter 5 - Rheological properties of PDAC cells under varying confinement

Cancer cells have ECM with large amounts of collagen I (Col I) and hyaluronic acid (HA). The presence of hyaluronic acid, especially, is unusual in cancers but typical to PDAC. Collagen I can disrupt the E-cadherin-based interaction of PDAC cells [34] and also increase the expression of SNAIL, which is a supporter of EMT and cell proliferation [127]. Since E-cadherin-based interaction is key to maintaining the normal form of pancreatic tissue, this disruption might also alter the mechanical properties of cancer cells. Hyaluronic acid is known to increase the motility of PDAC cells [30]. This further indicates the roles of collagen I and hyaluronic acid in PDAC progression and metastasis.

In the experimental results described in this chapter, pancreatic cancer cell lines were grown under five different conditions. The first condition was as single cells because the majority of mechanical measurements comparing healthy and diseased cells are carried out on single cells. Experiments that measure drug treatments, protein, DNA, RNA expressions, and other molecular biology experiments are typically carried out on layers of cells. However, both conditions are 2-dimensional, and the next state of confinement could be to grow the cells on circular micropatterns. Although the confinement is artificial, it is similar to the maximum level of confinement cells face in the tumour. As collagen I is abundantly found in PDAC tumours, this ECM protein was used to prepare hydrogel substrates. Although hyaluronic acid is also present in the ECM of PDAC tumours, it was found that cells do not adhere to pure hyaluronic acid hydrogels, therefore, a hybrid hyaluronic acid-collagen I hydrogel was used.

Apparent Young's modulus is an indicator of the amount of cytoskeleton, more than the actual nature of the cytoskeleton of a cell. Microrheology experiments to determine the actual contribution of viscous and elastic components tell the nature or phenotype of the cytoskeleton and mechanical properties of cells. These properties were described using a power law function stemming from the structural damping model. The power law exponent is an indicator of how viscous or elastic a material is. Its value ranges from 0 to 1. The smaller the power-law exponent is, the more elastic the material is.

This Chapter presents a summary of cell mechanics measurements carried out for pancreatic cancer cell lines (both stiffness and power-law exponents).

5.1 Stiffness of hydrogel substrates

The hybrid collagen I-hyaluronic acid (HA-Col I) hydrogels have a stiffness of around 8 kPa. They are stiffer than the Col I hydrogels characterized by apparent Young's modulus of around 1.5 kPa (Fig. 5.1). These values are placed within the stiffness range characteristic of pancreatic cancer [72]. Remodelling by pancreatic stellate cells is correlated with increased collagen matrix stiffness. The stiffness of the collagen I matrix increases from 100 Pa to around 1 kPa [128]. While the mechanical properties of the ECM of PDAC tumours have not been measured, the stiffness of whole tumours is 5.46 ± 3.18 kPa [72]. The ECM components themselves might be stiffer than the collective tumour; hence, a higher stiffness was chosen for the hybrid hydrogel.

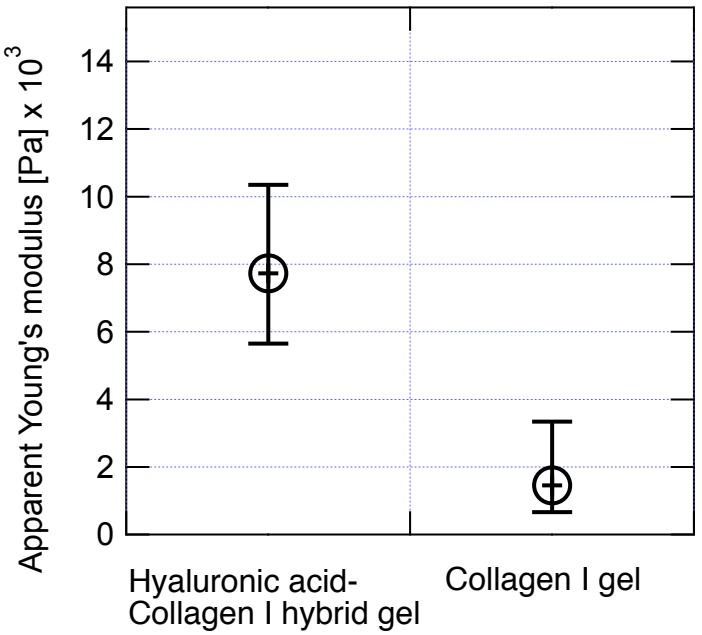

Fig. 5.1 The median ± interquartile region of the apparent Young's modulus of Col I and HA-Col I hydrogels used as substrates for pancreatic cancer cell growth. Hydrogel mechanics was measured with AFM. The hydrogels were prepared to a thickness of approximately 450 μm.

5.2 PANC-1 – primary site cell line

Figure 5.2 shows the distribution of the apparent Young's modulus of PANC-1 cells grown on different substrates/confinement conditions. The stiffness of cells falls under three groups: *(1)* moduli obtained for single cells and cells on circles being the softest, followed by *(2)* moduli obtained for cells grown on the hydrogels and, lastly, *(3)* moduli calculated for the cells cultured in layers. All histograms show wide, single maxima.

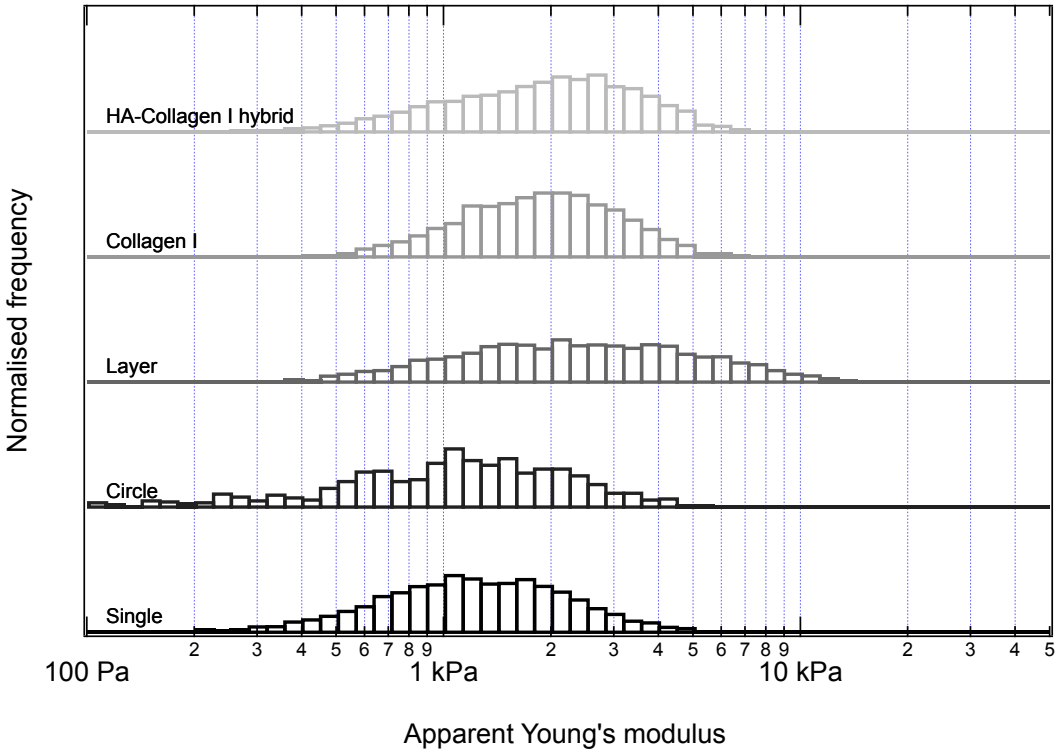

*Fig. 5.2 The distribution of the apparent Young's modulus of **PANC-1** cells measured by AFM. Cells were grown on various substrates and under various confinement conditions. Starting from the bottom to the top, the labels indicate – **single:** cells were grown for 1 day, and single cells were measured; **Circle:** cells were seeded on micropatterned fibronectin circles for 1 day; **Layer:** cells were seeded at a higher concentration and grown for 2 days, then cells which were enclosed by two lines of neighbors were measured; **Collagen I:** cells were grown on Collagen I hydrogels for 2 days; **HA-Collagen I hybrid:** cells were grown on Collagen I-hyaluronic acid hydrogels for 2 days.*

There is no difference between the following pairs: *(1)* single cells and cells cultured in circles and *(2)* cells cultured on Col I and on HA-Col I hydrogels. The mechanical measurements showed that cells cultured as a layer are stiffer than cells cultured as single cells or cells in circular confinement or cells cultured on hydrogel substrates. The single cells and cells in circles are significantly softer than the rest of the conditions, with a large effect size. Although wide distributions for cells cultured as layers and cells cultured on hydrogel substrates (Col I and HA-Col I), the apparent Young's modulus median for cells cultured as layers was the largest (2288 Pa). Table 5.1 summarizes statistical tests carried out to check the significance and effect size of the difference to show the same trend.

*Table 5.1. The results of statistical tests evaluating changes in the apparent Young's modulus of **PANC-1** cells cultured at various conditions (substrates confinements). Cohen's d test checks the effect size of using a different substrate/confinement. The outcome of the test is a parameter d. The medium effect size is 0.5 < d < 0.8 (gray), and the large effect size is 0.8 < d (red). Wilcoxon's rank test shows the significance of the difference between the two compared conditions. p < 0.01 (gray) and p < 0.001 (red). The value at the end of each row is the median.*

Confinement state	**Single cell**	**Circle**	**Layer**	**Collagen I**	**HA-Collagen I hybrid**
HA-Collagen I hybrid	$p = 2.1 \times 10^{-7}$ d = 0.98	$p = 7.9 \times 10^{-9}$ d = 1.3	$p = 2.1 \times 10^{-3}$ d = 0.54	p = 0.77 d = 0.12	1972 Pa
Collagen I	$p = 1.0 \times 10^{-9}$ d = 0.84	$p = 1.4 \times 10^{-11}$ d = 1.3	$p = 2.6 \times 10^{-3}$ d = 0.66	1629 Pa	
Layer	$p = 1.5 \times 10^{-13}$ d = 1.3	$p = 2.5 \times 10^{-12}$ d = 1.5	2288 Pa		
Circle	p =0.012 d =0.49	981 Pa			
Single cell	1160 Pa				

The distributions of the power law exponent of PANC-1 cells cultured at various conditions/confinements were characterized by a single peak (Figure 5.3).

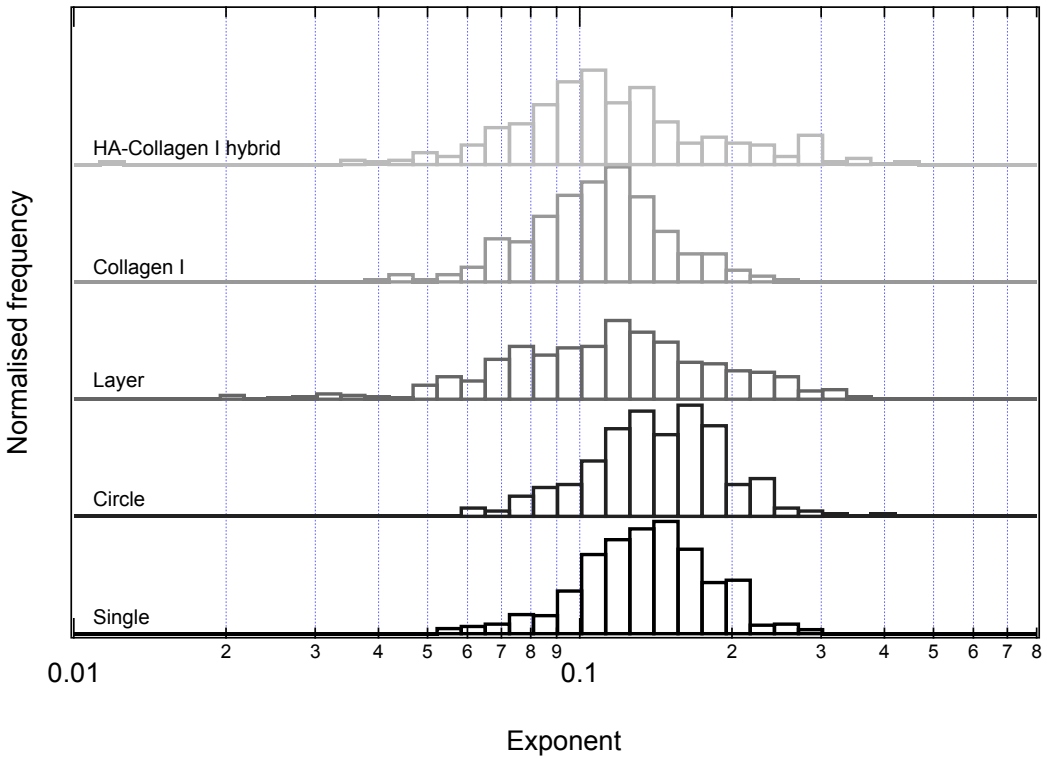

Fig. 5.3. The distribution of the power-law exponent characterizing the viscoelasticity of PANC-1 cells measured by AFM. Cells were grown on various substrates and under various confinement conditions. Starting from the bottom to the top, the labels indicate – single: cells were grown for 1 day and single cells were measured; ***Circle****: cells were seeded on micropatterned fibronectin circles for 1 day;* ***Layer****: cells were seeded at a higher concentration and grown for 2 days, then cells which were enclosed by two lines of neighbors were measured;* ***Collagen I****: cells were grown on Collagen I hydrogels for 2 days;* ***HA-Collagen I hybrid****: cells were grown on Collagen I-hyaluronic acid hydrogels for 2 days.*

The obtained results showed the largest viscous component in single cells cultured on circular confinement (0.136), followed by single cells cultured without confinements (0.126). The viscous components of cells cultured as layers or on hydrogel surfaces were similar (0.108, 0.098, 0.100, respectively). The statistical significance is summarised in Table 5.2, which shows a statistical test carried out to check the significance and effect size of the difference.

*Table 5.2. The results of statistical tests evaluating changes in the power-law exponent of **PANC-1** cells grown on various substrates and under various confinement conditions. Cohen's d test checks the effect size of using a different substrate/confinement. The outcome of the test is a parameter d. The medium effect size is 0.5 < d < 0.8 (gray), and the large effect size is 0.8 < d (red). Wilcoxon's rank test shows the significance of the difference between the two compared conditions. p < 0.01 (gray) and p < 0.001 (red). The value at the end of each row is the median.*

Confinement state	**Single cell**	**Circle**	**Layer**	**Collagen I**	**HA-Collagen I hybrid**
HA-Collagen I hybrid	p = 0.0034 d = 0.45	p = 0.0037 d = 0.67	p = 0.76 d = 0.18	p = 0.48 d = 0.12	0.100
Collagen I	p = 3.4×10^{-6} d = 0.83	p = 1.3×10^{-5} d = 1.2	p = 0.21 d = 0.39	0.098	
Layer	p = 0.027 d = 0.29	p = 0.0099 d = 0.63	0.108		
Circle	p = 0.13 d = 0.50	0.136			
Single cell	0.126				

The most significant difference and large effect size are observed between single cells cultured with and without circular confinements and cells cultured on the Col I hydrogel substrates. The former cells are more viscous than the latter. A moderate difference in the power law exponent is observed for these cells compared to cells cultured on the HA-Col I substrates and between cells cultured in circular confinements and cells cultured as layers.

As reported in Figs. 5.3 and Table 5.2, some of the softest cells have the highest power law exponent, indicating large contributions of viscous components in cell mechanics. Here, single cells cultured with and without circular confinements are highly viscous. Moreover, PANC-1 cells are indifferent to both the material nature and stiffness of the hydrogels.

5.3 PL-45 – primary site cell line

Figure 5.4 shows the distribution of the apparent Young's modulus of PL-45 cells grown on different substrates/confinement conditions.

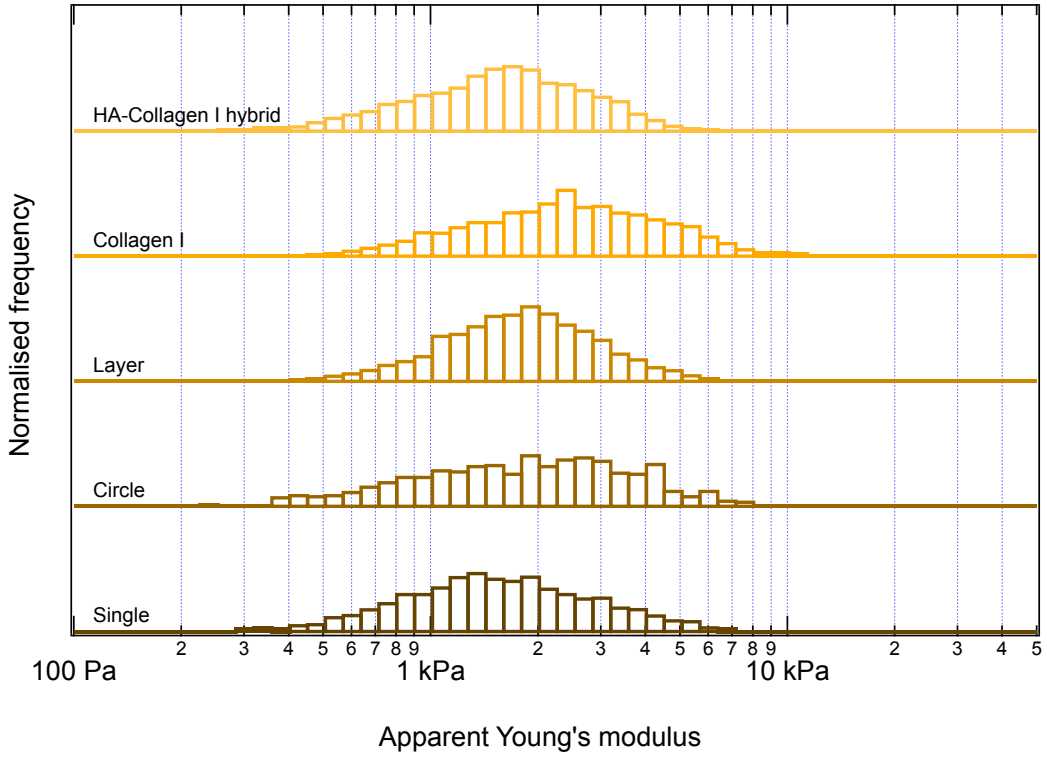

*Fig. 5.4 The distribution of the apparent Young's modulus of **PL-45** cells measured by AFM. Cells were grown on various substrates and under various confinement conditions. Starting from the bottom to the top, the labels indicate – **Single:** cells were grown for 2 days and single cells were measured; **Circle:** cells were seeded on micropatterned fibronectin circles for 2 days; **Layer:** cells were seeded at a higher concentration and grown for 3 days, then cells which were enclosed by two lines of neighbors were measured; **Collagen I:** cells were grown on Collagen I hydrogels for 3 days; **HA-Collagen I hybrid:** cells were grown on Collagen I-hyaluronic acid hydrogels for 3 days.*

The obtained results on cell stiffness fall into three groups. The first group includes moduli determined for single cells and cells cultured on the HA-Col I substrates, revealing the softest cells. The next group gatherers the moduli obtained for cells grown on circles and in layers. The last group are moduli determined for cells grown on collagen-I hydrogel substrate. All histograms show single peaks. The statistical tests (Table 5.3) were carried out to verify the significance and effect size of the difference.

*Table 5.3. The results of statistical tests evaluating changes in the apparent Young's modulus of **PL-45** cells grown on various substrates and under various confinement conditions. Cohen's d test checks the effect size of using a different substrate/confinement. The outcome of the test is a parameter d. The medium effect size is 0.5 < d < 0.8 (gray), and the large effect size is 0.8 < d (red). Wilcoxon's rank test shows the significance of the difference between the two compared conditions. p < 0.01 (gray) and p < 0.001 (red). The value at the end of each row is the median.*

Confinement state	**Single cell**	**Circle**	**Layer**	**Collagen I**	**HA-Collagen I hybrid**
HA-Collagen I hybrid	p = 0.68 d = 0.13	p = 0.91 d = 0.17	p = 0.052 d = 0.33	p = 1.2×10^{-5} d = 0.75	1514 Pa
Collagen I	p = 1.4×10^{-5} d = 0.75	p = 0.045 d = 0.50	p = 2.1×10^{-3} d = 0.43	2168 Pa	
Layer	p = 0.028 d = 0.40	p = 0.95 d = 0.13	1736 Pa		
Circle	p = 0.165 d = 0.25	1751 Pa			
Single cell	1415 Pa				

Significant differences and effect sizes were observed between cells cultured *(1)* on glass (referred to here as single cells group) and collagen-I substrates, *(2)* on Col I hydrogels surface and layers, and *(3)* Col I and HA-Col I hydrogel surfaces.

The power-law exponent shows a very different story than the apparent Young's modulus and clearly highlights the need for characterizing viscoelasticity or fluidity. Figure 5.5 shows the distributions of the power-law exponents determined for PL-45 pancreatic cells grown at various substrates/confinement conditions. All histograms show single peaks.

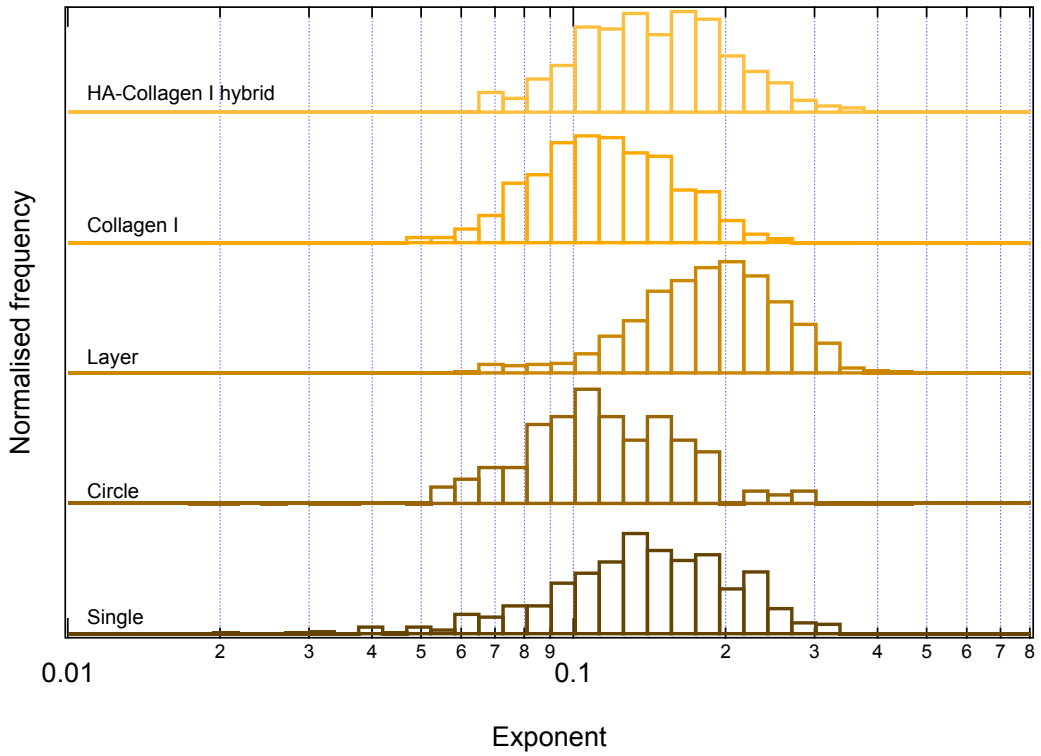

*Fig. 5.5 The distributions of the power-law exponent obtained for **PL-45** cells measured by AFM. Cells were grown on various substrates and under various confinement conditions. Starting from the bottom to the top, the labels indicate – **Single:** cells were grown for 2 days and single cells were measured; **Circle:** cells were seeded on micropatterned fibronectin circles for 2 days; **Layer:** cells were seeded at a higher concentration and grown for 3 days, then cells which were enclosed by two lines of neighbors were measured; **Collagen I:** cells were grown on Collagen I hydrogels for 3 days; **HA-Collagen I hybrid:** cells were grown on Collagen I-hyaluronic acid hydrogels for 3 days.*

The most significant difference and large effect size are observed for cells cultured as layers and cells grown in all the other conditions. Notably, there is a large size effect between the results obtained for cells cultured on the Col I and HA-Col I hydrogel substrates. A moderate difference is observed between the following pairs: (1) single cells and cells cultured on the Col I hydrogel substrates and cells cultured on the circles and on the HA-Col I hydrogel substrates.

*Table 5.4. The results of statistical tests evaluating changes in the power-law exponent of **PL-45** cells grown on various substrates and under various confinement conditions. Cohen's d test checks the effect size of using a different substrate/confinement. The outcome of the test is a parameter d. The medium effect size is 0.5 < d < 0.8 (gray), and the large effect size is 0.8 < d (red). Wilcoxon's rank test shows the significance of the difference between the two compared conditions. p < 0.01 (gray) and p < 0.001 (red). The value at the end of each row is the median.*

Confinement state	**Single cell**	**Circle**	**Layer**	**Collagen I**	**HA-Collagen I hybrid**
HA-Collagen I hybrid	p = 0.74 d = 0.26	p = 0.089 d = 0.65	p = 5.3×10^{-5} d = 0.76	p = 0.0075 d = 0.93	0.130
Collagen I	p = 0.034 d = 0.51	p = 0.6 d = 0.23	p = 3.3×10^{-10} d = 1.6	0.108	
Layer	p = 1.1×10^{-5} d = 0.91	p = 1.5×10^{-6} d = 1.33	0.177		
Circle	p = 0.14 d = 0.28	0.105			
Single cell	0.132				

In the case of PL-45, the pattern of mechanical properties is more complex. Single cells are softer and more viscous. Cells in layers are highly viscous with moderate stiffness. The cells cultured on the HA-Col I hydrogel substrates are among the softest, with a moderate viscosity. Cells in circles are among the least viscous with moderate stiffness. Cells cultured on the Col I hydrogel substrates are the stiffest but also among the least viscous.

5.4 Hs 766T – lymph node metastasis

Figure 5.6 shows the distribution of the apparent Young's modulus of Hs 766T cells grown on different substrates/confinement conditions. All histograms show single peaks except the histogram obtained for cells on a circle, which have a broad distribution with multiple peaks.

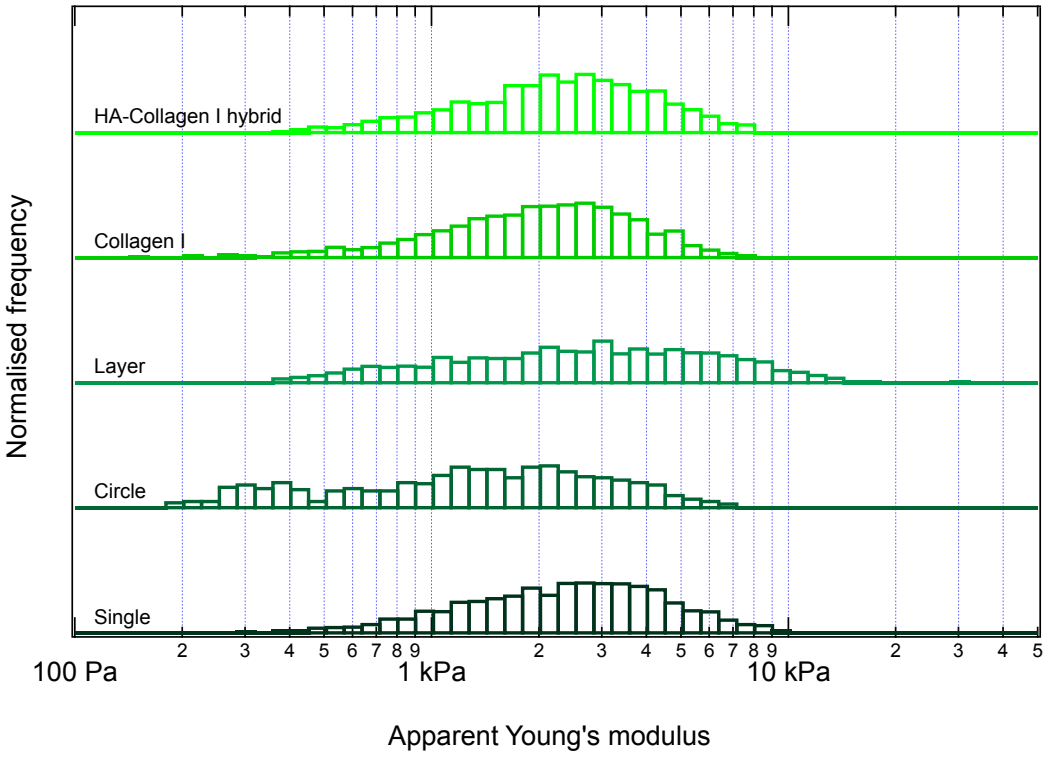

Fig. 5.6. The distributions of the apparent Young's modulus of ***Hs 766T*** *cells measured by AFM. Cells were grown on various substrates and under various confinement conditions. Starting from the bottom to the top, the labels indicate –* ***Single:*** *cells were grown for 1 day and single cells were measured;* ***Circle:*** *cells were seeded on micropatterned fibronectin circles for 1 day;* ***Layer:*** *cells were seeded at a higher concentration and grown for 2 days, then cells which were enclosed by two lines of neighbors were measured;* ***Collagen I:*** *cells were grown on Collagen I hydrogels for 2 days;* ***HA-Collagen I hybrid:*** *cells were grown on Collagen I-hyaluronic acid hydrogels for 2 days.*

The stiffness of cells falls under three groups, i.e., the softest, moderate, and stiffest cells. The first group are the cells cultured in circular confinements. Next are the cells cultured as single cells and on hydrogel surfaces. The third and last group are cells cultured in layers. Table 5.5 shows statistical tests carried out to verify the significance and effect size of the difference.

*Table 5.5 The results of statistical tests comparing the apparent Young's modulus of **Hs 766T** cells grown on various substrates and under various confinement conditions. Cohen's d test checks the effect size of using a different substrate/confinement and is the parameter d. Medium effect size is 0.5 < d < 0.8 (gray), and large effect size is 0.8 < d (red). Wilcoxon's rank test shows the significance of the difference between the two compared conditions. p<0.01 is in gray and p < 0.001 (red). The value at the end of each row is the median.*

Confinement state	**Single cell**	**Circle**	**Layer**	**Collagen I**	**HA-Collagen I hybrid**
HA-Collagen I hybrid	p = 0.56 d = 0.047	p = 0.0014 d = 0.93	p = 7.5×10^{-3} d = 0.38	p = 0.20 d = 0.26	2026 Pa
Collagen I	p = 0.10 d = 0.27	p = 0.024 d = 0.68	p = 6.9×10^{-4} d = 0.52	1796 Pa	
Layer	p = 0.013 d = 0.36	p = 2.1×10^{-5} d = 0.93	2689 Pa		
Circle	p = 6.1×10^{-4} d = 0.94	1389 Pa			
Single cell	2290 Pa				

Cells cultured in circles are significantly softer than both single cells and those cultured as layers. There is also a stark difference between the following pairs of cells cultured: (1) as layers and on the Col I hydrogel substrates, and (2) in circles and on the HA-Col I hydrogel substrates.

Figure 5.7 shows the distribution of power law exponents determined for Hs766T cells cultured at various conditions/confinements. All histograms show single peaks that fall in the same region. The determined power law exponents for Hs766T cells cultured at various conditions/confinements are very similar within the range of 0.125 – 0.144.

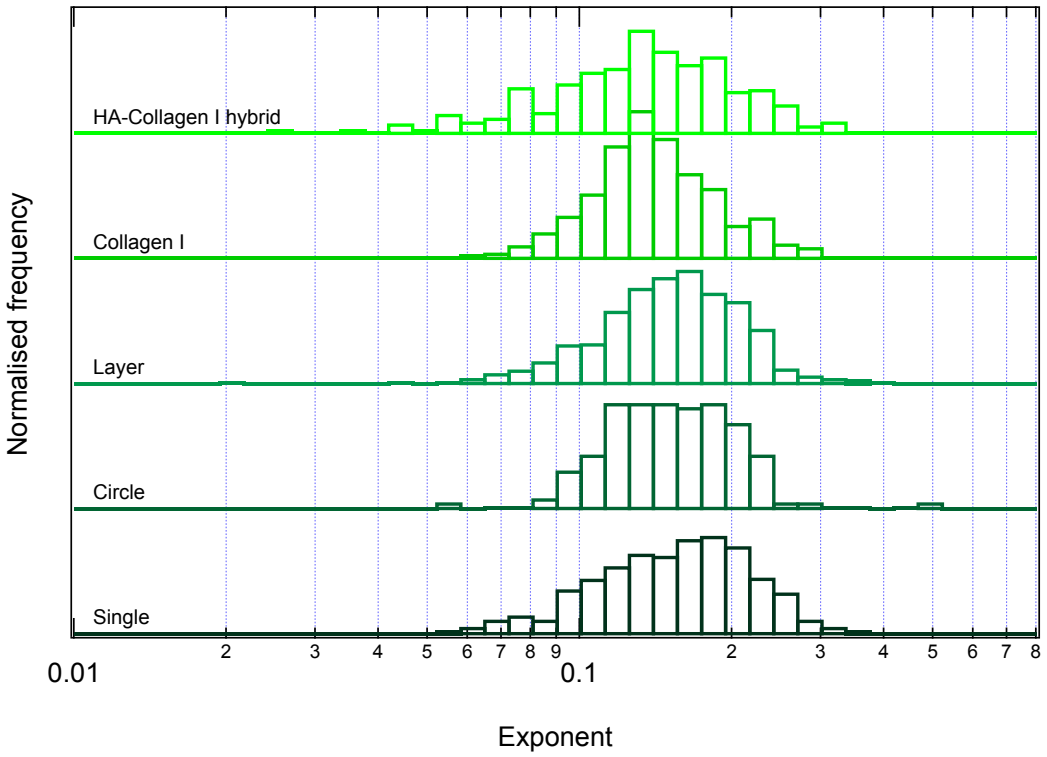

*Fig. 5.7 The distributions of the power-law exponent of **Hs 766T** cells measured by AFM. Cells were grown on various substrates and under various confinement conditions. Starting from the bottom to the top, the labels indicate – **Single:** cells were grown for 1 day and single cells were measured; **Circle:** cells were seeded on micropatterned fibronectin circles for 1 day; **Layer:** cells were seeded at a higher concentration and grown for 2 days, then cells which were enclosed by two lines of neighbors were measured; **Collagen I:** cells were grown on Collagen I hydrogels for 2 days; **HA-Collagen I hybrid:** cells were grown on Collagen I-hyaluronic acid hydrogels for 2 days.*

*Table 5.6 The results of statistical tests comparing the power-law exponent of **Hs 766T** cells grown on various substrates and under various confinement conditions. Cohen's d test checks the effect size of using a different substrate/confinement and is the parameter d. The medium effect size is 0.5 < d < 0.8 (gray), and the large effect size is 0.8 < d (red). Wilcoxon's rank test shows the significance of the difference between the two compared conditions. p < 0.01 (gray) and p < 0.001 (red). The value at the end of each row is the median.*

Confinement state	**Single cell**	**Circle**	**Layer**	**Collagen I**	**HA-Collagen I hybrid**
HA-Collagen I hybrid	p = 0.011 d = 0.047	p = 0.11 d = 0.92	p = 0.12 d = 0.38	p = 0.42 d = 0.26	0.125
Collagen I	p = 0.052 d = 0.27	p = 0.26 d = 0.68	p = 0.25 d = 0.52	0.125	
Layer	p = 0.18 d = 0.36	p = 0.85 d = 0.93	0.135		
Circle	p = 0.81 d = 0.94	0.134			
Single cell	0.144				

Table 5.6 summarizes the outcome of the applied statistical tests carried out to verify the significance and effect size of the difference. No statistically valid difference in the power law exponent for all groups of data is observed, though some effect size-related changes are observed. However, this alone is insufficient to validate the difference in the power-law exponent.

The biomechanical characterization of Hs766T shows limited sensitivity of these cells to culture conditions/confinements as only the apparent Young's modulus alters. The softening of cells is observed for cultures in circular confinements and on the Col I hydrogel substrates. The power law exponent of similar values and the lack of statistical significance indicates the viscous component of these cells hardly varies with the culture conditions.

5.5 CFPAC-1 – liver metastasis

The distributions of the apparent Young's modulus for CFPAC-1 cells originating from liver metastasis grown on different substrates/confinement conditions are presented in Fig. 5.8. All histograms show single peaks.

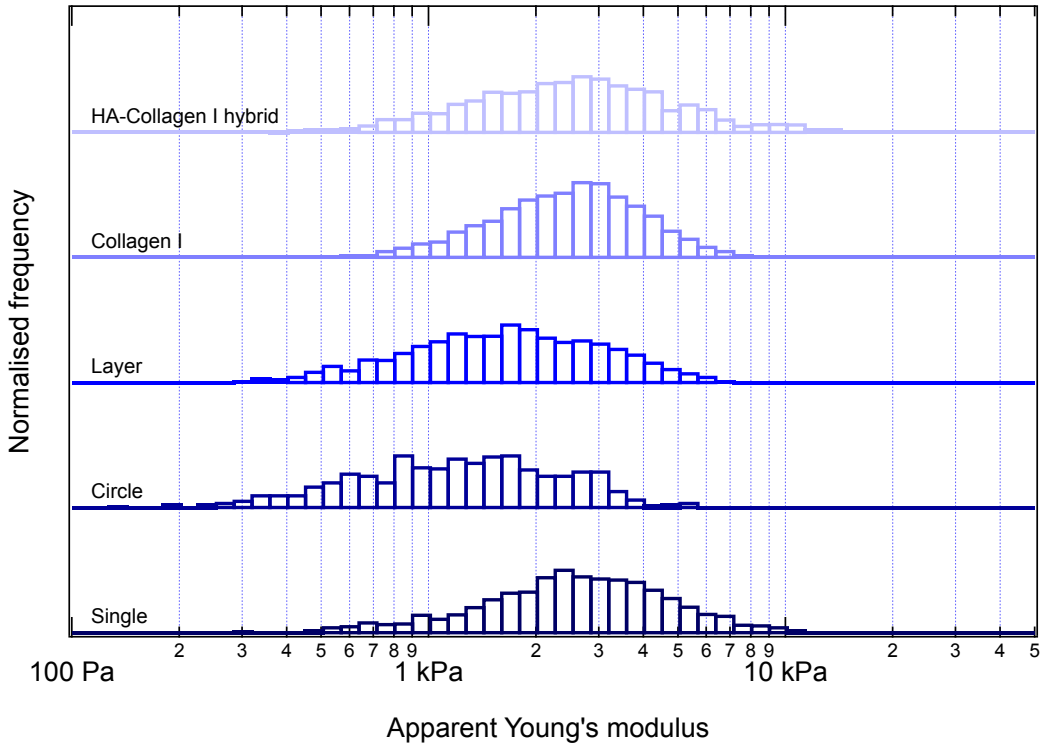

*Fig. 5.8 The distributions of the apparent Young's modulus of **CFPAC-1** cells measured by AFM. Cells were grown on various substrates and under various confinement conditions. Starting from the bottom to the top, the labels indicate – **Single:** cells were grown for 2 days and single cells were measured; **Circle:** cells were seeded on micropatterned fibronectin circles for 2 days; **Layer:** cells were seeded at a higher concentration and grown for 3 days, then cells which were enclosed by two lines of neighbors were measured; **Collagen I:** cells were grown on Collagen I hydrogels for 3 days; **HA-Collagen I hybrid:** cells were grown on Collagen I-hyaluronic acid hydrogels for 3 days.*

The determined cell stiffness can be divided into two groups. The first one encompasses the results obtained for cells cultured in layers and on circular confinements. The other gathers the results for cells cultured as single cells and both types of hydrogels. The former values oscillate around 1.2 – 1.5 kPa, while the latter around 2.3 – 2.4 kPa.

*Table 5.7 The results of statistical tests comparing the apparent Young's modulus of **CFPAC-1** cells grown on various substrates and under various confinement conditions. Cohen's d test checks the effect size of using a different substrate/confinement and is the parameter d. The medium effect size is 0.5 < d < 0.8 (gray), and the large effect size is 0.8 < d (red). Wilcoxon's rank test shows the significance of the difference between the two compared conditions. p < 0.01 (gray) and p < 0.001 (red). The value at the end of each row is the median.*

Confinement state	**Single cell**	**Circle**	**Layer**	**Collagen I**	**HA-Collagen I hybrid**
HA-Collagen I hybrid	p = 0.87 d = 0.20	p = 6.4×10^{-5} d = 1.6	p = 4.0×10^{-5} d = 0.91	p = 0.90 d = 0.31	2434 Pa
Collagen I	p = 0.58 d = 0.023	p = 3.2×10^{-5} d = 1.6	p = 1.7×10^{-6} d = 0.74	2295 Pa	
Layer	p = 7.7×10^{-7} d = 0.67	p = 0.0025 d = 0.70	1212 Pa		
Circle	p = 4.4×10^{-9} d = 1.3	1523 Pa			
Single cell	2320 Pa				

Table 5.7 shows the outcome of the statistical tests carried out to check the significance and effect size of the difference. The tests show significant changes within cells cultured *(1)* as single cells and in circular confinements, *(2)* as layers and on hydrogel substrates (Col I and HA-Col I), and *(3)* in circles and hydrogel substrates (Col I and HA-Col I). A moderate difference is observed between the cells cultured as layers and in circles.

The viscous component of CFPAC-1 cells grown on different substrates/confinement conditions is obtained by analysing the distributions of the power-law exponent determined for these cells (Fig. 5.9). All histograms show single peaks.

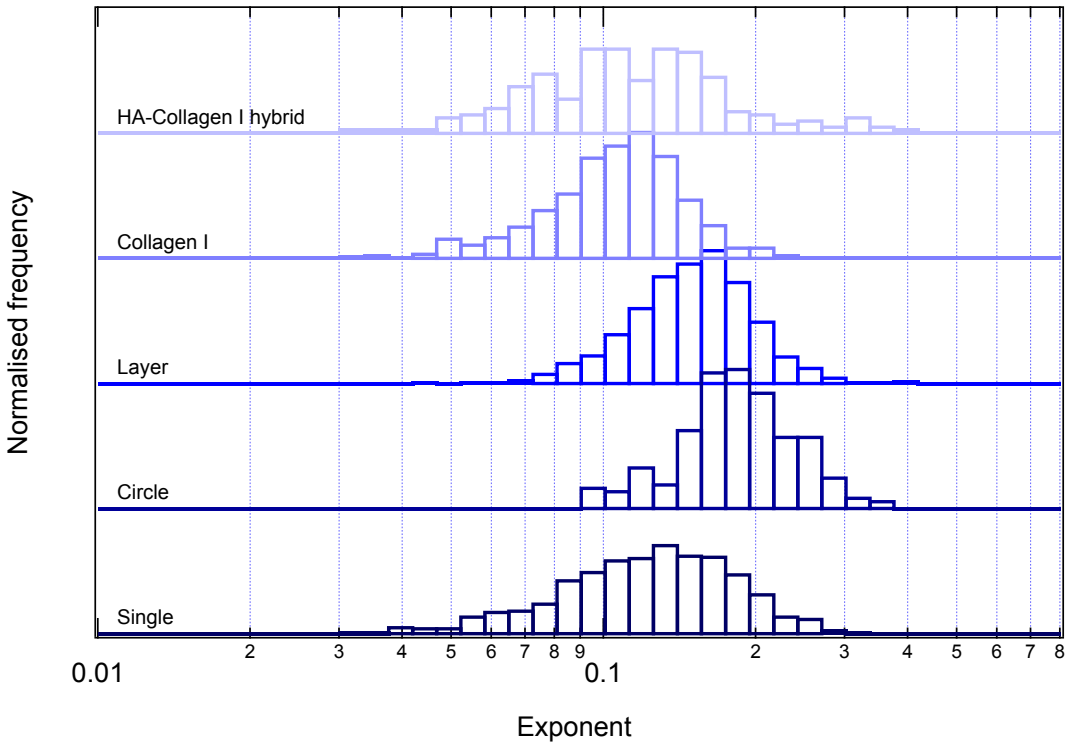

*Fig. 5.9 The distribution of the power-law exponent of **CFPAC-1** cells measured by AFM. Cells were grown on various substrates and under various confinement conditions. Starting from the bottom to the top, the labels indicate – **Single:** cells were grown for 2 days and single cells were measured; **Circle:** cells were seeded on micropatterned fibronectin circles for 2 days; **Layer:** cells were seeded at a higher concentration and grown for 3 days, then cells which were enclosed by two lines of neighbors were measured; **Collagen I:** cells were grown on Collagen I hydrogels for 3 days; **HA-Collagen I hybrid:** cells were grown on Collagen I-hyaluronic acid hydrogels for 3 days.*

The power-law exponent can be grouped as follows. The viscous component in CFPAC-1 cells was observed when cultured either as single cells, in circular confinements or as layers. Their growth on both Col I and HA-Col I hydrogel substrates leads to cell solidification, characterized by a smaller power law exponent. Table 5.8 shows the outcome of statistical tests carried out to check the significance and effect size of the difference.

Table 5.8 The results of statistical tests comparing the power-law exponent of CFPAC-1 cells grown on various substrates and under various confinement conditions. Cohen's d test checks the effect size of using a different substrate/confinement and is the parameter d. The medium effect size is 0.5 < d < 0.8 (gray), and the large effect size is 0.8 < d (red). Wilcoxon's rank test shows the significance of the difference between the two compared conditions. p < 0.01 (gray) and p < 0.001 (red). The value at the end of each row is the median.

Confinement state	**Single cell**	**Circle**	**Layer**	**Collagen I**	**HA-Collagen I hybrid**
HA-Collagen I hybrid	p = 0.39 d = 0.13	p = 8.0×10^{-5} d = 1.4	p = 1.8×10^{-4} d = 1.2	p = 0.38 d = 0.41	0.108
Collagen I	p = 0.016 d = 0.59	p = 8.3×10^{-9} d = 2.3	p = 3.6×10^{-10} d = 1.9	0.099	
Layer	p = 1.1×10^{-5} d = 0.96	p =0.0040 d = 0.94	0.146		
Circle	p = 4.9×10^{-6} d = 1.4	0.165			
Single cell	0.117				

The tests show significant changes within cells cultured *(1)* as single cells and as layers, *(2)* as single cells and in circles, *(3)* in circles and hydrogel substrates (Col I and HA-Col I), and *(4)* in layers and hydrogel substrates (Col I and HA-Col I). A moderate difference is observed between the cells cultured as single cells and on the Col I hydrogel surface.

In summary, the results of CFPAC-1 pancreatic cancer cells show that the softest cells are also the most viscous ones. Smaller power law exponents characterize stiffer cells. The softest cells were observed for cells cultured as layers and in circular confinements. CPFAC-1 cells are indifferent to the stiffness or material nature of hydrogels, as in both conditions, similar stiffness and power-law exponent are obtained for these cells.

5.6 Summary

Four cell lines from different parts of the PDAC disease were compared, and their mechanical response to various culture/confinement conditions was measured. Two cell lines from the primary site, PANC-1 and PL-45, one from lymph node metastasis, Hs 766T, and one from liver metastasis, CFPAC-1, were used. The following five conditions were used: single cell, cell on a circular pattern, cells in layers, cells on a collagen I hydrogel and cells on a hyaluronic acid-collagen I hydrogel. The power-law exponent is around the expected value for soft glassy materials. This justifies the use of the structural damping model to obtain a single power-law for measuring the extent of viscous and elastic contributions. To characterise the responses of cells to different conditions, we see how the apparent Young's modulus and power-law exponent change or stay similar.

Despite the fact that all cells originate from the same cancer type, the relation between the apparent Young's modulus and power law exponent is strongly cell-type dependent. However, a few conclusions can be drawn in terms of the comparison between cells from primary tumor sites and metastatic sites. The first main observation is that when cells are measured as single cells, the median of the apparent Young's modulus is lower (1160 Pa and 1425 Pa, for PANC-1 and PL-45 cells, respectively) than the median determined for metastatic cells (2290 Pa and 2320 Pa for Hs766T and CFPAC-1 cells, correspondingly). This relation vanished for cultures as layers, in circular confinements, and on the Col I hydrogel substrate. It stays for cells cultured on the HA-col I hydrogel surface (1972 Pa and 1514 Pa, for PANC-1 and PL-45 cells, 2026 Pa and 2434 Pa for for Hs766T and CFPAC-1cells, respectively). Surprisingly, these relations are not translated to similar dependence for power law exponent, which describes the viscous contribution. To understand this, each cell line must be considered separately. In the case of PANC-1, soft cells (cultured as single cells and circular conditions) were characterized by a greater power law exponent, indicating that these cells are more viscous. The other culture conditions (layers and hydrogel substrate) induce the stiffening of these cells manifested in smaller power-law exponents (except cells cultured as layers). For PL-45, originating from the primary tumor site as PANC-1 cells, the relations between the apparent Young's modulus/power law exponent and culture conditions are different. However, still stiffer cells are characterized by smaller power law exponent (again, except results obtained for cells cultured as layers). For metastatic cells, the softest and, simultaneously, viscous cells are observed only for CFPAC-1 cells, while it is not possible to draw such a relation for Hs766T cells. Moreover, in the case of PL-45, the apparent Young's modulus is very similar for most conditions, while in the case of Hs 766T, the power law exponent is very similar.

The following observations can be drawn when considering the effect of different culture conditions on pancreatic cancer mechanics in terms of their sensitivity to the surrounding environment. PANC-1 and CFPAC-1 cells display a very similar trend when grown on different substrates/confinement, where the cells with the lowest apparent Young's modulus are also the most viscous. These cells appeared to be more sensitive to culture conditions. The confinement realized via hydrogel substrates results in stiffer cells, potentially expressing diverse and high cytoskeleton capable of pushing more invasive activity. The Hs766T cells appeared insensitive to culture conditions, which could be linked to the high plasticity and adaptability of metastatic cells.

In the cells possessing a larger apparent Young's modulus, its higher value can be explained by the presence of more actin in the overall structure of the cytoskeleton rather than because of a change in the structure of the cytoskeleton [129]. The viscoelasticity is more representative of the cell ability to exert force and to be more flexible during cell migration and metastasis. Softer cells might also have a lower amount of other types of cytoskeletal networks like vimentin, which is often found in more aggressive forms of PDAC [89]. In a comparison between two cell lines, more invasive PDAC cells were shown to become less viscous in higher-concentration/stiffer 3D collagen gels, as compared to non-invasive cancer cells, which showed no change. Increased cellular viscosity marks more invasive activity of cancer cells [130].

Chapter 6 - Cell-cell interaction of the PDAC cell lines

The structure and order of the pancreatic epithelium are disrupted during pancreatic cancer progression. Consequently, such an outcome is possible because the adhesive properties of healthy cells are changed [131]–[133]. On the molecular level, changes observed for many cell-cell interactions originate from alterations in the conformation of various protein complexes, like catenins or cadherins, involved in adhesion, which differs from healthy to cancerous pancreatic epithelium. Semi-epithelial to mesenchymal transition occurs in PDAC, where both epithelial and mesenchymal markers are expressed in cancer cells [45]. Both cadherin type and structure are similar [134]; however, as shown in single-molecule AFM-based measurements, the interaction force between N-cadherin antibody and N-cadherin alone present in the surface of normal and cancer cells is different [69]. Here, the aim was to elaborate on how cadherin interaction changes in relation to specific pancreatic cancer and endothelial cells. To verify the specificity of the measured interaction, a potential PDAC simple peptide drug called Adherex (ADH-1, N-cadherin inhibitor [135], [136]) was used. It was applied to inhibit intercellular cadherin interactions. It also might be used because it might halt mechanisms of metastasis [137], [138].

In the presented set of experiments, the adhesive interactions between cancer or endothelial cells were characterised using AFM, working in single-cell force spectroscopy mode [59], [93]. In this mode, a single cell, either a cancer or endothelial cell, was attached to a chemically functionalised cantilever. Such a prepared AFM probe is called a cell-cantilever. An interaction experiment between the cancer cell layer probed with a cell-cantilever of the same type is a self-interaction experiment revealing how strongly the cells of the same type interact with each other. Here, self-interactions were measured for pancreatic cancer cells of the same type, i.e., PANC-1 – PANC -1, Hs766T – Hs766T, and CFPAC-1 – CFPAC-1 cells. An interaction experiment between the cancer cell layer and a cell-cantilever of different types of cells is focused on the cancer–endothelium adhesion. Therefore, the interaction between pancreatic cancer cells and endothelial cells from the cell line EA.hy926 was measured. PANC-1 from the primary tumour site was used as a control. The other cell lines studied were metastatic cell lines, one from the liver (CFPAC-1) and one from the lymph node (Hs766T).

The two parameters studied here were the total work of adhesion and the number of ruptures. The total work of adhesion is the amount of energy spent to detach the cells completely from each other. This parameter is more general

and gives a broad overview of the adhesiveness of cells. The number of ruptures is a more specific parameter, because rupture events are observed when sharp breaks occur between detaching cells. These are usually caused by the detachment of proteins or clusters of proteins. The aim of this part was to observe if there are any differences in the adhesive properties of metastatic cells with self-cells as compared to the endothelial cells. The tables below summarise the results of the experiments.

Table 6.1 The median work of adhesion and results of a statistical test comparing the work of adhesion with and without treatment with 4 mg/mL ADH-1 for 3h. Wilcoxon's rank test shows the significance of the difference between the two compared conditions. $p < 0.01$ (gray) and $p < 0.001$ (red).

	Condition	PANC-1	Hs 766T	CFPAC-1
Interaction with self-cancer cells	No ADH-1	15.3 fJ	17.6 fJ	1.76 fJ
	0.4 mg/mL ADH-1	12.4 fJ	11.1 fJ	0.882 fJ
	p-value	0.17	0.11	0.73
Interaction with endothelial cells	No ADH-1	6.36 fJ	8.46 fJ	5.17 fJ
	0.4 mg/mL ADH-1	5.49 fJ	5.86 fJ	7.24 fJ
	p-value	0.95	0.48	0.14

Table 6.2 The median number of ruptures and results of a statistical test comparing the work of adhesion with and without treatment with 4 mg/mL ADH-1 for 3h. Wilcoxon's rank test shows the significance of the difference between the two compared conditions. $p < 0.01$ (gray) and $p < 0.001$ (red).

	Condition	PANC-1	Hs 766T	CFPAC-1
Interaction with self-cancer cells	No ADH-1	4	15	0
	0.4 mg/mL ADH-1	5	6	0
	p-value	0.85	9.9×10^{-6}	0.044
Interaction with endothelial cells	No ADH-1	1.25	10	4
	0.4 mg/mL ADH-1	0	2	2.5
	p-value	0.024	2.4×10^{-4}	0.34

6.1 PANC-1 – primary site cell line

The distribution of the work of adhesion between PANC-1 cells as a layer on a petri dish and either a single PANC-1 or an EA.hy926 cell adhered to the cantilever is shown in Fig. 6.1.

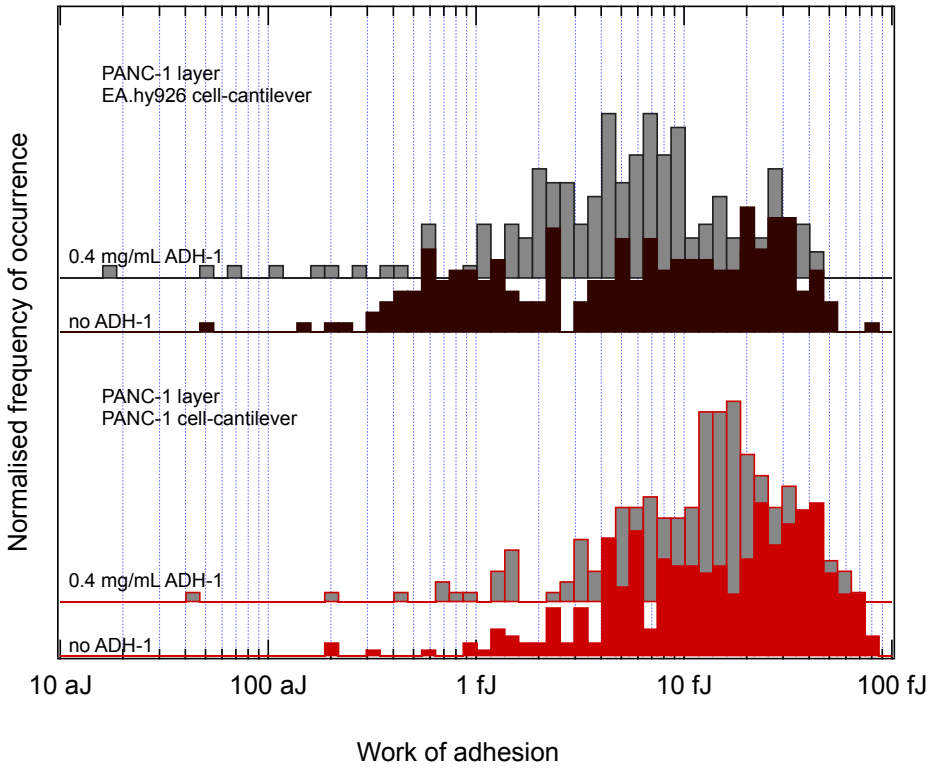

*Fig. 6.1 The distribution of the work of adhesion measured by AFM. **PANC-1** cells were grown on Petri dishes in a cell layer. Either **PANC-1** or **EA.hy926** cells were attached to the cantilever. Red and dark red histograms show the work of adhesion between cells without the N-cadherin inhibitor ADH-1, while the gray histograms show the work of adhesion between **PANC-1** layer treated with 0.4 mg/mL ADH-1 for 3 h and cell-cantilever.*

The adhesion work ranges from 10 aJ to 100 fJ, with double maxima around 10 fJ and 40 fJ. The addition of ADH-1 does not affect the adhesion significantly, although a qualitative decrease is observed, i.e., the maximum of larger values shifts to lower work of adhesion values (~15 fJ). Such results might indicate that N-cadherins govern part of the cadherins interaction characterized by larger interaction forces. In the case of PANC-1 and EA.hy926 cells, the work of adhesion shows double peaks, with lower around 1 fJ and higher around 10 fJ values. The presence of an N-cadherin inhibitor leads to a wide histogram with a peak value of 7 fJ. After blocking N-cadherins on PANC-1 cells, the cell-cell interaction probably is mostly governed by E-cadherins.

The number of ruptures ranges up to 40 events (Fig. 6.2); however, the majority of rupture occurrence stays up to 20 events, and they are cell- and treatment-

dependent. For PANC-1 – PANC-1 adhesion, the occurrence is similar for the interaction with and without the presence of an N-cadherin inhibitor. Thus, the addition of ADH-1 does not show a significant change (Table 6.2). For PANC-1 – EA.hy929 adhesion, the occurrence of rupture events after ADH-1 treatment blocks multiple N-cadherin interactions, and the frequency of lower number of ruptures per force curve increases.

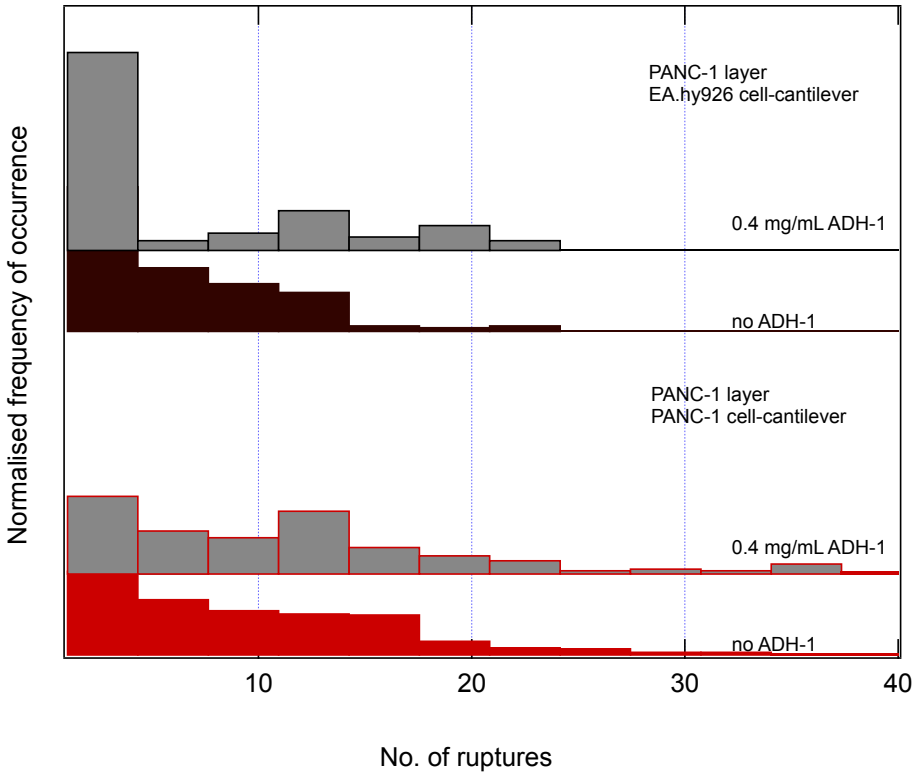

*Fig. 6.2 The distribution of the number of ruptures measured by AFM. **PANC-1** cells were grown on Petri dishes in a cell layer. Either **PANC-1** or **EA.hy926** cells were attached to the cantilever to make cell-cantilevers. Red and dark red histograms show the no. of ruptures between cells without the N-cadherin inhibitor ADH-1, while the gray histograms show the work of adhesion between **PANC-1** layer treated with 0.4 mg/mL ADH-1 for 3 h and cell-cantilever.*

Altogether, the obtained results show that the PANC-1 – PANC-1 cell adhesion is larger than PANC-1 – EA.hy929 cell adhesion, but the number of rupture events (single and multiple ones) is similar. The addition of the N-cadherin inhibitor shows, regardless of the interaction type, that the presence of ADH-1 manifests in narrowing the work of adhesion histograms and shifts the maximum to lower values. The larger effect of AHD-1 in the PANC-1 – EA.hy929 cell adhesion is probably linked with the sensitivity of the measurements. Possibly, the high abundance of N-cadherins allows for multiple binding events, making the experiments less sensitive to the addition of N-cadherin inhibitor.

6.2 Hs 766T – lymph node metastasis

The distribution of the work of adhesion between Hs 766T cells as a layer on a petri dish and either a single Hs 766T cell or an EA.hy926 cell adhered to the cantilever is shown in Fig. 6.3. Only a qualitative decrease is observed in the work of adhesion. In general, only one peak is observed. The work of adhesion is very close for the interaction of Hs766T (~10 fJ) with endothelial cells and with self-cells (~20 fJ).

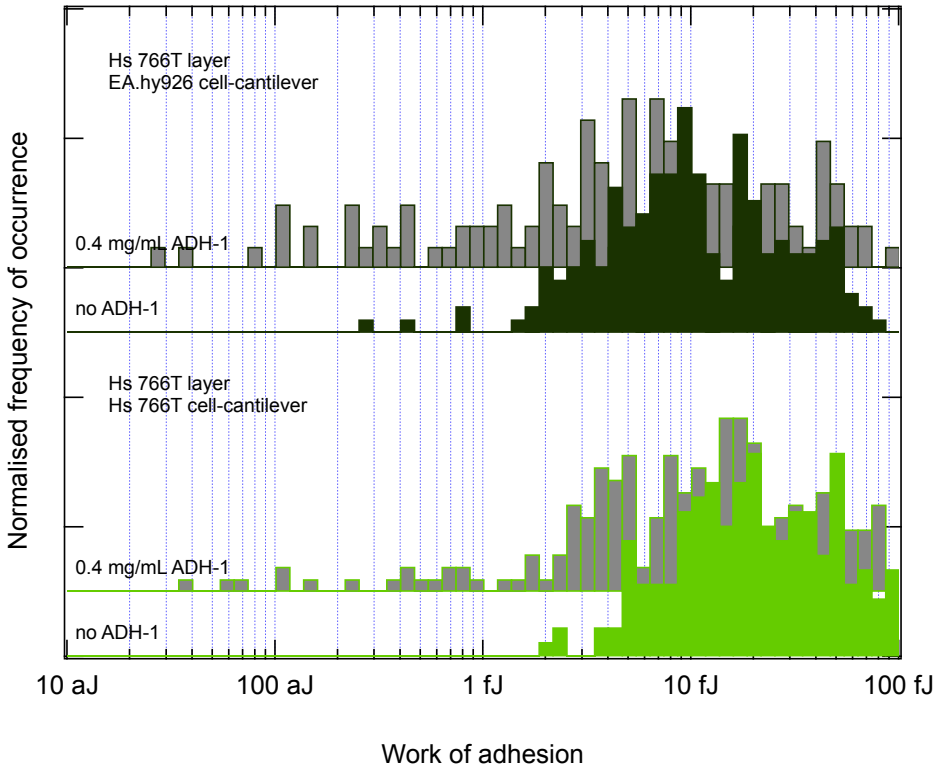

Fig. 6.3 The distribution of the work of adhesion measured by AFM. HS 766T cells were grown on Petri dishes in a cell layer. Either HS 766T or EA.hy926 cells were attached to the cantilever to make cell-cantilevers. Green and dark green histograms show the work of adhesion between cells without the N-cadherin inhibitor ADH-1, while the gray histograms show the work of adhesion between HS 766T layer treated with 0.4 mg/mL ADH-1 for 3 h and cell-cantilever.

Hs 766T self-interaction has a higher frequency of occurrence of no. of ruptures than with endothelial cells. In both cases, the addition of ADH-1 greatly reduces the number of ruptures. This is shown in the histogram distribution in Fig. 6.4 and by the results of Wilcoxon's rank test (Table 6.2).

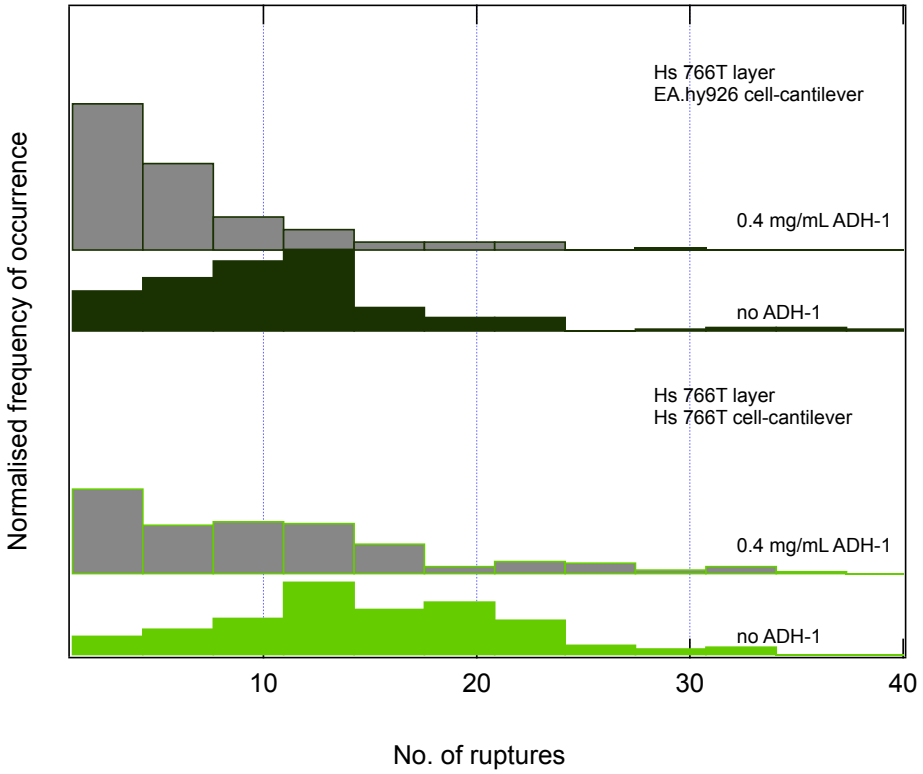

*Fig. 6.4 The distribution of the number of ruptures measured by AFM. **HS 766T** cells were grown on Petri dishes in a cell layer. Either **HS 766T** or **EA.hy926** cells were attached to the cantilever to make cell-cantilevers. Green and dark green histograms show the work of adhesion between cells without the N-cadherin inhibitor ADH-1, while the gray histograms show the work of adhesion between **HS 766T** layer treated with 0.4 mg/mL ADH-1 for 3 h and cell-cantilever.*

When comparing the cell-cell interaction of PANC-1 with Hs 766T, the work of adhesion shows very similar numbers (Table 6.1). However, the number of ruptures is significantly reduced in Hs 766T than in PANC-1 when the cells are treated with ADH-1. This indicates the possibility that ADH-1 is more effective in hindering N-cadherin based adhesion in lymph node metastasis. Since patients without lymph node metastasis had much better prognostic outcomes than those with lymph node metastasis [139], this result offers promising additions to hindering lymph node metastasis.

6.3 CFPAC-1 – liver metastasis

The distribution of the work of adhesion between CFPAC-1 cells as a layer on a petri dish and either a single CFPAC-1 or an EA.hy926 cell adhered to the cantilever is shown in Fig. 6.5. The work of adhesion between self- CFPAC-1 cells falls under two distributions. One is on the lower side and ranges from 0.1 – 1 fJ. The other falls between 1 – 10 fJ and overlaps with the range of the distribution of the work between CFPAC-1 cells and endothelial cells. This clearly indicates two populations of CFPAC-1 cells based on their self-adhesiveness.

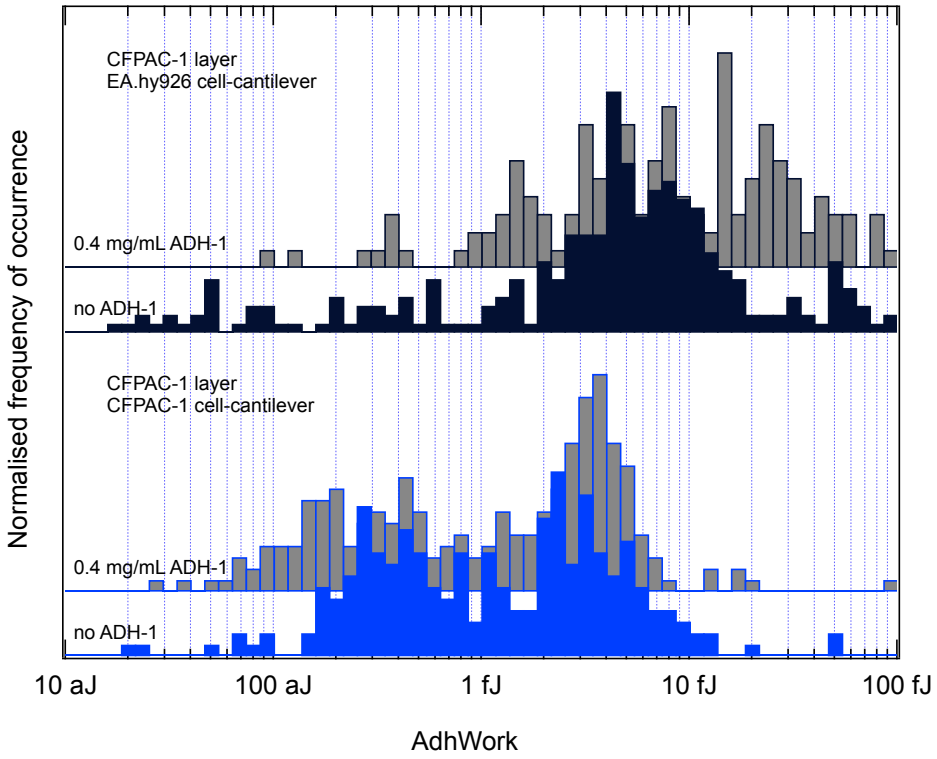

*Fig. 6.5 The distribution of the work of adhesion measured by AFM. **CFPAC-1** cells were grown on Petri dishes in a cell layer. Either **CFPAC-1** or **EA.hy926** cells were attached to the cantilever to make cell-cantilevers. Blue and dark blue histograms show the work of adhesion between cells without the N-cadherin inhibitor ADH-1, while the gray histograms show the work of adhesion between **CFPAC-1** layer treated with 0.4 mg/mL ADH-1 for 3 h and cell-cantilever.*

The histogram distribution of the number of ruptures (Fig. 6.6) shows much the same as the work of adhesion. There are more rupture events occurring when the EA.hy926 cell interacts with the CFPAC-1. This is highly unusual, because if there are not enough adhesion proteins on the CFPAC-1 to cause rupture events during self-adhesion experiments, then there would not be enough to interact with EA.hy926. This points to a unique mechanism of interacting with EA.hy926 cells.

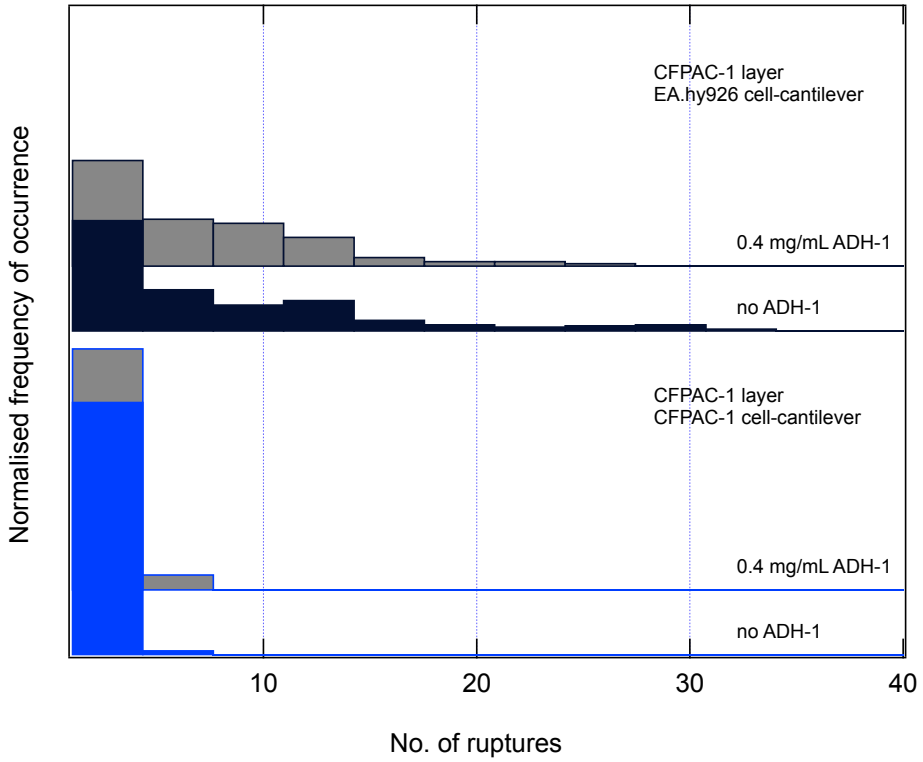

*Fig. 6.6 The distribution of the number of ruptures measured by AFM. **CFPAC-1** cells were grown on Petri dishes in a cell layer. Either **CFPAC-1** or **EA.hy926** cells were attached to the cantilever to make cell-cantilevers. Blue and dark blue histograms show the work of adhesion between cells without the N-cadherin inhibitor ADH-1, while the gray histograms show the work of adhesion between **CFPAC-1** layer treated with 0.4 mg/mL ADH-1 for 3 h and cell-cantilever.*

The adhesiveness of CFPAC-1 is very low, and in fact, it appears that any cell-cell interaction that CFPAC-1 cells show is due to the adhesiveness of EA.hy926 cells. Adding ADH-1 has no quantitative effect on the adhesion for either pair of interacting cells.

6.4 Summary

The adhesive properties of three pancreatic cancer cell lines were evaluated in terms of the work of adhesion (the work needed to detach cell-cell interaction) and number of ruptures (jumps in cell-cell detachment caused by the breaking apart of clusters of adhesion proteins on the detaching cells). PANC-1 cells from the primary site of the pancreas were used as the control, and the two metastatic cell lines were compared to it, namely, Hs 766T cells from lymph node metastasis and CFPAC-1 cells from liver metastasis. The main conclusion that can be drawn from this part of the experiment is the following. First, the work of adhesion between cells of the same origin is much larger than the adhesion between pancreatic cancer cells and endothelial EA.hy292 cells for PANC-1 and Hs766T cells. The reverse relation was observed for CFPAC-1 cells that bind stronger to endothelial cells. Although the binding of the studied pancreatic cancer cells was similar (of the order of 5 – 8 fJ), the adhesion pattern can be found, i.e., cells with high self-adhesion bind weaker to endothelial cells, while cells with low self-adhesion bind stronger to endothelial cells. Since cells can metastasize single or in groups, self-adhesion may be a marker of how cells metastasis to specific distant sites. Hs766T cells are more self-adhesive than adhesive to endothelial cells. PANC-1 cells are from an aggressive tumour at the primary site and show similar behaviour. Cells metastasizing to the rest of the body, often encounter the lymphatic system first. This might explain the similarity in adhesive properties between PANC-1 and Hs 766T. Cells metastasising to the liver would need high adhesion to the endothelial lining as they have to extravasate from the pancreas into blood vessels, and then intravasate into the liver. This is the adhesion pattern followed by CFPAC-1 cells.

Recalling that during the cancer progression, E-cadherins are replaced by N-cadherins, an inhibitor ADH-1 applied to block N-cadherins binding. Simultaneously, this inhibitor confirms the specificity of the interaction and reveals the contribution of N-cadherins binding in cancer cells interacting with endothelial cells. The results show that cells interacting with similar cell types are less sensitive to the presence of the ADH-1 inhibitor. For PANC-1 cells, the obtained medians of the number of ruptures were 4 and 5 without and with ADH-1 inhibitor, which indicates that PANC-1 – PANC-1 adhesion is weakly dependent on the N-cadherins interactions, despite its presence as reported for these cell lines, for example in [140]. For CFPAC-1 cells, the median equals zero (without and with ADH-1), showing that cell-cell adhesion is weak. Only a few force curves showed rupture events leading to a 50 percentile equals zero. The largest rupture number was observed for Hs766T – Hs766T cellular adhesion. The blocking of N-cadherin interaction with ADH-1 inhibitor for these cells reveals more than 50% drop (from 15 to 6 rupture events), simultaneously

indicating that self-adhesion strongly depends on N-cadherin involvement. When mowing to pancreatic cancer cell interaction with endothelial cells, the results show that various contributions of N-cadherins are present depending on the cell type. For all cells measured before and after adding the AHD-1 inhibitor, the number of ruptures decreases after blocking this interaction type. The largest decrease was observed for Hs766T cells, indicating that their interaction with endothelial cells also depends on the N-cadherins.

Chapter 7 - Conclusion and Outlook

7.1 Conclusion

This thesis aimed to evaluate the mechanical properties of pancreatic cancer cells originating from different stages of cancer progression. Thus, two cell lines from the primary site were studied, i.e., PL-45 and PANC-1 cells, alongside two cell lines from metastatic sites, namely, Hs766T and CFPAC-1 cells. Following the reports showing the relativeness of the apparent Young's modulus of cells on culture conditions, the aim was to evaluate the influence of culture conditions, especially the concentration of CO_2, load force, and substrate types, on the apparent Young's modulus and power law exponent in the chosen pancreatic cancer cells. Alongside, the adhesive interactions between cells of the same type and between pancreatic cancer and endothelial cells were evaluated to complete the image of the biophysical characteristics of pancreatic cancer cells.

- PANC-1 single cells, both with and without confinement, were highly viscous and also had low stiffness. The layers of cells and cells on hydrogels were stiffer and more elastic. Their adhesive properties were relatively high in self-interactions and interaction with endothelial cells.
- PL-45 cells have a rather mixed trend of viscoelastic properties regarding their reaction to the different substrates/confinements. Since PANC-1 is used more often to study other cancer paradigms, it was chosen over PL-45 as the control cell line to compare with the metastatic cell lines.
- Hs766T cells have no change in viscoelastic properties with changing conditions. There are, however, mild variations in the stiffness of cells. Overall, it could be considered not to be very mechanosensitive. This is unlike the PANC-1 cells. However, they share similar adhesive properties, with higher self-adhesion than adhesion with endothelial cells.
- CFPAC-1 cells display a similar trend of viscoelastic properties as PANC-1 cells. These cells in a layer and on fibronectin-coated circles are the softest and most viscous cells. Thus, while PANC-1 cells are softer as cultured as single cells, CFPAC-1c cells are softer as cultured as layers. The confinement of CFPAC-1 cells via hydrogels or the lack of confinement in a single cell results in stiffer cells. The adhesive properties of CFPAC-1 are the opposite of PANC-1 cells. The magnitude of the work of adhesion is lower. CFPAC-1 cells have lower self-adhesion as compared to adhesion with endothelial cells.

In summary, the following conclusions can be drawn:

- The load force has a mild effect on determining the median for the apparent Young's modulus.
- The apparent Young's modulus depends on the CO_2 presence during AFM measurements. For cells from primary tumour sites (PANC-1 & PL-45 cells), the presence of CO_2 leads to a decrease in the median values (cells become softer), while in the case of metastatic cells, the effect is the opposite as the medians of the apparent Young's modulus increases (cells become stiffer).
- The power law exponent describing the viscous component depends on the CO_2 presence during AFM measurements. For all studied pancreatic cancer cells, the presence of 5% CO_2 leads to an increase in the median values (cells become more viscous).
- Culture conditions, i.e., the way to culture cells and the substrates used, affect cells differently. Cells from primary tumour sites (PANC-1 & PL-45 cells) are softer than cells from metastatic sites (Hs766T & CFPAC-1 cells) only when cultured as single cells and on HA-Col I hydrogel substrates.
- Softer cells are not necessarily more viscous, pointing out that the characterization of actin cytoskeleton organization and content has to be taken into account to obtain a complete image of the mechanical phenotype of pancreatic cancer cells.
- Cell adhesion and involvement of N-cadherins is fully cell-dependent.

Importantly, one can note that the magnitude of all observed changes is cell-type dependent, indicating differences in the ability to sense the surrounding environment.

7.2 Outlook

The most obvious caveat of studying one aspect of any disease progression is that the process does not occur in isolation. While partly inspiring this work, the role of internal genetic and epigenetic changes also adds to the complexity of pancreatic cancer progression. On the other hand, external and environmental factors and the reaction of the body's immune system are also to be considered.

The cell lines used in this study are from different patients. Mechanical properties of cancer tissue and cells derived from different patients could have inherent variations. This has been observed in studies reporting the mechanical properties of other cancers [141] and PDAC [72]. Obtaining all cell types from the same patient, like in this study of renal cancer [65], would be the ideal option. PDAC and stellate cell co-culture has also been established from cells derived from the same tumour [142]. This can be an interesting system to study the mechanical dependence in PDAC, because stellate cells are a major source of cancer-associated fibroblasts in the tumour. While many cancer studies investigate cells from primary and metastatic sites, actively metastasising cells are difficult to obtain. These usually circulate in the blood or lymph networks and would be the ideal mechanical system to study changes in cell mechanical properties caused by metastasis accurately.

When trying to understand changes in the stiffness of cells, measurement of the stiffness, viscoelasticity and fluidity is important. However, the biochemical or physiological drivers like cytoskeleton, cell membrane, and nuclear stiffness could be behind the changes. Thus, changes in their composition and structure could also be investigated. Similarly, the presence and distribution of cell-cell interaction molecules and complexes on the cell membrane can also provide information about cancer cell adhesive properties.

This work focused on studying the mechanical properties of cells. While the cells were studied under various substrates, confinements and grouping, this is still an *in vitro* study on monotypic samples. Any studies in the medical field require further study into more complex systems that resemble the human body. This usually means mammalian systems like mice, rats etc. [15], [143], [144]. While not much progress has been made in studying the mechanics of PDAC in these systems, new alternatives that could be more ethical are emerging. Tumour spheroids and organoids incorporate more elements if the real tumours are being developed [72], [145], [146]. Using these model systems can give more realistic estimates of the biophysical properties of pancreatic cancer.

The application of AFM was extended beyond previous applications to the study of the mechanics of cancer cells. The viscoelasticity and adhesiveness of

PDAC cell lines under various conditions were characterised. However, the AFM can investigate only the top layer of the cell. Application of techniques such as traction force microscopy [147], [148] and micropipette aspiration [149], [150] can help capture the stiffness or viscoelastic properties of cells in different configurations.

There is a wide scope for using advanced cell culture models and biophysical techniques to study the mechanical properties of PDAC. It is a disease showing slow progress concerning treatment in the last few decades, especially when compared to other cancers. Translational and clinical research is on-going, with promising breakthroughs in immune therapy. However, pursuing different perspectives, like the mechanical perspective of disease progression, is useful to help uncover new treatment targets.

List of Publications

Published articles

1. S. Pérez-Domínguez*, S.G. Kulkarni*, C. Rianna, C. and M. Radmacher, "Atomic force microscopy for cell mechanics and diseases." *Neuroforum*, vol *26*, no. 2, pp.101-109, Apr 2020.
2. S. G. Kulkarni*, S. Pérez-Domínguez*, and M. Radmacher, "Influence of cantilever tip geometry and contact model on AFM elasticity measurement of cells," *J. Mol. Recognit.*, vol. 36, no. 7, p. e3018, Jul. 2023.
3. S. Pérez-Domínguez, S.G. Kulkarni *et al.*, "Reliable, standardized measurements for cell mechanical properties," *Nanoscale*, vol. 15, no. 40, pp. 16371–16380, Oct. 2023.

Articles under preparation

1. S. G. Kulkarni, N. Messerschmidt, M. Lekka and M. Radmacher, "Effect of cantilever force and ambient CO2 on AFM-based mechanical measurement of pancreatic cancer cell lines."
2. S. G. Kulkarni, E. Werkmeister, *et al.,* "Cell environment modulates rheological properties of pancreatic cancer cells."
3. S. G. Kulkarni, J. Pabijan, M. Radmacher and M. Lekka," Single-cell force spectroscopy reveals interaction between cancer and endothelial cells."
4. L. Martinez-Vidal, S.G. Kulkarni, *et al.,* "Standardization of AFM measurements on tissues"
5. S. Pérez-Domínguez*, S.G. Kulkarni*, *et al.,* "Measuring viscoelastic properties of cells using continuous multi-frequency microrheology."
6. K. Polemidiotou, S.G. Kulkarni, *et al*., "Sarcoma cells remodel their cytoskeleton in order to enhance their invasion and migration."

*Equal contribution

Appendix

A. Hydrodynamic drag correction

Force measurements with atomic force microscopy (AFM) in liquid are subject to a hydrodynamic drag force artefact (F_d) caused by the viscous friction generated by the cantilever moving in the liquid medium. An experiment was performed using the sweep frequency methodology to calculate the hydrodynamic drag (b(0)) of the PFQNM-LC-A-CAL cantilever, based on the method elaborated in [151]. In this approach, the F_d is estimated at a certain distance above the sample by performing a modified sweep frequency force curve out of contact with the substrate on Petri dish containing only culture medium. F_d is then subtracted from the contact force measured on the sample. However, since fluid dynamics theory predicts an increase in the drag force on a body moving close to a rigid plane wall, this assumption of constant F_d is expected to underestimate the actual hydrodynamic force in contact. The drag factor, b(0), can be estimated by measuring the hydrodynamic drag at different distances from the surface. Thus, force curves out of contact were performed at various distances from the surface. The modification of the force curve was as follows: after approaching at a trigger point of 1 nN, the cantilever was retracted to a height (h) varied logarithmically from 0 - 5000 nm and the z-oscillation identical to a sweep frequency methodology force curve was carried out. Force maps with 4X4 curves were captured, with 1 map per oscillation amplitude (100 nm, 200 nm and 500nm). Figure A.1 shows that the hydrodynamic drag correction factor to be used for the PFQNM-LC-A-CAL cantilever is 4.16×10^{-6} N.s/m.

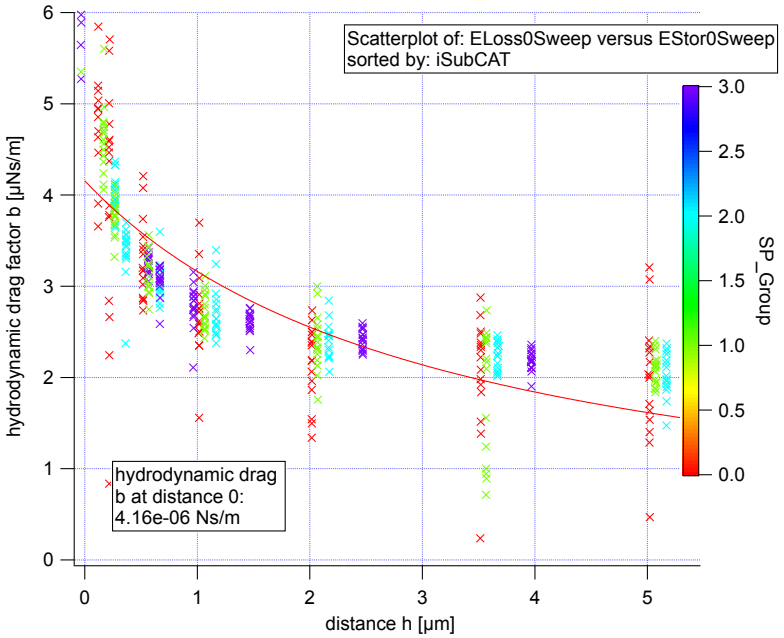

Fig. A.1 shows the hydrodynamic drag factor b for PFQNM-LC-A-CAL cantilever. The distance of the cantilever from the surface, at the time of oscillation is plotted on the x-axis and the hydrodynamic drag correction factor at that distance is plotted on the y-axis.

B. Storage and loss moduli of cell lines at 1 Hz, 10 Hz and 100 Hz.

The sweep frequency methodology yields the storage and loss modulus of the measured sample at multiple frequencies, across decades, within the same force curve. The general trend that is observed in all four cell lines and across the substrate/confinement used, is that the loss modulus increases with frequency much more sharply than the storage modulus does, as shown in Fig. A2 – A9.

PANC-1 – primary site cell line

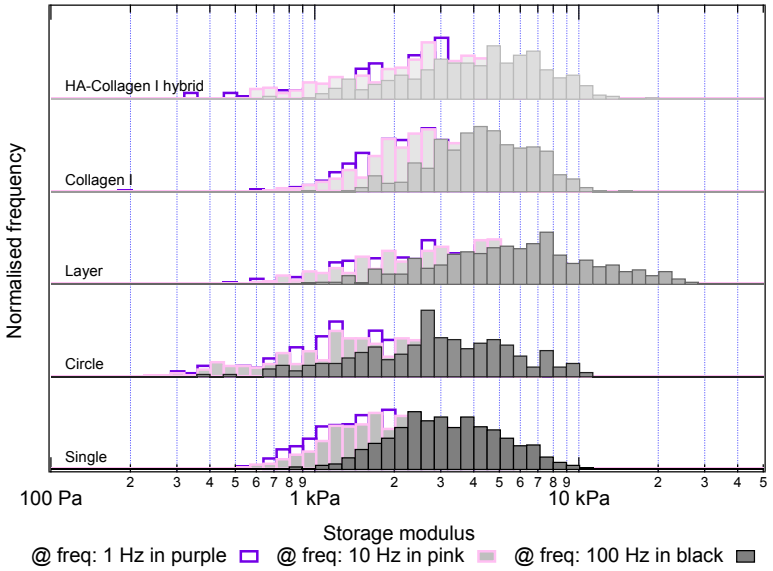

Fig. A.2 Storage modulus of PANC-1 cells across multiple frequencies and for cells on multiple substrates/confinements.

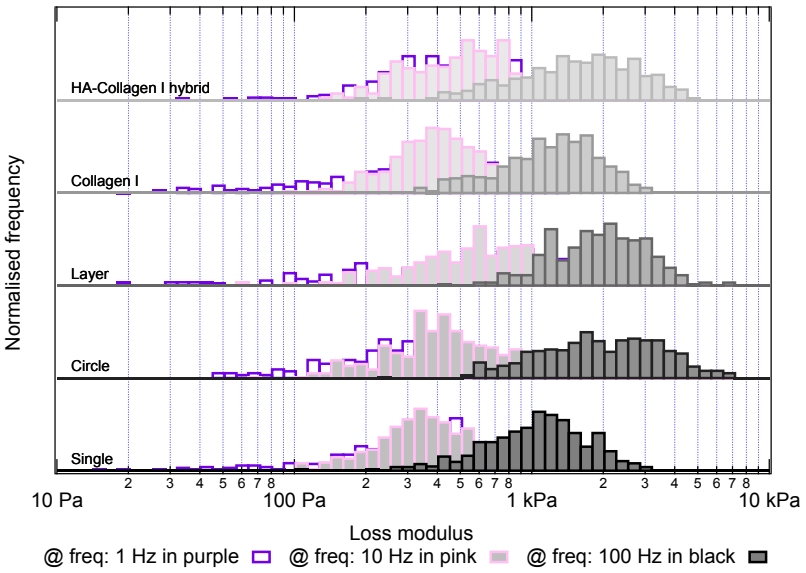

Fig. A.3 Loss modulus of PANC-1 cells across multiple frequencies and for cells on multiple substrates/confinements.

PL-45 – primary site cell line

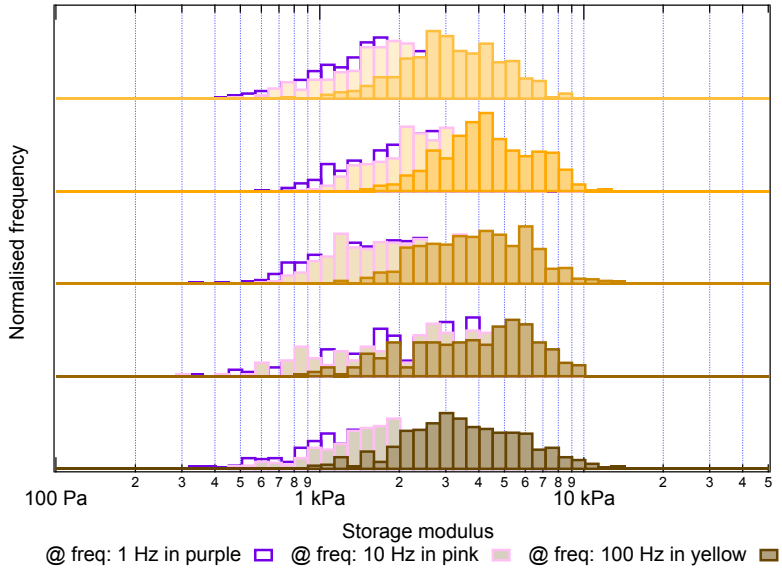

Fig. A.4 Storage modulus of PL-45 cells across multiple frequencies and for cells on multiple substrates/confinements.

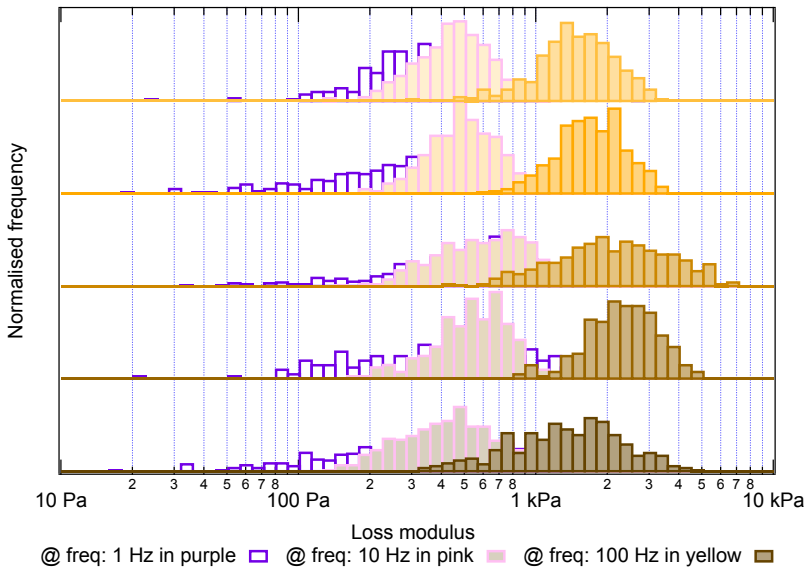

Fig. A.5 Loss modulus of PL-45 cells across multiple frequencies and for cells on multiple substrates/confinements.

Hs 766T – lymph node metastasis

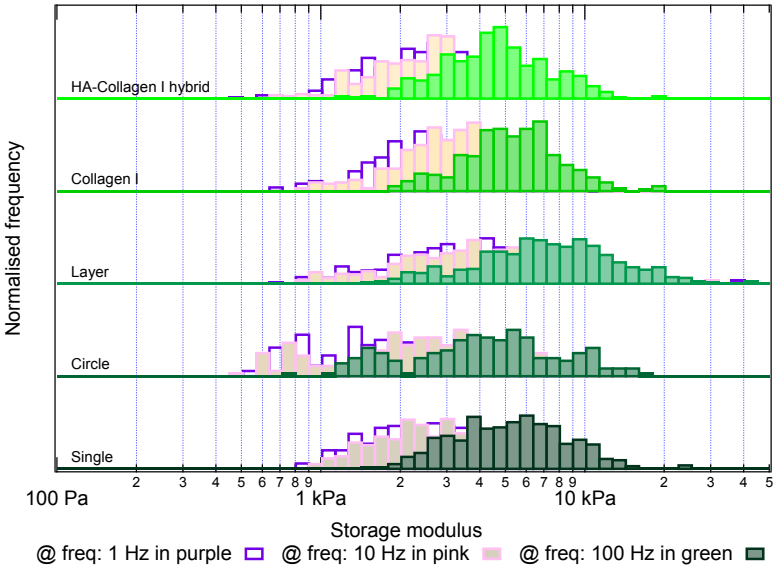

Fig. A.6 Storage modulus of Hs 766T cells across multiple frequencies and for cells on multiple substrates/confinements.

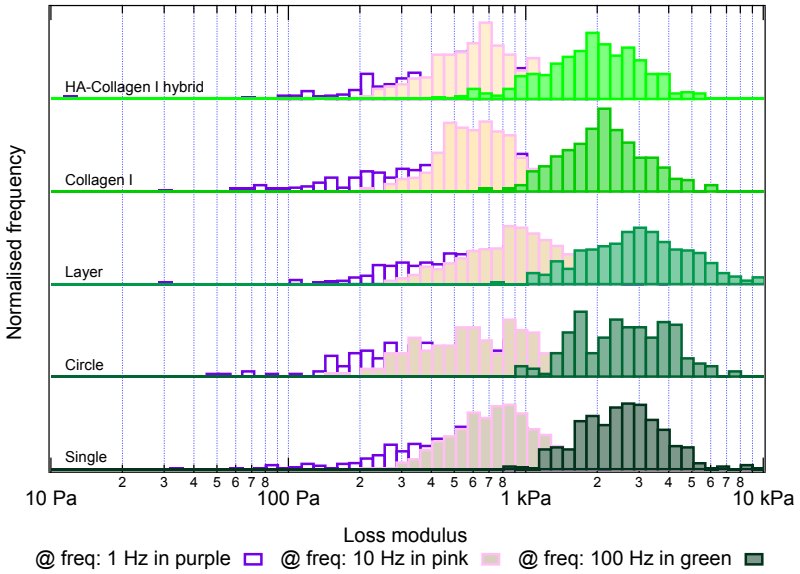

Fig. A.7 Loss modulus of Hs 766T cells across multiple frequencies and for cells on multiple substrates/confinements.

CFPAC-1 – liver metastasis

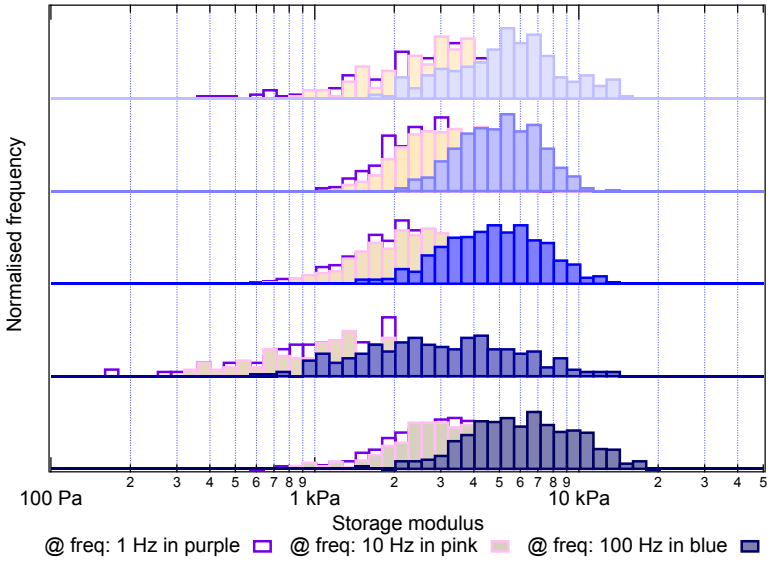

Fig. A.8 Storage modulus of CFPAC-1 cells across multiple frequencies and for cells on multiple substrates/confinements.

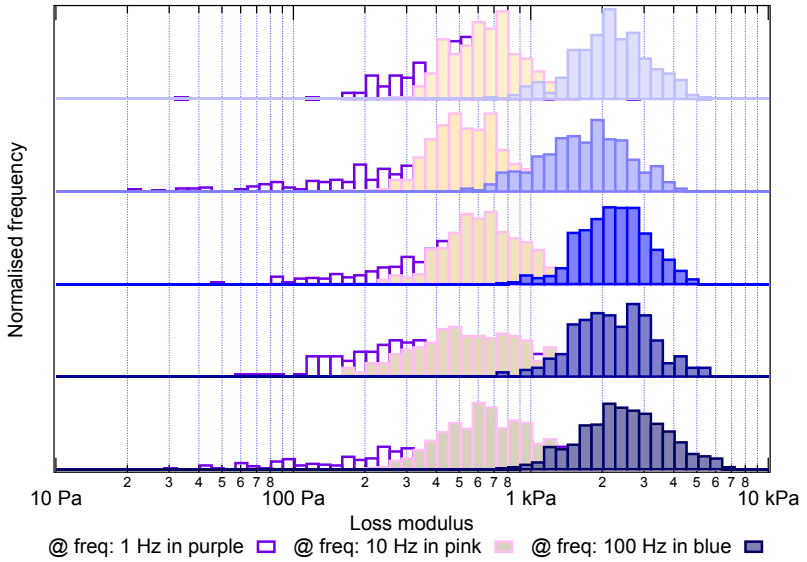

Fig. A.9 Loss modulus of CFPAC-1 cells across multiple frequencies and for cells on multiple substrates/confinements.

Bibliography

[1] M. Ilic and I. Ilic, "Epidemiology of pancreatic cancer," *World J. Gastroenterol.*, vol. 22, no. 44, p. 9694, Nov. 2016.

[2] A. D. Singhi, E. J. Koay, S. T. Chari, and A. Maitra, "Early Detection of Pancreatic Cancer: Opportunities and Challenges.," *Gastroenterology*, vol. 156, no. 7, pp. 2024–2040, May 2019.

[3] A. Teague, K.-H. Lim, and A. Wang-Gillam, "Advanced pancreatic adenocarcinoma: a review of current treatment strategies and developing therapies," *Ther. Adv. Med. Oncol.*, vol. 7, no. 2, pp. 68–84, Mar. 2015.

[4] A. Bengtsson, R. Andersson, and D. Ansari, "The actual 5-year survivors of pancreatic ductal adenocarcinoma based on real-world data," *Sci. Reports 2020 101*, vol. 10, no. 1, pp. 1–9, Oct. 2020.

[5] P. Procacci, C. Moscheni, P. Sartori, M. Sommariva, and N. Gagliano, "Tumor-Stroma Cross-Talk in Human Pancreatic Ductal Adenocarcinoma: A Focus on the Effect of the Extracellular Matrix on Tumor Cell Phenotype and Invasive Potential," 2018.

[6] T. Kamisawa, L. D. Wood, T. Itoi, and K. Takaori, "Pancreatic cancer," *Lancet*, vol. 388, no. 10039, pp. 73–85, Jul. 2016.

[7] S. Gillen, T. Schuster, C. M. Zum Büschenfelde, H. Friess, and J. Kleeff, "Preoperative/Neoadjuvant Therapy in Pancreatic Cancer: A Systematic Review and Meta-analysis of Response and Resection Percentages," *PLOS Med.*, vol. 7, no. 4, p. e1000267, Apr. 2010.

[8] Y. Jiang and D. P. S. Sohal, "Pancreatic Adenocarcinoma Management," *JCO Oncol. Pract.*, vol. 19, no. 1, pp. 19–32, Jan. 2023.

[9] Z. Xu, S. P. Pothula, J. S. Wilson, and M. V. Apte, "Pancreatic cancer and its stroma: A conspiracy theory," *World J. Gastroenterol.*, vol. 20, no. 32, pp. 11216–11229, 2014.

[10] S. Y. G. Friedlander *et al.*, "Context-Dependent Transformation of Adult Pancreatic Cells by Oncogenic K-Ras," *Cancer Cell*, vol. 16, no. 5, pp. 379–389, Nov. 2009.

[11] S. Puri, A. E. Folias, and M. Hebrok, "Plasticity and Dedifferentiation within the Pancreas: Development, Homeostasis, and Disease," *Cell Stem Cell*, vol. 16, no. 1, pp. 18–31, Jan. 2015.

[12] J. Y. Kim and S.-M. Hong, "Precursor Lesions of Pancreatic Cancer," *Oncol. Res. Treat.*, vol. 41, no. 10, pp. 603–610, 2018.

[13] M. Orth *et al.*, "Pancreatic ductal adenocarcinoma: biological hallmarks, current status, and future perspectives of combined modality treatment approaches," *Radiat. Oncol. 2019 141*, vol. 14, no. 1, pp. 1–20, Aug. 2019.

[14] N. Waddell *et al.*, "Whole genomes redefine the mutational landscape of pancreatic cancer," *Nat. 2015 5187540*, vol. 518, no. 7540, pp. 495–501, Feb. 2015.

[15] S. Mueller *et al.*, "Evolutionary routes and KRAS dosage define pancreatic

cancer phenotypes," *Nature*, vol. 554, no. 7690, pp. 62–68, Feb. 2018.

[16] D. A. Altomare *et al.*, "Frequent activation of AKT2 kinase in human pancreatic carcinomas.," *J. Cell. Biochem.*, vol. 87, no. 4, pp. 470–476, Jan. 2002.

[17] H. Ying *et al.*, "Genetics and biology of pancreatic ductal adenocarcinoma," *Genes Dev.*, vol. 30, no. 4, pp. 355–385, Feb. 2016.

[18] Z. I. Hu *et al.*, "Evaluating Mismatch Repair Deficiency in Pancreatic Adenocarcinoma: Challenges and Recommendations," *Clin. Cancer Res.*, vol. 24, no. 6, pp. 1326–1336, Mar. 2018.

[19] P. E. Ferdek and M. A. Jakubowska, "Biology of pancreatic stellate cells-more than just pancreatic cancer.," *Pflugers Arch.*, vol. 469, no. 9, pp. 1039–1050, 2017.

[20] J. Barbazán and D. Matic Vignjevic, "Cancer associated fibroblasts: is the force the path to the dark side?," *Current Opinion in Cell Biology*, vol. 56. pp. 71–79, 2019.

[21] D. Öhlund *et al.*, "Distinct populations of inflammatory fibroblasts and myofibroblasts in pancreatic cancer," *J. Exp. Med.*, vol. 214, no. 3, pp. 579–596, 2017.

[22] J. A. McCarroll *et al.*, "Role of pancreatic stellate cells in chemoresistance in pancreatic cancer," *Frontiers in Physiology*, vol. 5 APR. Frontiers Media SA, p. 141, 09-Apr-2014.

[23] N. Sato, S. Kohi, K. Hirata, and M. Goggins, "Role of hyaluronan in pancreatic cancer biology and therapy: Once again in the spotlight," *Cancer Sci.*, vol. 107, no. 5, pp. 569–575, May 2016.

[24] M. Sarper, E. Cortes, T. J. Lieberthal, and A. Del Río Hernández, "ATRA modulates mechanical activation of TGF-β by pancreatic stellate cells," *Sci. Rep.*, vol. 6, no. February, pp. 1–10, 2016.

[25] A. Haage and I. C. Schneider, "Cellular contractility and extracellular matrix stiffness regulate matrix metalloproteinase activity in pancreatic cancer cells," *FASEB J.*, vol. 28, no. 8, pp. 3589–3599, 2014.

[26] H. Y. Tanaka *et al.*, "Pancreatic stellate cells derived from human pancreatic cancer demonstrate aberrant SPARC-dependent ECM remodeling in 3D engineered fibrotic tissue of clinically relevant thickness," *Biomaterials*, vol. 192, pp. 355–367, 2019.

[27] S. Coppola *et al.*, "A mechanopharmacology approach to overcome chemoresistance in pancreatic cancer," *Drug Resist. Updat.*, vol. 31, pp. 43–51, Mar. 2017.

[28] V. Mahlbacher, A. Sewing, H. P. Elsasser, and H. F. Kern, "Hyaluronan is a secretory product of human pancreatic adenocarcinoma cells.," *Eur. J. Cell Biol.*, vol. 58, no. 1, pp. 28–34, Jun. 1992.

[29] A. D. Theocharis, M. E. Tsara, N. Papageorgacopoulou, D. D. Karavias, and D. A. Theocharis, "Pancreatic carcinoma is characterized by elevated content of hyaluronan and chondroitin sulfate with altered disaccharide composition," *Biochim. Biophys. Acta - Mol. Basis Dis.*, vol. 1502, no. 2, pp. 201–206, Oct. 2000.

[30] X. B. Cheng, S. Kohi, A. Koga, K. Hirata, and N. Sato, "Hyaluronan stimulates pancreatic cancer cell motility," *Oncotarget*, vol. 7, no. 4, pp. 4829–4840, Dec. 2016.

[31] M. A. Jacobetz *et al.*, "Hyaluronan impairs vascular function and drug delivery in a mouse model of pancreatic cancer," *Gut*, vol. 62, no. 1, pp. 112–120, Jan. 2013.

[32] X.-B. Cheng, N. Sato, S. Kohi, and K. Yamaguchi, "Prognostic Impact of Hyaluronan and Its Regulators in Pancreatic Ductal Adenocarcinoma," *PLoS One*, vol. 8, no. 11, p. e80765, Nov. 2013.

[33] M. A. Shields, S. Dangi-Garimella, A. J. Redig, and H. G. Munshi, "Biochemical role of the collagen-rich tumour microenvironment in pancreatic cancer progression," *Biochem. J.*, vol. 441, no. 2, pp. 541–552, Jan. 2012.

[34] A. Koenig, C. Mueller, C. Hasel, G. Adler, and A. Menke, "Collagen type I induces disruption of E-cadherin-mediated cell-cell contacts and promotes proliferation of pancreatic carcinoma cells," *Cancer Res.*, vol. 66, no. 9, pp. 4662–4671, May 2006.

[35] T. Armstrong *et al.*, "Type I collagen promotes the malignant phenotype of pancreatic ductal adenocarcinoma," *Clin. Cancer Res.*, vol. 10, no. 21, pp. 7427–7437, Nov. 2004.

[36] Y. Imamichi, A. König, T. Gress, and A. Menke, "Collagen type I-induced Smad-interacting protein 1 expression downregulates E-cadherin in pancreatic cancer," *Oncogene*, vol. 26, no. 16, pp. 2381–2385, Apr. 2007.

[37] D. Hlund, C. Lundin, B. Ardnor, M. Man, P. Naredi, and M. Sund, "Type IV collagen is a tumour stroma-derived biomarker for pancreas cancer," *Br. J. Cancer*, vol. 101, no. 1, pp. 91–97, 2009.

[38] D. Öhlund, O. Franklin, E. Lundberg, C. Lundin, and M. Sund, "Type IV collagen stimulates pancreatic cancer cell proliferation, migration, and inhibits apoptosis through an autocrine loop," *BMC Cancer*, vol. 13, no. 1, pp. 1–11, Mar. 2013.

[39] S. Berchtold *et al.*, "Collagen type V promotes the malignant phenotype of pancreatic ductal adenocarcinoma," *Cancer Lett.*, vol. 356, no. 2, pp. 721–732, 2015.

[40] R. Curvello, V. Kast, M. H. Abuwarwar, A. L. Fletcher, G. Garnier, and D. Loessner, "3D Collagen-Nanocellulose Matrices Model the Tumour Microenvironment of Pancreatic Cancer," *Front. Digit. Heal.*, vol. 3, no. July, pp. 1–13, 2021.

[41] A. J. Rice *et al.*, "Matrix stiffness induces epithelial-mesenchymal transition and promotes chemoresistance in pancreatic cancer cells," *Oncogenesis*, vol. 6, no. 7, pp. e352–e352, Jul. 2017.

[42] I. Carnevale, M. Capula, E. Giovannetti, T. Schmidt, and S. Coppola, "A mechanical memory of pancreatic cancer cells," *bioRxiv*. bioRxiv, p. 730960, 09-Aug-2019.

[43] A. M. Krebs *et al.*, "The EMT-activator Zeb1 is a key factor for cell plasticity and promotes metastasis in pancreatic cancer," *Nat. Cell Biol.*, vol. 19, no. 5, pp. 518–529, 2017.

[44] N. Aceto, M. Toner, S. Maheswaran, and D. A. Haber, "En Route to Metastasis: Circulating Tumor Cell Clusters and Epithelial-to-Mesenchymal Transition," *Trends in Cancer*, vol. 1, no. 1, pp. 44–52, 2015.

[45] E. Toyoda *et al.*, "Analysis of E-, N-cadherin, α-, β-, and γ-catenin expression in human pancreatic carcinoma cell lines," *Pancreas*, vol. 30, no. 2, pp. 168–173, Mar. 2005.

[46] N. Gagliano *et al.*, "Epithelial-to-mesenchymal transition in pancreatic ductal adenocarcinoma: Characterization in a 3D-cell culture model," *World J. Gastroenterol.*, vol. 22, no. 18, pp. 4466–4483, May 2016.

[47] Y. Shichi *et al.*, "Enhanced morphological and functional differences of pancreatic cancer with epithelial or mesenchymal characteristics in 3D culture," *Sci. Rep.*, vol. 9, no. 1, pp. 1–10, Dec. 2019.

[48] J. L. Carstens *et al.*, "Stabilized epithelial phenotype of cancer cells in primary tumors leads to increased colonization of liver metastasis in pancreatic cancer," *CellReports*, vol. 35, p. 108990, 2021.

[49] B. A. Purnell, "Cell mechanics indicate cell fate," *Science (80-.).*, vol. 358, no. 6370, pp. 1552.3-1553, Dec. 2017.

[50] G. Binnig, C. F. Quate, and C. Gerber, "Atomic force microscope," *Phys. Rev. Lett.*, vol. 56, no. 9, pp. 930–933, 1986.

[51] G. Binnig and H. Rohrer, "Scanning tunneling microscopy," *Surf. Sci.*, vol. 126, no. 1–3, pp. 236–244, Mar. 1983.

[52] R. W. Tillmann, M. Radmacher, and H. E. Gaub, "Surface structure of hydrated amorphous silicon oxide at 3 Å resolution by scanning force microscopy," *Appl. Phys. Lett.*, vol. 60, no. 25, pp. 3111–3113, 1992.

[53] M. Fritz, M. Radmacher, and H. E. Gaub, "Granula motion and membrane spreading during activation of human platelets imaged by atomic force microscopy," *Biophys. J.*, vol. 66, no. 5, pp. 1328–1334, 1994.

[54] M. Radmacher, M. Fritz, and P. K. Hansma, "Imaging soft samples with the atomic force microscope: gelatin in water and propanol," *Biophys. J.*, vol. 69, no. 1, pp. 264–270, 1995.

[55] S. W. Schneider, R. Matzke, M. Radmacher, and H. Oberleithner, "Shape and volume of living aldosterone-sensitive cells imaged with the atomic force microscope.," *Methods Mol. Biol.*, vol. 242, no. 19, pp. 255–279, 2004.

[56] C. Roduit, S. Sekatski, G. Dietler, S. Catsicas, F. Lafont, and S. Kasas, "Stiffness tomography by atomic force microscopy," *Biophys. J.*, vol. 97, no. 2, pp. 674–677, Jul. 2009.

[57] C. Rotsch, K. Jacobson, and M. Radmacher, "Dimensional and mechanical dynamics of active and stable edges in motile fibroblasts investigated by using atomic force microscopy," *Proc. Natl. Acad. Sci. U. S. A.*, vol. 96, no. 3, pp. 921–

926, 1999.

[58] M. Lekka, P. Laidler, D. Gil, J. Lekki, Z. Stachura, and A. Z. Hrynkiewicz, "Elasticity of normal and cancerous human bladder cells studied by scanning force microscopy," *Eur. Biophys. J.*, vol. 28, no. 4, pp. 312–316, 1999.

[59] P. H. Puech, K. Poole, D. Knebel, and D. J. Muller, "A new technical approach to quantify cell-cell adhesion forces by AFM," *Ultramicroscopy*, vol. 106, no. 8–9, pp. 637–644, 2006.

[60] H. H. Lin *et al.*, "Mechanical phenotype of cancer cells: Cell softening and loss of stiffness sensing," *Oncotarget*, vol. 6, no. 25, pp. 20946–20958, 2015.

[61] C. Rianna and M. Radmacher, "Comparison of viscoelastic properties of cancer and normal thyroid cells on different stiffness substrates," 2016.

[62] R. Omidvar, M. Tafazzoli-shadpour, M. A. Shokrgozar, and M. Rostami, "Atomic force microscope-based single cell force spectroscopy of breast cancer cell lines: An approach for evaluating cellular invasion," *J. Biomech.*, vol. 47, no. 13, pp. 3373–3379, 2014.

[63] Y. Wang *et al.*, "Quantitative analysis of the cell-surface roughness and viscoelasticity for breast cancer cells discrimination using atomic force microscopy," *Scanning*, vol. 38, no. 6, pp. 558–563, Nov. 2016.

[64] Y. Lv, C. Chen, B. Zhao, and X. Zhang, "Regulation of matrix stiffness on the epithelial-mesenchymal transition of breast cancer cells under hypoxia environment," *Sci. Nat.*, vol. 104, no. 5–6, Jun. 2017.

[65] C. Rianna and M. Radmacher, "Influence of microenvironment topography and stiffness on the mechanics and motility of normal and cancer renal cells," *Nanoscale*, vol. 9, no. 31, pp. 11222–11230, 2017.

[66] J. Raczkowska *et al.*, "Patterning of cancerous cells driven by a combined modification of mechanical and chemical properties of the substrate," *Eur. Polym. J.*, vol. 93, pp. 726–732, 2017.

[67] Y. Abidine, V. M. Laurent, R. Michel, A. Duperray, and C. Verdier, "Local mechanical properties of bladder cancer cells measured by AFM as a signature of metastatic potential," *Eur. Phys. J. Plus*, vol. 130, no. 10, Oct. 2015.

[68] K. Gnanachandran, S. Kędracka-Krok, J. Pabijan, and M. Lekka, "Discriminating bladder cancer cells through rheological mechanomarkers at cell and spheroid levels," *J. Biomech.*, vol. 144, p. 111346, Nov. 2022.

[69] M. Lekka *et al.*, "Characterization of N-cadherin unbinding properties in non-malignant (HCV29) and malignant (T24) bladder cells.," *J. Mol. Recognit.*, vol. 24, no. 5, pp. 833–842, 2011.

[70] V. Palmieri *et al.*, "Biomechanical investigation of colorectal cancer cells," *Appl. Phys. Lett.*, vol. 105, no. 12, 2014.

[71] M. M. Brás *et al.*, "Mechanical Properties of Colorectal Cancer Cells Determined by Dynamic Atomic Force Microscopy: A Novel Biomarker," *Cancers (Basel).*, vol. 14, no. 20, p. 5053, Oct. 2022.

[72] A. Rubiano *et al.*, "Viscoelastic properties of human pancreatic tumors and in vitro constructs to mimic mechanical properties," *Acta Biomater.*, vol. 67, pp. 331–340, Feb. 2018.

[73] A. Stylianou, C. Voutouri, F. Mpekris, and T. Stylianopoulos, "Pancreatic Cancer Presents Distinct Nanomechanical Properties During Progression," *Ann. Biomed. Eng.*, vol. 51, no. 7, pp. 1602–1615, Jul. 2023.

[74] D. Kpeglo *et al.*, "Modeling the mechanical stiffness of pancreatic ductal adenocarcinoma," *Matrix Biol. Plus*, vol. 14, p. 100109, Jun. 2022.

[75] N. Walter, T. Busch, T. Seufferlein, and J. P. Spatz, "Elastic moduli of living epithelial pancreatic cancer cells and their skeletonized keratin intermediate filament network," *Biointerphases*, vol. 6, no. 2, pp. 79–85, 2011.

[76] X. Liang, S. Liu, X. Wang, D. Xia, and Q. Li, "Alteration of nanomechanical properties of pancreatic cancer cells through anticancer drug treatment revealed by atomic force microscopy," *Beilstein J. Nanotechnol. 12101*, vol. 12, no. 1, pp. 1372–1379, Dec. 2021.

[77] A. V. Nguyen *et al.*, "Stiffness of pancreatic cancer cells is associated with increased invasive potential," *Integr. Biol. (United Kingdom)*, vol. 8, no. 12, pp. 1232–1245, 2016.

[78] C. Verdier, J. Etienne, A. Duperray, and L. Preziosi, "Review: Rheological properties of biological materials," *Comptes Rendus Phys.*, vol. 10, no. 8, pp. 790–811, 2009.

[79] C. Braunsmann, R. Proksch, I. Revenko, and T. E. Schäffer, "Creep compliance mapping by atomic force microscopy," *Polymer (Guildf).*, vol. 55, no. 1, pp. 219–225, Jan. 2014.

[80] A. Yango, J. Schäpe, C. Rianna, H. Doschke, and M. Radmacher, "Measuring the viscoelastic creep of soft samples by step response AFM," *Soft Matter*, vol. 12, no. 40, pp. 8297–8306, 2016.

[81] J. Alcaraz *et al.*, "Microrheology of Human Lung Epithelial Cells Measured by Atomic Force Microscopy," *Biophys. J.*, vol. 84, no. 3, pp. 2071–2079, Mar. 2003.

[82] A. R. Bausch, F. Ziemann, A. A. Boulbitch, K. Jacobson, and E. Sackmann, "Local measurements of viscoelastic parameters of adherent cell surfaces by magnetic bead microrheometry," *Biophys. J.*, vol. 75, no. 4, pp. 2038–2049, Oct. 1998.

[83] R. E. Mahaffy, C. K. Shih, F. C. MacKintosh, and J. Käs, "Scanning Probe-Based Frequency-Dependent Microrheology of Polymer Gels and Biological Cells," *Phys. Rev. Lett.*, vol. 85, no. 4, p. 880, Jul. 2000.

[84] B. Fabry, G. N. Maksym, J. P. Butler, M. Glogauer, D. Navajas, and J. J. Fredberg, "Scaling the microrheology of living cells," *Phys. Rev. Lett.*, vol. 87, no. 14, pp. 1–4, 2001.

[85] M. Puig-De-Morales *et al.*, "Measurement of cell microrheology by magnetic twisting cytometry with frequency domain demodulation," *J. Appl. Physiol.*, vol. 91, no. 3, pp. 1152–1159, 2001.

[86] A. W. Holle, M. Kalafat, A. S. Ramos, T. Seufferlein, R. Kemkemer, and J. P.

Spatz, "Intermediate filament reorganization dynamically influences cancer cell alignment and migration," *Sci. Rep.*, vol. 7, no. 1, pp. 1–14, Mar. 2017.

[87] L. Roa-Peña *et al.*, "Keratin 17 identifies the most lethal molecular subtype of pancreatic cancer," *Sci. Rep.*, vol. 9, no. 1, p. 11239, 2019.

[88] V. Karantza, "Keratins in health and cancer: More than mere epithelial cell markers," *Oncogene*, vol. 30, no. 2, pp. 127–138, 2011.

[89] A. Handra-Luca, S. M. Hong, K. Walter, C. Wolfgang, R. Hruban, and M. Goggins, "Tumour epithelial vimentin expression and outcome of pancreatic ductal adenocarcinomas," *Br. J. Cancer 2011 1048*, vol. 104, no. 8, pp. 1296–1302, Mar. 2011.

[90] W. Wang *et al.*, "Girdin interaction with vimentin induces EMT and promotes the growth and metastasis of pancreatic ductal adenocarcinoma," *Oncol. Rep.*, vol. 44, no. 2, pp. 637–649, Aug. 2020.

[91] P. Kollmannsberger and B. Fabry, "Active soft glassy rheology of adherent cells," *Soft Matter*, vol. 5, no. 9, pp. 1771–1774, 2009.

[92] D. Ingber, J. Madri, and J. Jamieson, "Neoplastic Disorganization of Pancreatic Epithelial Cell-Cell Relations," *Am J Pathol*, vol. 121, pp. 248–60, 1985.

[93] J. Friedrichs *et al.*, "A practical guide to quantify cell adhesion using single-cell force spectroscopy," *Methods*, vol. 60, no. 2, pp. 169–178, Apr. 2013.

[94] V. Kanoldt, L. Fischer, and C. Grashoff, "Unforgettable force-crosstalk and memory of mechanosensitive structures," *Biol. Chem.*, vol. 400, no. 6, pp. 687–698, May 2019.

[95] G. Ariel *et al.*, "Thermorheology of living cells—impact of temperature variations on cell mechanics," *New J. Phys.*, vol. 15, no. 4, p. 045026, Apr. 2013.

[96] M. Zambito, F. Viti, A. G. Bosio, I. Ceccherini, T. Florio, and M. Vassalli, "The Impact of Experimental Conditions on Cell Mechanics as Measured with Nanoindentation," *Nanomater. 2023, Vol. 13, Page 1190*, vol. 13, no. 7, p. 1190, Mar. 2023.

[97] B. Codan, V. Martinelli, L. Mestroni, and O. Sbaizero, "Atomic force microscopy of 3T3 and SW-13 cell lines: An investigation of cell elasticity changes due to fixation," *Mater. Sci. Eng. C*, vol. 33, no. 6, pp. 3303–3308, Aug. 2013.

[98] T. Kulkarni, A. Tam, D. Mukhopadhyay, and S. Bhattacharya, "AFM study: Cell cycle and probe geometry influences nanomechanical characterization of Panc1 cells," *Biochim. Biophys. Acta - Gen. Subj.*, vol. 1863, no. 5, pp. 802–812, 2019.

[99] A. Weber, J. Iturri, R. Benitez, and J. L. Toca-Herrera, "Measuring biomaterials mechanics with atomic force microscopy. 1. Influence of the loading rate and applied force (pyramidal tips)," *Microsc. Res. Tech.*, vol. 82, no. 9, pp. 1392–1400, Sep. 2019.

[100] M. Zhao, C. Srinivasan, D. J. Burgess, and B. D. Huey, "Rate- and depth-dependent nanomechanical behavior of individual living Chinese hamster ovary cells probed by atomic force microscopy," *J. Mater. Res.*, vol. 21, no. 8, pp. 1906–1912, Aug. 2006.

[101] S. Wang, S. Huang, and Y. L. Sun, "Epithelial-mesenchymal transition in pancreatic cancer: A review," *Biomed Res. Int.*, vol. 2017, 2017.

[102] Y. W. Chiou, H. K. Lin, M. J. Tang, H. H. Lin, and M. L. Yeh, "The Influence of Physical and Physiological Cues on Atomic Force Microscopy-Based Cell Stiffness Assessment," *PLoS One*, vol. 8, no. 10, 2013.

[103] S. G. Kulkarni, S. Pérez-Domínguez, and M. Radmacher, "Influence of cantilever tip geometry and contact model on AFM elasticity measurement of cells," *J. Mol. Recognit.*, vol. 36, no. 7, p. e3018, Jul. 2023.

[104] L. Wang, L. Tian, W. Zhang, Z. Wang, and X. Liu, "Effect of AFM nanoindentation loading rate on the characterization of mechanical properties of vascular endothelial cell," *Micromachines*, vol. 11, no. 6, p. 562, Jun. 2020.

[105] H. Hertz, "Ueber die Berührung fester elastischer Körper," *J. fur die Reine und Angew. Math.*, vol. 1882, no. 92, pp. 156–171, Jan. 1882.

[106] R. A. Cairns, I. S. Harris, and T. W. Mak, "Regulation of cancer cell metabolism," *Nat. Rev. Cancer 2011 112*, vol. 11, no. 2, pp. 85–95, Jan. 2011.

[107] J. C. Tung *et al.*, "Tumor mechanics and metabolic dysfunction," *Free Radic. Biol. Med.*, vol. 79, pp. 269–280, 2015.

[108] P. Romani, L. Valcarcel-Jimenez, C. Frezza, and S. Dupont, "Crosstalk between mechanotransduction and metabolism," *Nat. Rev. Mol. Cell Biol. 2020 221*, vol. 22, no. 1, pp. 22–38, Nov. 2020.

[109] J. S. Park *et al.*, "Mechanical regulation of glycolysis via cytoskeleton architecture," *Nat. 2020 5787796*, vol. 578, no. 7796, pp. 621–626, Feb. 2020.

[110] J. Michl, K. C. Park, and P. Swietach, "Evidence-based guidelines for controlling pH in mammalian live-cell culture systems," *Commun. Biol. 2019 21*, vol. 2, no. 1, pp. 1–12, Apr. 2019.

[111] E. L. Stuenkel, T. E. Machen, and J. A. Williams, "pH regulatory mechanisms in rat pancreatic ductal cells," *https://doi.org/10.1152/ajpgi.1988.254.6.G925*, vol. 254, no. 6, 1988.

[112] H. Schillers *et al.*, "Standardized Nanomechanical Atomic Force Microscopy Procedure (SNAP) for Measuring Soft and Biological Samples," *Sci. Rep.*, vol. 7, no. 1, pp. 1–9, 2017.

[113] J. Bobrowska *et al.*, "Biophysical and biochemical characteristics as complementary indicators of melanoma progression," *Anal. Chem.*, vol. 91, no. 15, pp. 9885–9892, Aug. 2019.

[114] J. Bao, S. Wang, L. K. Gunther, S. ichiro Kitajiri, C. Li, and T. Sakamoto, "The actin-bundling protein TRIOBP-4 and -5 promotes the motility of pancreatic cancer cells," *Cancer Lett.*, vol. 356, no. 2, pp. 367–373, 2015.

[115] T. Yin, C. Wang, T. Liu, G. Zhao, Y. Zha, and M. Yang, "Expression of Snail in Pancreatic Cancer Promotes Metastasis and Chemoresistance," *J. Surg. Res.*, 2007.

[116] G. Lazzari, V. Nicolas, M. Matsusaki, M. Akashi, P. Couvreur, and S. Mura,

"Multicellular spheroid based on a triple co-culture: A novel 3D model to mimic pancreatic tumor complexity," *Acta Biomater.*, vol. 78, pp. 296–307, 2018.

[117] A. Azioune, M. Storch, M. Bornens, M. Théry, and M. Piel, "Simple and rapid process for single cell micro-patterning," *Lab Chip*, vol. 9, no. 11, pp. 1640–1642, Jun. 2009.

[118] J. R. Tse and A. J. Engler, "Preparation of hydrogel substrates with tunable mechanical properties," *Curr. Protoc. Cell Biol.*, no. SUPPL. 47, pp. 1–16, 2010.

[119] Z. Charles Ying, M. G. Reitsma, and R. S. Gates, "Direct measurement of cantilever spring constants and correction for cantilever irregularities using an instrumented indenter," 2007.

[120] J. M. Neumeister and W. A. Ducker, "Lateral, normal, and longitudinal spring constants of atomic force microscopy cantilevers," *Rev. Sci. Instrum.*, vol. 65, no. 8, pp. 2527–2531, Aug. 1994.

[121] N. Gavara, "A beginner's guide to atomic force microscopy probing for cell mechanics," *Microsc. Res. Tech.*, vol. 80, no. 1, pp. 75–84, 2017.

[122] N. Schierbaum, J. Rheinlaender, and T. E. Schäffer, "Viscoelastic properties of normal and cancerous human breast cells are affected differently by contact to adjacent cells," *Acta Biomater.*, vol. 55, pp. 239–248, 2017.

[123] M. Lekka, "Discrimination Between Normal and Cancerous Cells Using AFM," *Bionanoscience*, vol. 6, no. 1, pp. 65–80, Mar. 2016.

[124] E. Bertseva *et al.*, "Intracellular nanomanipulation by a photonic-force microscope with real-time acquisition of a 3D stiffness matrix," *Nanotechnology*, vol. 20, no. 28, 2009.

[125] C. Rianna and M. Radmacher, "Cell mechanics as a marker for diseases: Biomedical applications of AFM," *AIP Conf. Proc.*, vol. 1760, no. 1, Aug. 2016.

[126] K. Pogoda *et al.*, "Depth-sensing analysis of cytoskeleton organization based on AFM data," *Eur. Biophys. J.*, vol. 41, no. 1, pp. 79–87, 2012.

[127] M. A. Shields, S. Dangi-Garimella, S. B. Krantz, D. J. Bentrem, and H. G. Munshi, "Pancreatic cancer cells respond to type I collagen by inducing snail expression to promote membrane type 1 matrix metalloproteinase-dependent collagen invasion," *J. Biol. Chem.*, vol. 286, no. 12, pp. 10495–10504, Mar. 2011.

[128] B. K. Robinson, E. Cortes, A. J. Rice, M. Sarper, and A. D. R. Hernañdez, "Quantitative analysis of 3D extracellular matrix remodelling by pancreatic stellate cells," *Biol. Open*, vol. 5, no. 6, pp. 875–882, 2016.

[129] J. R. Ramos, J. Pabijan, R. Garcia, and M. Lekka, "The softening of human bladder cancer cells happens at an early stage of the malignancy process," *Beilstein J. Nanotechnol. 552*, vol. 5, no. 1, pp. 447–457, Apr. 2014.

[130] L. Wullkopf *et al.*, "Cancer cells' ability to mechanically adjust to extracellular matrix stiffness correlates with their invasive potential," *Mol. Biol. Cell*, vol. 29, no. 20, pp. 2378–2385, Oct. 2018.

[131] A. J. Knights, A. P. W. Funnell, M. Crossley, and R. C. M. Pearson, "Holding

Tight: Cell Junctions and Cancer Spread.," *Trends Cancer Res.*, vol. 8, pp. 61–69, 2012.

[132] T. A. Martin, "The role of tight junctions in cancer metastasis," *Seminars in Cell and Developmental Biology*, vol. 36. Academic Press, pp. 224–231, 01-Dec-2014.

[133] V. Vasioukhin, "Adherens junctions and cancer," *Subcell. Biochem.*, vol. 60, pp. 379–414, 2012.

[134] J. M. Gooding, K. L. Yap, and M. Ikura, "The cadherin–catenin complex as a focal point of cell adhesion and signalling: new insights from three-dimensional structures," *BioEssays*, vol. 26, no. 5, pp. 497–511, May 2004.

[135] O. W. Blaschuk, "Discovery and development of N-cadherin antagonists," *Cell and Tissue Research*, vol. 348, no. 2. Springer, pp. 309–313, 27-May-2012.

[136] M. Eslami *et al.*, "Deep analysis of N-cadherin/ADH-1 interaction: a computational survey," *J. Biomol. Struct. Dyn.*, vol. 37, no. 1, pp. 210–228, 2019.

[137] O. W. Blaschuk, "N-cadherin antagonists as oncology therapeutics," *Philosophical Transactions of the Royal Society B: Biological Sciences*, vol. 370, no. 1661. Royal Society of London, 05-Jan-2015.

[138] Y. Shintani *et al.*, "ADH-1 suppresses N-cadherin-dependent pancreatic cancer progression," *Int. J. Cancer*, vol. 122, no. 1, pp. 71–77, Jan. 2008.

[139] M. B. Slidell *et al.*, "Impact of total lymph node count and lymph node ratio on staging and survival after pancreatectomy for pancreatic adenocarcinoma: A large, population-based analysis," *Ann. Surg. Oncol.*, vol. 15, no. 1, pp. 165–174, Jan. 2008.

[140] S. Nakajima *et al.*, "N-cadherin expression and epithelial-mesenchymal transition in pancreatic carcinoma," *Clin. Cancer Res.*, vol. 10, no. 12 I, pp. 4125–4133, 2004.

[141] E. Lorenc *et al.*, "Correlation between biological and mechanical properties of extracellular matrix from colorectal peritoneal metastases in human tissues," *Sci. Reports 2023 131*, vol. 13, no. 1, pp. 1–13, Jul. 2023.

[142] M. Amrutkar *et al.*, "Establishment and Characterization of Paired Primary Cultures of Human Pancreatic Cancer Cells and Stellate Cells Derived from the Same Tumor," *Cells*, vol. 9, no. 1, p. 227, Jan. 2020.

[143] E. Vernucci *et al.*, "Metabolic Alterations in Pancreatic Cancer Progression," *Cancers 2020, Vol. 12, Page 2*, vol. 12, no. 1, p. 2, Dec. 2019.

[144] A. J. Rice *et al.*, "Matrix stiffness induces epithelial-mesenchymal transition and promotes chemoresistance in pancreatic cancer cells," *Oncogenesis*, vol. 6, no. 7, p. 352, Jul. 2017.

[145] L. A. Baker, H. Tiriac, H. Clevers, and D. A. Tuveson, "Modeling Pancreatic Cancer with Organoids," *Trends in Cancer*, vol. 2, no. 4, pp. 176–190, 2016.

[146] M. Ermis *et al.*, "Tunable hybrid hydrogels with multicellular spheroids for modeling desmoplastic pancreatic cancer," *Bioact. Mater.*, vol. 25, pp. 360–373, Jul. 2023.

[147] M. Gupta, L. Kocgozlu, B. R. Sarangi, F. Margadant, M. Ashraf, and B. Ladoux, *Micropillar substrates: A tool for studying cell mechanobiology*, vol. 125. Elsevier Ltd, 2015.

[148] R. W. Style *et al.*, "Traction force microscopy in physics and biology," *Soft Matter*, vol. 10, no. 23, pp. 4047–4055, 2014.

[149] E. H. Zhou, S. T. Quek, and C. T. Lim, "Power-law rheology analysis of cells undergoing micropipette aspiration," *Biomech. Model. Mechanobiol.*, vol. 9, no. 5, pp. 563–572, 2010.

[150] L. Guillou *et al.*, "Measuring Cell Viscoelastic Properties Using a Microfluidic Extensional Flow Device," *Biophys. J.*, vol. 111, no. 9, pp. 2039–2050, Nov. 2016.

[151] J. Alcaraz, L. Buscemi, M. Puig-De-Morales, J. Colchero, A. Baró, and D. Navajas, "Correction of microrheological measurements of soft samples with atomic force microscopy for the hydrodynamic drag on the cantilever," *Langmuir*, vol. 18, no. 3, pp. 716–721, Feb. 2002.